Doctoral Dissertation (Shinshu University)

Study on carbon nanomaterials modified NF membrane and Mg^{2+}/Li^{+} separation performance

カーボンナノ材料修飾 NF 膜とその Mg^{2+}/Li^{+}分離性能に関する研究

March 2022

XU PING

Abstract

The rapid developments of electric-energy storage technology, especially in the application of electric vehicles, have promoted an increasing demand for lithium resources. Owing to the low cost and large lithium reserves, lithium recovery from salt-lake brines has become a growing trend in the lithium recovery industry. Effectively separate Li^+ and the co-exist Mg^{2+} is critical for enriching and extracting high purity lithium products from salt-lake brines. Nanofiltration (NF) technology is promising for separating Mg^{2+} and Li^+ in salt-lake brines. Till now, it is still challenging to obtain both high separation ability and high flux at the same time, which is the bottleneck of the industrial application of NF membrane for lithium extraction. For industrial applications, an optimization of the membrane structure and chemical composition is necessary to ensure highly selective separation, anti-pollution, and long-term stable performance. In this work, we adopted several carbon materials to improve the Mg^{2+}/Li^+ separation performance and efficiency of NF membranes, and comprehensively discussed the results and mechanism of the resulted carbon-based NF membranes from the perspectives of multiple aspects. Based on the above research process, the main research contents of this paper are as follows:

(1) A novel NF membrane was optimized by doping graphene oxide (GO) additives into the ultrafiltration (UF) base membrane. The effects of GO doping content on the morphology, structure and surface properties of UF membrane and the final NF membrane were studied comprehensively. The hydrophilic GO acted as a “bridge” between UF membrane and polyamide layer due to the “anchor effect”, which significantly enhanced the interaction between base membrane and polyamide layer. The results revealed that with ultra-low GO doping content of 0.05 wt%, the final NF membrane exhibited a high selective separation capacity for Mg^{2+} and Li^+, and the flux increased by about 119% compared with the pure NF membrane without GO.

Additionally, due to the high stability of membrane, the excellent separation capacity of modified NF membrane only changed slightly after 7-day cycle filtration test. Importantly, a small amount of GO doping greatly improved the permeability of both UF and NF membranes, which correspondingly improved the separation efficiency and accelerated the filtration rate.

(2) We developed another novel NF membrane by incorporating nano-sized aminated graphene quantum dots (GQDs-NH_2). The effect of GQDs-NH_2 dosage on the structure and properties of the NF membrane was systematically investigated by several characterization methods. The modified NF membrane with optimized GQDs-NH_2 incorporation of 0.03 wt% exhibited a higher positive chargeability, a high separation ability and a higher difference of up to 77% between Mg^{2+} and Li^{+} rejection, suggesting its excellent Mg^{2+}/Li^{+} separation capability. Importantly, the modified NF membrane had a high permeation flux of 11.94 L/m^2hbar, which was 137.8 % more than that of pure NF membrane with no GQDs-NH_2. Furthermore, the (GQDs-NH_2)-optimized morphology structure and hydrophilicity led to strong anti-fouling and stability of the final NF composite membrane.

(3) We successfully synthesized a new functional nano-additive called potassium carboxylate functionalized multi-wall carbon nanotubes (MWCNTs-COOK) and introduced it into the interfacial polymerization system to fine-tune the structure and properties of the NF membrane. The embedded MWCNTs-COOK (150ppm) tightened the network-crosslink structure of the selective layer and contributed to a dense hydrophilic membrane surface with high positive chargeability. In addition, MWCNTs-COOK nano-additives in membrane created some intrinsic fast transport channels for water molecules. The MWCNTs-COOK (150ppm)-assisted NF membrane exhibited a remarkable high flux of 12.23 L/m^2hbar, a high separation ability, and a high difference in Li^{+} and Mg^{2+} rejections around 77%, indicating an excellent Li^{+} enrichment and Mg^{2+} removal capabilities, and breaking through the trad-off limit of permeate flux. Simultaneously, the comprehensive performance of the NF membrane can be maintained stably even in long-term utilization.

(4) Herein, we proposed another (MWCNTs-COOK)-engineered substrate membrane to regulate the NF membrane for fast and efficient separation of Li^+ and co-existing Mg^{2+} in brines. Results proved that the fixed MWCNTs-COOK strengthened the connection between the substrate and the formed polyamide layer, and it endowed both the substrate and the final NF membrane with higher water permeability. The membrane performance characterization indicated that with a low MWCNTs-COOK content of 0.012 wt% in the NF membrane, the difference between rejections of Mg^{2+} and Li^+ reached up to 86.94 %. Note that the modified NF membrane showed a high flux of high flux of 11.46 (L/m^2hbar), which was 2.28 times as high as that of the NF membrane without MWCNTs-COOK. Moreover, the NF membrane also performed stable during the long-time filtration due to the improved structure and hydrophilicity of membrane.

In summary, the incorporation of carbon nanomaterials is an effective way to improve the Mg^{2+}/Li^+ separation efficiency of NF membrane. This work opens a simple and effective pathway for accelerating Li^+ enrichment and Mg^{2+} removal, which has great potential for lithium extraction application from salt-lake brines that loaded with high concentration of Mg^{2+}

CONTENTS

Chapter 1

General introduction

1 General introduction

1.1 Lithium resources and distribution

Lithium is the lightest metal element and has been proven to possess several excellent characteristics, such as extremely high electrochemical activity, high specific heat capacity, and a low thermal expansion coefficient [1-4]. Lithium metal and lithium compounds have been widely applied in commercial fields due to their excellent physical and chemical properties, and the demand for lithium has rapidly accelerated in recent years [4-7]. According to the current data of global lithium resources in the end-use market surveyed by the United States Geological Survey [8], following is the 2019 distribution of lithium consumption: batteries (65%); ceramics and glass (18%); lubricating greases (5%); polymer production (3%); continuous casting mold flux powders (3%); air treatment (1%); and other uses (5%). The total global demand for lithium resources has recently increased owing to the rapid economic and technological development. The battery industry consumes the largest share of global lithium resource. Batteries, including rechargeable and non-rechargeable batteries, are widely used in devices such as portable electronic devices and electrical tools. The rapid development of the electric vehicle industry and increasing use of portable electronic equipment have led to increased annual lithium resource consumption for applications in rechargeable lithium batteries. For example, the global end-use production for batteries increased from 23% in 2009 to 65% in 2019 [8, 9]. The global lithium consumption in 2019 was estimated to be 57,700 tons, which is an 18% increase from 49,100 tons in 2018 [8, 10]. Compared with fossil fuel vehicles, electric vehicles that use rechargeable lithium batteries have lower operating costs [6], and do not emit pollutants into the atmosphere. The global popularity of electric vehicles and reduction in the number of fossil fuel vehicles will effectively reduce greenhouse gases, which is an important environmental concern and lead towards a low-carbon energy future. The United Kingdom and France announced that the sale of all gasoline and diesel vehicles will be banned by 2040 [6].

Fossil fuels are depleting non-renewable energy resources that are increasingly difficult to mine. The extraction of renewable green-energy lithium resources is, therefore, critical for a sustainable development of the global economy and technology.

Global identified lithium resources reached 80 million tons (Mt) in 2019 and are mainly distributed in the United States (6.8 Mt), Bolivia (21 Mt), Argentina (17 Mt), Chile (9 Mt), Australia (6.3 Mt), China (4.5 Mt), Congo (Kinshasa) (3 Mt), and Germany (2.5 Mt) [8]. Lithium does not exist in pure metal form in nature; its single outer-shell valence electron is easily lost to form compounds, particularly with oxygen [6]. The global lithium reserves were about 17 Mt in 2019. Lithium resources are usually found in brines, seawater, clays and ores [11-14]. Previous studies on the geographical distribution of global lithium resources have reported that, ~61.8% of verified lithium resources exist in brines, 25% in minerals [5, 6], and ~59% in continental brines [15]. Lithium extraction from salt-lake brines is cost-effective and relatively simple to operate, compared to traditional ore extraction [16-18]. Lithium-bearing mineral deposits offer a means to supplement lithium production from brines, which can alleviate concerns regarding future lithium shortages. Due to the resources and cost advantages, global lithium extraction is mostly based on salt-lake brines.

However, various ions (e.g., Mg^{2+}, Ca^{2+}, K^{+}, and Na^{+}) co-exist with Li^{+} in salt-lake brines, which are typically rich in Mg^{2+} [19-22]. To extract high-purity lithium products from salt-lake brines, it is necessary to separate lithium from other coexisting ions. Compared to other ions, Li^{+} and Mg^{2+} share a similar ionic hydration radius and chemical characteristics, which make it more difficult to separate them [16]. According to the Mg^{2+}/Li^{+} mass ratio, salt lake brines can be divided into low Mg^{2+}/Li^{+} salt lake brine, where $Mg^{2+}/Li^{+} < 8$, and high Mg^{2+}/Li^{+} salt lake brine, where $Mg^{2+}/Li^{+} > 8$ [23]. Lithium recovery is known to be easier in low Mg^{2+}/Li^{+} brines, due to the relatively high lithium content. However, an effective separation of Mg^{2+} and Li^{+} from high Mg^{2+}/Li^{+} brines is more difficult and must follow a strict process at higher relative cost [24, 25]. The Mg^{2+}/Li^{+} mass ratio exceeds 8 in many well-known salt-lake brines, and some values even reach tens to thousands, which poses substantial challenges for

extracting lithium resources from these salt lakes. To effectively recover lithium resources from salt-lake brines, it is, therefore, necessary to simplify the Mg^{2+} and Li^{+} separation process.

An increase in the global lithium resource consumption has also increased the cost of lithium products, thereby promoting rapid development of the lithium industry. In recent years, Mg^{2+}/Li^{+} separation technology has received increasing attention. Previous methods for separating Mg^{2+} and Li^{+} from salt-lake brines mainly include precipitation, solvent extraction, adsorption, electrodialysis, nanofiltration, and electrochemical techniques [14, 19, 20, 30, 31]. However, no universal extraction process exists for recovering lithium, because the process is typically designed according to the brine composition of the salt-lake brine, particularly the mass ratio of Mg^{2+}/Li^{+}.

1.2 Li^{+} recovery methods

1.2.1 Precipitation materials

Precipitation is a method that separates the target component from the solution by via a chemical reaction, and has been widely applied in large-scale industrial lithium extraction [18]. The extraction of lithium resources from salt lakes using traditional evaporative precipitation methods requires multiple steps [15, 32, 33]. Lithium-containing brine is first pumped from underground into a large open-air pond, and then concentrated by solar evaporation and wind to obtain an appropriate lithium concentration of ~6000ppm. The precipitation process is accompanied by continuous evaporation in successive evaporation ponds to remove various coexisting ions in the concentrated brine. Na^{+} and K^{+} can be removed by precipitation above each saturation point, and borate can be removed by solvent extraction using aliphatic alcohol. The residual Mg^{2+}, Ca^{2+}, and sulfate can be precipitated with lime $Ca(OH)_2$, Na_2CO_3, oxalate, and $BaCl_2$. According to the various precipitant materials used for extracting lithium resources, this process can be divided into carbonate precipitation, aluminate

precipitation, carbonization precipitation, boron (B), and Li co-operation [33-36], which can be summarized as two major types depending on the brine composition: associated ion precipitation and aluminum-based materials precipitate.

Traditional precipitation is common in industrial applications, and more suitable for extracting lithium from brines with low Mg^{2+}/Li^{+}. In recent years, these new precipitants have been shown to be able to separate Mg^{2+} and Li^{+} in brines with high Mg^{2+}/Li^{+}, but consume a range of chemicals and produce extensive sludge. When extracting lithium from salt-lake brines, it is necessary to comprehensively develop and use other mineral resources in the salt-lake to reduce the production cost of lithium salt products. To sustainably develop lithium resources from salt-lake brines, it is necessary to develop some novel cost-effective and environmentally friendly precipitants.

1.2.2 Adsorption extraction materials

Adsorption is an effective and promising approach for the selective extraction of lithium resources from salt-lake brines with high Mg^{2+}/Li^{+}, and has the advantages of simplicity and environmental cleanliness [37, 38]. During extraction, Li^{+} is captured by an adsorbent with high Li^{+} selectivity and desorbed by some solvents, thereby separating Li^{+} from other coexisting ions [39]. The key to this method identifying excellent adsorption materials with high Li^{+} selectivity, high adsorption capacity, and reasonable operation stability. Adsorbents can be summarized into two major categories: containing inorganic and organic adsorption materials.

The inorganic ion adsorption method mainly relies on the unique memory effect and selectivity of inorganic ion adsorbents for Li^{+}. Inorganic adsorbents mainly include aluminum salt adsorbent, natural ore and carbon materials, and lithium ion sieve. A lithium ion sieve is an adsorbent with Li^{+} memory that can be used to extract lithium from salt lake or seawater. The precursor is first formed by introducing target Li^{+} into the inorganic compound. Li^{+} is then extracted from the precursor by the eluent without changing the crystal structure of the precursor, thereby obtaining a lithium ion sieve adsorbent with a pore structure matched with that of Li^{+} [40,41]. The formed vacant

crystal sites can hold ions that possess a smaller or equal radius of the target Li^+ [42]. Li^+ has the smallest ionic radius compared to other metal ions [41], which is why the lithium ion sieve selectively adsorbs Li^+ selectively and is a key to the adsorption process. Lithium ion sieves can be divided into two categories depending on their chemistry: lithium manganese oxide (Li-Mn-O) type and lithium titanium oxide (Li-Ti-O) type. Compared to the Li-Ti-O type lithium ion sieves, Li-Mn-O type lithium ion sieves exhibit higher lithium selectivity and adsorption capacity, as well as excellent regeneration properties [41]. However, the Li-Mn-O type lithium ion sieve faces the fatal problem of manganese dissolution during desorption, which can lead to severe water pollution, and therefore, restrict its development [38]. Both Li-Mn-O type lithium ion sieve and Li-Ti-O type lithium ion sieve also suffer from dissolution loss. Although titanium compounds are harmless to water environments [40], dissolution loss decreases the adsorption capacity of the ion sieve. In summary, Li-Ti-O and Li-Mn-O type lithium ion sieves have their advantages and disadvantages, and more efforts must be made to overcome the shortcomings.

Lithium ion sieve adsorbents are mostly in powder form, with poor fluidity and permeability. The fatal problem of dissolution loss during adsorption-desorption increases with the use of lithium ion sieves and can cause harm to the water environment. A small amount of the core framework of an ion sieve can also be dissolved during the acid treatment, resulting adsorbent loss. To avoid dissolution of the powder ionic sieves, the use of suitable adhesive materials to form lithium ion sieve composites while not reducing the lithium adsorption performance of the ion sieves is extremely important to promote their industrial application.

Organic adsorbents can be synthesized by chemically bounded organic ligand which can specifically coordinate Li^+ with various substrates, such as particles, fibers, and porous materials. The commonly used ligand crown ethers are macrocyclic polyethers containing multiple C-O-C structural units which can form complexes with cations, especially alkali metal ions. Owing to the macrocyclic effects, the cavities of 12-crown-4-ether can coordinate with Li^+ due to the appropriate size match [43,44].

Organic adsorption materials with imprinting effects similar to those of ion sieve, preserve the memory of lithium, and have a high lithium adsorption specificity. However, the organic ligands of crown ethers and calixarene face the problems of difficulty during synthesis and poor solubility in solution. Phosphate ligands must be synergistic with ferric chloride during lithium extraction. Thus, novel organic ligands and substrates must be explored for the urgently needed development of organic adsorption materials.

The special memory effect on Li^+ is beneficial to improve the Li^+ selectivity of lithium ion sieves, thereby achieving high Li^+ adsorption capacity with environmentally friendly performance. However, drawbacks such as harsh synthesis demand and high adsorbent dissolution limit its application in large-scale industries. The optimization of synthesis methods and exploration of novel preparation approaches are, therefore, effective for controlling the crystal form of lithium ion sieves. Making ion sieves into different composite forms (e.g., membrane, foam, magnetization fiber, and granulation) can reduce the dissolution of ion sieves and improve their stability, while simultaneously reducing the adsorption capacity. Further exploration of lithium ion sieves must still focus on the design and synthesis of new ligands with great adsorption capacity, high selectivity, long-time stability, and easy synthesis and elution. The chemical bonding of a lithium ion sieve to the substrate with a suitable structure and morphology effectively prepares a lithium ion sieve adsorbent composite with excellent lithium extraction performance.

1.2.3 Solvent extraction materials

Solvent extraction uses the difference in partition coefficients of Li^+ between the liquid and organic phases to achieve purification or concentration of lithium resources. The solvent extraction method performs excellently in extracting lithium from brines with a high Mg^{2+}/Li^+ mass ratio. Due to the advantages of low cost, simplicity and high efficiency, solvent extraction offers good prospects in industrial applications. However, the fatal drawbacks of this method, including solvent dissolution and corrosiveness to

equipment, limit its industrial application. The key to this method is the selected extractant materials, which can be divided into several categories: crown ether system extractants, β-diketone system extractants, organophosphorus system extractants, and ion liquid system extractants.

According to several previous studies, crown-ether-type extractants can achieve Li^+ extraction, however, with weak the selective Li^+ affinity. High Li^+ extraction efficiency using crown-ether-type extractants remains difficult, especially for brines with high Mg^{2+}/Li^+. In terms of commercial applications, the synthesis process of crown ethers is complicated and expensive, which makes it difficult for industrial applications. Further exploration of chemical mechanisms and extensive in-depth studies are urgently needed for industrial applications.

Ionic liquids are novel environmentally friendly liquid melting salt solvent composed of anions and cations that exhibit remarkable performance properties, such as high thermal stability, low volatility, low saturated vapor pressure, tunable viscosity, and nonflammability [45,46]. Compared to organic solvent systems, ion liquid systems exhibit different extraction properties due to their polyfunctionality, asymmetry, flexibility, and large ionic size of in the liquid structure [47]. Ion liquid systems have recently been recognized as a promising alternative to traditional organic solvent systems.

The Li^+ extraction ability and back-extraction effect of ionic liquids can be improved by introducing functional groups that can coordinate with Li^+ in the ionic liquid structure. As a green medium that replaces conventional extractants, ionic liquids have excellent selectivity and extraction efficiency for lithium, and can avoid environmental pollution problems caused by organic solvents when using conventional solvent extraction methods. However, the high cost and large molecular weight of the functionalized ionic liquid can result in a higher viscosity of the extraction system, which is not conducive to operations and mass transfer during extraction. It is, therefore, urgent to develop novel functional ionic liquids with high extraction capacity and selectivity.

Liquid extractant is an effective separation approach that can achieve Li^+ extraction from brines with high Mg^{2+}/Li^+ and the resulting lithium product can reach high purity. However, from industrial viewpoint, the equipment must possess high solvent resistance due to the leakage of organic solvents. Note that the fatal problem of extractant loss can be prevented by applying a supported liquid membrane, which is in line with the environmentally friendly requirement in industrial application. However, few related studies have been reported, and thus, more in-depth studies must be conducted in the future for further developments in industrial applications. From an industrial viewpoint, extractants with high selective extraction ability, low cost and stable structure are the core for an ideal solvent extraction technique.

1.2.4 Electrodialysis technology

Electrodialysis (ED) is a dialysis phenomenon without phase inversion [48], in which charged ions in solution migrate through the ion-exchange membrane under an applied electric field [40, 50]. In the presence of an electric potential difference, cations and anions can directionally migrate through the selective ion-exchange membrane with ion-selective permeability, thereby separating and concentrating ions. During the migration process [51], cations migrate toward the cathode, while anions migrate toward the anode. Cations can easily pass through the negatively charged cation-exchange membrane, while anions can easily pass through the positively charged anion-exchange membrane. However, cations and anions will be rejected by positively and negatively charged cation-exchange membrane, respectively. Monovalent selective ion exchange membranes were demonstrated to have high selective permeability for monovalent ions, which can be applied to separate monovalent and divalent/ multivalent ions [52, 53]. The application of ED ion-exchange membranes in the separation of Mg^{2+}/Li^+ has been rapidly developed.

Lithium in brine can be effectively enriched by the ED technique, which is an alternative and promising method for lithium recovery from brines with high Mg^{2+}/Li^+. Lithium recovery rate can also be further improved by integrating ED with other

techniques or materials that are selective for lithium. Although the ED process is technically feasible and performs well during lithium extraction, the reduction of capital and operating costs remains a major challenge for industrial applications. Membranes play an important role in the ED process, whereas high concentration polarization greatly decreases the membrane separation capability, thus limiting the application of ED technology in industry [54]. From an economic and environmental protection perspective, the development of durable membranes with highly selective permeability for monovalent Li^+ cations are urgent needed. This novel electrochemical technique presents a promising and competitive prospect for lithium extraction fields. Further optimizations should focus on: (1) exploring electrode materials with a stable structure to obtain a good balance between extraction capacity and long-time stability; (2) designing an electrochemical cell that is suitable for applications using real brine; and (3) adjusting the extraction process to achieve high efficiency.

1.2.5 Electrochemical technology

Electrochemical methods are another novel environmentally friendly and energy-efficient technique proposed for lithium extraction, which refers to the insertion and extraction of lithium in lithium-ion batteries through controlled potential [55]. Various adsorption materials have been exploited as electrodes, and the insertion or extraction of Li^+ can be controlled by applying electric field. Compared to the traditional lithium ion sieve, the fatal problem of adsorbent dissolution during the Li^+ extraction process can be largely avoided using this electrochemical process. The co-existence ions in brine seriously affect the lithium extraction efficiency, and thus, electrode materials with high lithium selectivity are the key to improving the lithium extraction rate. Common electrode materials currently used for lithium extraction can be mainly divided into two types: lithium iron phosphate (LFP) type and LMO type.

The electrochemical method clearly offers promising prospects for lithium recovery from salt lake brines or seawater due to the simple operation, low energy cost, high efficiency, and environmental friendliness. However, there remain some

shortcomings that limit its commercial application. The composition of salt-lake brine is complex and variable. For example, in different regions, the composition of various anions and cations in brines may differ [56]. In these electrochemical lithium extraction systems, due to the influence of coexisting ions, the kinetics of Li^+ diffusion at the interface of the electrode brine and electrode material nanopores are also very different, which directly affect the lithium extraction rate. It is still remains difficult to achieve large-scale production and preparation of high-efficiency lithium electrode materials, as well as the assembly of electrolytic cells in large-scale lithium extraction operations [57]. To resolve these limitations, considerable work is still required to realize industrial applications, including electrode materials, electrochemical cell equipment, and extraction process.

1.2.6 NF membrane technology

There is no general extraction process for recovering lithium from different brines because the process of extracting lithium for each salt-lake brine is composition-specific, especially regarding the mass ratio of Mg^{2+}/Li^+. Due to its specific characteristics, NF membrane has outstanding performance for water treatment. The pore size of the charged NF membrane is less than 2 nm, making it the popular choice for separating divalent and monovalent ions, which is promising for lithium enrichment during lithium extraction. Note that, NF membrane separation techniques show excellent separation performance among several traditional approaches. NF membrane techniques with low consumption cost and simple operation processes offer high prospects for separating Mg^{2+} and Li^+. Especially in brines with high Mg^{2+}/Li^+, positively charged NF membranes show high selectivity during Mg^{2+} and Li^+ separation. For industrial applications, an optimization of the membrane structure and chemical composition is necessary to ensure highly selective separation, anti-pollution, and long-term stable performance.

1.3. Mg^{2+}/Li^{+} separation with NF membrane

1.3.1 NF membrane separation technology

NF membranes possess nanopores less than 2 nm and are used in the membrane separation technology driven by low pressure [58, 59]. The NF membrane surface usually exhibits chargeability because the ionizable groups dissociate from the membrane surface or pores. During the filtration process, electrostatic interactions between the membrane and ions can directly affect the mass transfer of ions [60-62]. Ions with higher hydration energy or larger ion radius in the solution are more likely to be trapped by the membrane [29, 54]. Owing to its special pore size and charge ability, the rejection of multivalent ions by an NF membrane is higher than that of monovalent ions.

NF membrane is commonly composed of the substrate membrane and selective thin polyamide layer. The dual-effect of membrane chargeability and structure determines the separation capacity of divalent and monovalent ions. The current NF membrane fabricated method mainly contains phase inversion, dip-coating process, interfacial polymerization, and layer-by-layer self-assembly [58]. Interfacial polymerization is the most widely used method in which a polymerization reaction occurs at the interface of mutually incompatible solvents to form an active functional selective thin layer.

Several parameters during the interface polymerization process, such as concentration of aqueous and organic phase monomers, reaction temperature, and reaction time, can direct determine the formation and properties (e.g. chargeability, thickness, pore size and surface morphology) of the formed polyamide layer. The lower the polymerization temperature, the slower the monomer diffusion, the milder the reaction, and the thinner polyamide layer can be obtained. Small-molecule amine monomers, such as piperazine (PIP) and m-phenylenediamine (MPD), have high reactivity, and their solubility in n-hexane solution is also large, which can quickly crosslink with organic phase monomers and form a thick and dense polyamide layer.

However, macromolecular amine monomers, such as polyethyleneimine (PEI), will diffuse slowly during the interfacial polymerization process due to the primary steric hindrance effect, contributing to a relatively loose and thin polyamide layer. Therefore, choosing different amine monomers or adding nanomaterials can note only control the diffusion rate and uniformity of the aqueous monomers, but also can effectively regulate the structure and properties of the formed polyamide layer and the obtained NF membrane [63].

Embedding the inorganic nanomaterials into the monomer solution will not only change the crosslink reaction during the interfacial polymerization process and improve the permeability of the final NF membrane. On the other hand, some inorganic nanoparticles have inherent low-resistance water channels, and the inter-gap between the inorganic nanoparticles and the polymer interface, can further increases the permeability of the NF membrane.

It is also worth noting that the substrate membrane can not only support the polyamide layer, but also affect the formation process of the active polyamide layer. During the process of interfacial polymerization, the pore size, hydrophilicity/hydrophobicity, and chargeability of the substrate membrane can directly affect the distribution of the aqueous monomer, thereby affecting the properties (e.g. thickness, pore size, morphology and chargeability) of the formed polyamide layer and the final NF membrane.

1.3.2 Mg^{2+}/Li^{+} separation research and difficulty

The synthesis effect of steric hindrance and Donnan exclusion make NF membrane a promising approach for enriching high purity Li^{+}. For separating Mg^{2+} and Li^{+} with similar hydrate radius of 0.428 nm and 0.382 nm, respectively, it is difficult to achieve high separation capacity by only adjusting pore size of membrane. In this case, electrostatic interaction between ions and membrane is crucial for separating ions with similar size but different chargeability. Charged NF membranes can be divided into positively and negatively charged membranes, the latter of which are more commonly

used for commercial purpose. Several commercial NF membranes have been tested to explore their feasibility for lithium separation, such as commercial NF membrane NF90 [29], Desal-5 DL [64], and DK-1812 [62]. Somorani et al. applied the commercial NF membrane NF90 and low-pressure reverse osmosis (LPRO) membrane to investigate the separation performance of lithium in the diluted Chott Djerid (Tunisia) brine [29]. The results showed that membrane NF90 is more suitable for lithium extraction from brine, due to its higher hydraulic permeability to water. The membrane NF90 showed 100% rejection of Mg^{2+} in the first separation step of the diluted brine, where the concentrations of Mg^{2+}, Li^{+}, and Na^{+} were ~0.30, 8.0, and 0.006 g/L, respectively. In the next step, NF90 showed difficulty in effectively separating Li^{+} in the presence of Na^{+}. However, after filtering the diluted brine for 6h, the membrane's performance was reduced by 50% due to membrane fouling. To improve the long-term stability of the membrane performance in industrial applications, the anti-fouling property must be improved in further studies. Some additional factors can directly affect the separation efficiency during the separation process, including operation pressure, Mg^{2+}/Li^{+} mass ratio, feed solution concentration, and the existence of other ions during the separation process [60-62]. A commercial Desal (DL) NF membrane was adopted to extract lithium from simulated East and West Taijiner brine with high Mg^{2+}/Li^{+} [60]. The results indicated that increased operation pressure and lower pH can have a positive effect on the separation performance. However, increased feed temperature and Mg^{2+}/Li^{+} can negatively impact the separation efficiency.

Commercial NF membranes usually exhibit negative chargeability and are not a preferred way of selectively separating Li^{+} and Mg^{2+}. The separation mechanism of NF membrane is dominated by the Donnan exclusion effect and steric hindrance effect [65]. Li^{+} and Mg^{2+} have a hydrate ion radius difference of less than 0.1nm, and thus, the selective separation performance is dominated by the Donnan exclusion effect during filtration. There is a stronger exclusion effect between a positively charged NF membrane and Mg^{2+} compared with Li^{+}, because Mg^{2+} carries more charge than monovalent Li^{+}. Therefore, for separating Mg^{2+} and Li^{+}, a positively charged NF

membrane is a preferred choice. The separation factor $S_{Mg,Li}$ can be calculated to evaluate the selective rejection of NF membrane for Mg^{2+} and Li^{+}:

$$S_{\mathrm{Mg,Li}} = \frac{C_{Mg,p}/C_{Li,p}}{C_{Mg,f}/C_{Lif}} \quad (13)$$

Where $C_{Mg,p}$ and $C_{Mg,f}$ represent the concentrations of Mg^{2+} in the permeate and feed solution, respectively, and the same applies to $C_{Li,p}$ and $C_{Li,f}$. When $S_{Mg,Li}$ <1, this indicates that Mg^{2+} and Li^{+} can be separated. Lower $S_{Mg,Li}$ values are associated with improved separation efficiency.

To improve the Mg^{2+}/Li^{+} separation performance of NF membranes, Li et al. prepared a hollow positively charged NF membrane via interfacial polymerization between 1,4-bis(3-aminopropyl) piperazine and trimesoyl chloride (TMC) on the PAN substrate membrane [65]. After filtration of the simulated brine at a pressure of 3 bar, the Mg^{2+}/Li^{+} mass ratio decreased from an initial value of 20 to 7.7 with a separation factor $S_{Mg,Li}$ of 0.38. Li et al. reported another positively charged NF membrane with a high separation ability for Mg^{2+} and Li^{+}. The membrane was fabricated by interfacial polymerization between branched poly(ethylene imine) and TMC on a crosslinked polyetherimide substrate membrane, which was then modified with ethylenediaminetetraacetic acid [25]. After filtration of the simulated brine with a Mg^{2+}/Li^{+} of 24 at 10 bar and pH near 5.5, the separation factor $S_{Mg,Li}$ and flux were ~ 0.1 and 6.0 L/(m^2h), respectively.

By regulating the preparation conditions during interfacial polymerization between polyethyleneimine and TMC on the PES support membrane, Xu et al. fabricated a high positively charged NF membrane with excellent Mg^{2+} and Li^{+} selective separation performance [59]. The results showed that the rejection difference between Mg^{2+} and Li^{+} reached up to 76%, and the permeation flux was ~5.02 L/(m^2hbar). Guo et al. fabricated a novel double-Janus composite NF membrane [66]. The middle layer of the composite membrane exhibited negative chargeability and the surface layer showed opposite chargeability, which is helpful for rejecting Mg^{2+} by the surface layer and attracting Li^{+} by the middle layer. The Janus composite NF membrane possessed excellent selective separation properties for the simulated brines with high

Mg^{2+}/Li^{+}. $S_{Mg,Li}$ reached 0.08 and 0.17 after filtering a simulated brine with Mg^{2+}/Li^{+} of 30 and 60, respectively. According to the research by Zhang et al., the modification of multi-walled carbon nanotubes was achieved by grafting piperazine, and then mixing it with an aqueous solution during the interfacial polymerization process to obtain an NF membrane with high permeability [67]. After the filtration experiments, $S_{Mg,Li}$ was ~0.06 and the permeation flux reached up to 14.0 L/(m^2hbar), which shows promising selectively separation prosperities. A novel NF membrane was recently investigated by doping water-soluble polyhydroxylated fullerene onto a polyamide layer during the polymerization process between PIP and TMC on the PES base membrane [68]. Note that the water permeation of the membranes increased by 39.2%, and the membrane showed high anti-fouling properties.

Owing to the low energy consumption, simple operation process and high separation ability, NF membranes offer a promising approach for Mg^{2+}/Li^{+} separation in brines with high Mg^{2+}/Li^{+}. However, due to the trade-off effect, their use still faces difficulty in achieving both high separation performance and high permeation flux, which directly hinder the achievement of a higher lithium extraction efficiency. In addition, due to membrane fouling, both the separation performance and permeation flux of NF membranes directly decrease after long-time filtration processes. Therefore, considerable work requires to be conducted to develop novel anti-fouling NF membranes with both high separation ability and permeability.

1.4 Purposes and significances of research

Due to the existence of the “trade-off” effect, it is hard to simultaneously control both high separation ability and permeability of the NF membrane. The low permeation flux of NF membrane may significantly limit its work efficiency and practical applications. To improve the lithium recovery rates in industrial applications, further developments and optimization for separating materials should be carried out from the perspective of high separation selectivity, stability, low cost, and environmental friendliness.

It is well known that the morphological structure of the membranes can be substantially changed after introducing nano-additives with special characteristics to improve the membrane properties, such as mechanical behavior, hydrophilicity, separation ability, and anti-fouling performance. During the synthesis process, carbon-based nano-additives, such as carbon nanotube (CNT) and its derivatives as well as graphene oxide (GO) and its derivatives, have emerged as a promising alternative to improve the permeation flux of the NF membrane. After doping with such additives, the final membrane is endowed with superior properties of both polymer materials and carbon-based nanomaterials. Due to the unique structure and large quantities of oxygen-bearing functional groups (e.g., carboxyl, epoxy, and hydroxyl) at the edge of the GO nanosheet, the incorporated GO additives can optimize the properties of membrane (e.g., mechanical, antifouling, and hydrophilicity). Importantly, the nanomaterial CNTs have special smooth cylindrical nanostructure, large specific surface area, high biocidal and antioxidant ability, and high thermal and mechanical characteristics, which make it attractive in membrane optimization. In addition, the hollow structure of CNTs and inter-gaps between CNTs and polymer matrix can provide more nano-channels for water to pass through the membrane, which can greatly enhance the permeate flux of the membrane.

The purpose of this work is to develop the novel composite NF membrane which can effectively and quickly separate Li^+ and the co-existence Mg^{2+}, achieving high lithium recovery rate from salt-lake brines. For future research, it will be valuable to combine the advantages of the carbon nano-materials to fabricate lithium extraction NF membranes with high Mg^{2+}/Li^+ separation ability and efficiency.

1.5 Outline of dissertation

Most of the research on the modification of Mg^{2+}/Li^+ separation performance is mainly focused on the selective thin polyamide layer of NF membrane. Importantly, the structure and property of substrate membrane can directly affect the formation of the polyamide layer during interfacial polymerization. However, there are few reports focus

on the optimizing properties of the NF membrane by adjusting the substrate membrane. In this work, we have designed and constructed four novel NF membrane system from the perspective of regulating the substrate membrane and polyamide layer with the help of carbon nano-additives. This dissertation is organized to summarize carbon nanomaterials modified NF membrane and Mg^{2+}/Li^{+} separation performance by six chapters.

In chapter 1, an overview of global lithium resources and distribution, commonly used lithium retraction methods, and research status and difficulties of Mg^{2+}/Li^{+} separation using NF membrane has been presented.

In chapter 2, we proposed a new approach to optimize the NF membrane performance by regulating the substrate. From the perspective of optimizing the substrate film, we modified polyethersulfone (PES) ultrafiltration substrate membrane with GO nano-additives to improve the mechanism and hydrophilicity performance, followed with interfacial polymerization between PEI and TMC. Several analyze methods were applied to explore the chemical composition, microstructure, separation performance, etc. of the obtained composite membranes. In addition, the synergy effects of GO loading concentration on substrate membrane and polyamide layer were comprehensively studied.

In chapter 3, we embedded graphene oxide quantum dots (GQDs-NH_2) into the aqueous phase during polymerization to prepare a novel GQDs-NH_2 incorporated NF membrane with high Mg^{2+}/Li^{+} separation efficiency. By grafting amine groups (-NH_2) at the edge of GQDs, the obtained GQDs-NH_2 can not only inherit the advantage of GQDs but also carry some amine groups (-NH_2). The structure and properties of NF membranes with different incorporating content of GQDs-NH_2 were analyzed by several characterization methods. In addition, the effect of doped GQDs-NH_2 on the Mg^{2+}/Li^{+} separation capability, permeation efficiency and antifouling performance of the final NF membrane was extensively discussed.

In chapter 4, we first proposed an easy-to-operate and environmentally friendly functionalization method to synthesize a new class of potassium carboxylate

functionalized multi-wall CNTs (MWCNTs-COOK) with high hydrophilicity. Then, we designed a new class of positively charged NF membrane with high permeate flux for effectively enriching Li^+ and separating Mg^{2+}. The prepared MWCNTs-COOK were synthesized as nano-additives to regulate the interfacial polymerization process between PEI and TMC on the ultrafiltration substrate, thereby fine-tuning the microstructure and optimizing the performance of the final NF membrane. How the MWCNTs-COOK nano-additives improve the Li^+/Mg^{2+} separation efficiency of NF membrane was comprehensively investigated and evaluated from multiple aspects (e.g., morphology, structure, surface properties, and rejection ability) by using various characterization methods.

In chapter 5, On the fourth membrane system, we designed another novel NF membrane by anchoring the nano-additives MWCNTs-COOK into PES ultrafiltration substrate. The MWCNTs-COOK grown in PES substrate can work as a "connector" and influence the formation of polyamide layer. We have systematically studied and discussed how the loaded MWCNTs-COOK alter the final NF membrane from many aspects, including microstructure, chemical composition, surface properties and Mg^{2+}/Li^+ separation efficiency.

In chapter 6, a summary of this work and conclusions were presented.

References

[1] L.A. Gil-Alana, M. Monge. Lithium: Production and estimated consumption. Evidence of persistence, Resources Policy. 60 (2019)198-202.

[2] G. Martin, L. Rentsch, M. Höck, M. Bertau. Lithium market research – global supply, future demand and price development, Energy Storage Materials. 6 (2017) 171-179.

[3] D. Liu, X. Gao, H. An, Y. Qi, X. Sun, Z. Wang, Z. Chen, F. An, N. Jia. Supply and demand response trends of lithium resources driven by the demand of emerging renewable energy technologies in China, Resources, Conservation and Recycling. 145 (2019) 311-321.

[4] P. Maxwell. Transparent and opaque pricing: The interesting case of lithium,

Resources Policy. 45 (2015) 92-97.

[5] C. Grosjean, P.H. Miranda, M. Perrin, P. Poggi. Assessment of world lithium resources and consequences of their geographic distribution on the expected development of the electric vehicle industry, Renewable and Sustainable Energy Reviews. 16 (2012) 1735-1744.

[6] L. Kavanagh, J. Keohane, G. Garcia Cabellos, A. Lloyd, J. Cleary. Global lithium sources—industrial use and future in the electric vehicle Industry: A review, Resources. 7 (2018) 57.

[7] X. Sun, H. Hao, F. Zhao, Z. Liu. Tracing global lithium flow: A trade-linked material flow analysis, Resources, Conservation and Recycling. 124 (2017) 50-61.

[8] U.S. Geological Survey (2020) Mineral Commodity Summaries 2020, U.S. Geological Survey

[9] U.S. Geological Survey (2010) Mineral Commodity Summaries 2010, U.S. Geological Survey

[10] U.S. Geological Survey (2019) Mineral Commodity Summaries 2019, U.S. Geological Survey

[11] X. Li, Y. Mo, W. Qing, S. Shao, C.Y. Tang, J. Li. Membrane-based technologies for lithium recovery from water lithium resources: A review, Journal of Membrane Science. 591 (2019) 117317.

[12] T. Nguyen, M. Lee. A review on the separation of lithium ion from leach liquors of primary and secondary resources by solvent extraction with commercial extractants, Processes. 6 (2018) 55.

[13] P. Loganathan, G. Naidu, S. Vigneswaran. Mining valuable minerals from seawater: a critical review, Environmental Science: Water Research & Technology. 3 (2017) 37-53.

[14] N. Linneen, R. Bhave, D. Woerner. Purification of industrial grade lithium chloride for the recovery of high purity battery grade lithium carbonate, Separation and Purification Technology. 214 (2019) 168-173.

[15] B. Swain. Recovery and recycling of lithium: A review, Separation and Purification

Technology. 172 (2017) 388-403.

[16] X. Zhao, H. Yang, Y. Wang, Z. Sha. Review on the electrochemical extraction of lithium from seawater/brine, Journal of Electroanalytical Chemistry. 850 (2019) 113389.

[17] U. Bardi. Extracting minerals from seawater: an Energy analysis, Sustainability. 2 (2010) 980-992.

[18] Y. Zhang, Y. Hu, N. Sun, S.A. Khoso, L. Wang, W. Sun. A novel precipitant for separating lithium from magnesium in high Mg/Li ratio brine, Hydrometallurgy. 187 (2019) 125-133.

[19] G. Liu, Z. Zhao, L. He Highly selective lithium recovery from high Mg/Li ratio brines, Desalination. 474 (2020) 114185.

[20] J.F. Song, L.D. Nghiem, X.-M. Li, T. He. Lithium extraction from Chinese salt-lake brines: opportunities, challenges, and future outlook, Environmental Science: Water Research & Technology. 3 (2017) 593-597.

[21] X. Guo, S. Hu, C. Wang, H. Duan, X. Xiang. Highly efficient separation of magnesium and lithium and high-valued utilization of magnesium from salt lake brine by a reaction-coupled separation technology, Industrial & Engineering Chemistry Research. 57 (2018) 6618-6626.

[22] X. Liu, X. Chen, L. He, Z. Zhao. Study on extraction of lithium from salt lake brine by membrane electrolysis, Desalination. 376 (2015) 35-40.

[23] Z.-Y. Guo, Z.-Y. Ji, Q.-B. Chen, J. Liu, Y.-Y. Zhao, F. Li, Z.-Y. Liu, J.-S. Yuan. Prefractionation of LiCl from concentrated seawater/salt lake brines by electrodialysis with monovalent selective ion exchange membranes, Journal of Cleaner Production. 193 (2018) 338-350.

[24] Z.-y. Ji, Q.-b. Chen, J.-s. Yuan, J. Liu, Y.-y. Zhao, W.-x. Feng. Preliminary study on recovering lithium from high Mg^{2+}/Li^{+} ratio brines by electrodialysis, Separation and Purification Technology. 172 (2017) 168-177.

[25] W. Li, C. Shi, A. Zhou, X. He, Y. Sun, J. Zhang. A positively charged composite nanofiltration membrane modified by EDTA for $LiCl/MgCl_2$ separation, Separation and

Purification Technology. 186 (2017) 233-242.
[26] L. Li, V.G. Deshmane, M.P. Paranthaman, R. Bhave, B.A. Moyer, S. Harrison. Lithium recovery from aqueous resources and batteries: A brief review, Johnson Matthey Technology Review. 62 (2018) 161-176.
[27] H. Vikström, S. Davidsson, M. Höök. Lithium availability and future production outlooks, Applied Energy. 110 (2013) 252-266.
[28] J.W. An, D.J. Kang, K.T. Tran, M.J. Kim, T. Lim, T. Tran. Recovery of lithium from Uyuni salar brine, Hydrometallurgy. 117-118 (2012) 64-70.
[29] A. Somrani, A.H. Hamzaoui, M. Pontie. Study on lithium separation from salt lake brines by nanofiltration (NF) and low pressure reverse osmosis (LPRO), Desalination. 317 (2013) 184-192.
[30] P.K. Choubey, M.-s. Kim, R.R. Srivastava, J.-c. Lee, J.-Y. Lee. Advance review on the exploitation of the prominent energy-storage element: Lithium. Part I: From mineral and brine resources, Minerals Engineering. 89 (2016) 119-137.
[31] P. Meshram, B.D. Pandey, T.R. Mankhand. Extraction of lithium from primary and secondary sources by pre-treatment, leaching and separation: A comprehensive review, Hydrometallurgy. 150 (2014) 192-208.
[32] V. Flexer, C.F. Baspineiro, C.I. Galli. Lithium recovery from brines: A vital raw material for green energies with a potential environmental impact in its mining and processing, Sci Total Environ. 639 (2018) 1188-1204.
[33] Y. Zhang, Y. Hu, L. Wang, W. Sun. Systematic review of lithium extraction from salt-lake brines via precipitation approaches, Minerals Engineering. 139 (2019) 105868.
[34] Z. Xu, H. Zhang, R. Wang, W. Gui, G. Liu, Y. Yang. Systemic and direct production of battery-grade lithium carbonate from a saline Lake, Industrial & Engineering Chemistry Research. 53 (2014) 16502-16507.
[35] X. Liu, M. Zhong, X. Chen, Z. Zhao. Separating lithium and magnesium in brine by aluminum-based materials, Hydrometallurgy. 176 (2018) 73-77.
[36] Y. Liu, T. Deng. Progresses on the process and technique of lithium recovery from salt Lake brines around the world, World Sci-tech R & D. 28 (2006) 69-75.

[37] L. Tian, W. Ma, M. Han. Adsorption behavior of Li^+ onto nano-lithium ion sieve from hybrid magnesium/lithium manganese oxide, Chemical Engineering Journal. 156 (2010) 134-140.

[38] H. Jiang, Y. Yang, S. Sun, J. Yu. Adsorption of lithium ions on lithium-aluminum hydroxides: Equilibrium and kinetics, The Canadian Journal of Chemical Engineering. 98 (2019) 544-555.

[39] F. Yang, S. Chen, C. Shi, F. Xue, X. Zhang, S. Ju, W. Xing. A Facile Synthesis of Hexagonal Spinel λ-MnO_2 Ion-Sieves for Highly Selective Li^+ Adsorption, Processes. 6 (2018) 59.

[40] G. Liu, Z. Zhao, A. Ghahreman. Novel approaches for lithium extraction from salt-lake brines: A review, Hydrometallurgy. 187 (2019) 81-100.

[41] X. Xu, Y. Chen, P. Wan, K. Gasem, K. Wang, T. He, H. Adidharma, M. Fan. Extraction of lithium with functionalized lithium ion-sieves, Progress in Materials Science. 84 (2016) 276-313.

[42] R. Marthi, Y.R. Smith. Selective recovery of lithium from the Great Salt Lake using lithium manganese oxide-diatomaceous earth composite, Hydrometallurgy. 186 (2019)115-125.

[43] D.K. Cabbiness, D.W. Margerum. Macrocyclic effect on the stability of copper(II) tetramine complexes, Journal of the American Chemical Society. 91 (1969) 6540-6541.

[44] H.K. Frensdorff. Stability constants of cyclic polyether complexes with univalent cations, Journal of the American Chemical Society. 93 (1971) 600-606.

[45] C. Shi, Y. Jing, Y. Jia. Solvent extraction of lithium ions by tri-n-butyl phosphate using a room temperature ionic liquid, Journal of Molecular Liquids. 215 (2016) 640-646.

[46] X. Wang, Y. Jing, H. Liu, Y. Yao, C. Shi, J. Xiao, S. Wang, Y. Jia. Extraction of lithium from salt lake brines by bis[(trifluoromethyl)sulfonyl]imide-based ionic liquids, Chemical Physics Letters. 707 (2018) 8-12.

[47] C. Shi, D. Duan, Y. Jia, Y. Jing. A highly efficient solvent system containing ionic liquid in tributyl phosphate for lithium ion extraction, Journal of Molecular Liquids.

200 (2014) 191-195.

[48] Y. Song, Z. Zhao. Recovery of lithium from spent lithium-ion batteries using precipitation and electrodialysis techniques, Separation and Purification Technology. 206 (2018) 335-342.

[49] Z.L. Ye, K. Ghyselbrecht, A. Monballiu, T. Rottiers, B. Sansen, L. Pinoy, B. Meesschaert. Fractionating magnesium ion from seawater for struvite recovery using electrodialysis with monovalent selective membranes, Chemosphere. 210 (2018) 867-876.

[50] N. Parsa, A. Moheb, A. Mehrabani-Zeinabad, M.A. Masigol. Recovery of lithium ions from sodium-contaminated lithium bromide solution by using electrodialysis process, Chemical Engineering Research and Design. 98 (2015) 81-88.

[51] S. Gmar, A. Chagnes Recent advances on electrodialysis for the recovery of lithium from primary and secondary resources, Hydrometallurgy. 189 (2019) 105124.

[52] Y. Kim, W.S. Walker, D.F. Lawler. Competitive separation of di- vs. mono-valent cations in electrodialysis: effects of the boundary layer properties, Water Res. 46 (2012) 2042-2056.

[53] Y. Zhang, S. Paepen, L. Pinoy, B. Meesschaert, B. Van der Bruggen. Selectrodialysis: fractionation of divalent ions from monovalent ions in a novel electrodialysis stack, Separation and Purification Technology. 88 (2012) 191-201.

[54] M. Pontié, A. Lhassani, C.K. Diawara, A. Elana, C. Innocent, D. Aureau, M. Rumeau, J.P. Croue, H. Buisson, P. Hemery. Seawater nanofiltration for the elaboration of usable salty waters, Desalination. 167 (2004) 347-355.

[55] H. Kanoh, K. Ooi, Y. Miyai, S. Katoh. Electrochemical recovery of lithium Ions in the aqueous phase, Separation Science and Technology. 28 (1993) 643-651.

[56] D.E. Garrett, Handbook of lithium and natural calcium chloride, Elsevier Science (2004).

[57] X.-J. Pan, Z.-H. Dou, D.-L. Meng, X.-X. Han, T.-A. Zhang. Electrochemical separation of magnesium from solutions of magnesium and lithium chloride. Hydrometallurgy 191 (2020) 105166.

[58] X.Q. Cheng, Y.L. Zhang, Z.X. Wang, Z.H. Guo, Y.P. Bai, L. Shao. Recent advances in polymeric solvent-resistant nanofiltration membranes, Advances in Polymer Technology. 33 (2014) n/a-n/a.

[59] P. Xu, W. Wang, X. Qian, H. Wang, C. Guo, N. Li, Z. Xu, K. Teng, Z. Wang. Positive charged PEI-TMC composite nanofiltration membrane for separation of Li^+ and Mg^{2+} from brine with high Mg^{2+}/Li^+ ratio, Desalination. 449 (2019) 57-68.

[60] S.-Y. Sun, L.-J. Cai, X.-Y. Nie, X. Song, J.-G. Yu. Separation of magnesium and lithium from brine using a Desal nanofiltration membrane, Journal of Water Process Engineering. 7 (2015) 210-217.

[61] Y. Gang, S. Hong, W. Liu, X. Weihong, X. Nanping. Investigation of Mg^{2+}/Li^+ separation by nanofiltration, Chinese Journal of Chemical Engineering. 19 (2011) 586-591.

[62] Q. Bi, Z. Zhang, C. Zhao, Z. Tao. Study on the recovery of lithium from high Mg^{2+}/Li^+ ratio brine by nanofiltration, Water Sci Technol. 70 (2014) 1690-1694.

[63] Q.-H. Zhang, S.-P. Li, S.-Y. Sun, X.-S. Yin, J.-G. Yu. $LiMn_2O_4$ spinel direct synthesis and lithium ion selective adsorption, Chemical Engineering Science. 65 (2010) 169-173.

[64] X. Wen, P. Ma, C. Zhu, Q. He, X. Deng. Preliminary study on recovering lithium chloride from lithium-containing waters by nanofiltration, Separation and Purification Technology. 49 (2006) 230-236.

[65] X. Li, C. Zhang, S. Zhang, J. Li, B. He, Z. Cui. Preparation and characterization of positively charged polyamide composite nanofiltration hollow fiber membrane for lithium and magnesium separation, Desalination. 369 (2015) 26-36.

[66] C. Guo, N. Li, X. Qian, J. Shi, M. Jing, K. Teng, Z. Xu. Ultra-thin double Janus nanofiltration membrane for separation of Li^+ and Mg^{2+}: “drag” effect from carboxyl-containing negative interlayer, Separation and Purification Technology. 230 (2019) 115567

[67] H.-Z. Zhang, Z.-L. Xu, H. Ding, Y.-J. Tang. Positively charged capillary nanofiltration membrane with high rejection for Mg^{2+} and Ca^{2+} and good separation for

Mg^{2+} and Li^{+}, Desalination. 420 (2017) 158-166.

[68] Q. Shen, S.J. Xu, Z.L. Xu, H.Z. Zhang, Z.Q. Dong Novel thin-film nanocomposite membrane with water-soluble polyhydroxylated fullerene for the separation of Mg^{2+}/Li^{+} aqueous solution, Journal of Applied Polymer Science. 136 (2019) 48029.

Chapter 2

✵✵✵✵✵✵✵✵✵✵✵✵✵✵✵✵✵✵✵✵✵✵✵✵✵✵✵✵

“Bridge” graphene oxide modified positive charged nanofiltration thin membrane with high efficiency for Mg^{2+}/Li^{+} separation

✵✵✵✵✵✵✵✵✵✵✵✵✵✵✵✵✵✵✵✵✵✵✵✵✵✵✵✵

2 “Bridge” graphene oxide modified positive charged nanofiltration thin membrane with high efficiency for Mg^{2+}/Li^{+} separation

2.1 Introduction

Global lithium consumption in several industry fields has grown rapidly owing to the excellent characteristics of lithium[1]. Especially, the rapid development of the electric vehicle industry has led to a significant increase in the demand for green lithium resources[2, 3]. Global lithium resources are mainly distributed in ores and brines[4]. Due to the low consumption cost and great reserve (about 59%)[5], it has become a trend to extract lithium from continental brine resources. Co-existence ions, especially the diagonal element Mg^{2+}, limit the recovery purity for Li^{+}, which is caused by similar chemical characteristics and hydration ion size between Li^{+} and Mg^{2+}[6, 7]. It has been proved that many salt lakes in the world possess high mass ratio of Mg^{2+}/Li^{+}. However, the high Mg^{2+} concentration in salt-lake brine will make it more difficult to extract lithium. To separate Mg^{2+} and Li^{+}, several methods have been developed, including precipitation[8-10], solvent extraction[11-14], adsorption[15-18] and membrane separation[5, 7]. Traditional precipitation has been widely used for extracting lithium from salt lakes with low mass ratio of Mg^{2+}/Li^{+}. However, precipitation method requires several stages during the lithium extract process, which is extremely time-consuming and energy-consumption[5]. In addition, this method is not suitable for brines with high mass ratio of Mg^{2+}/Li^{+}[19]. As for solvent extraction and adsorption, both adsorbents and extractants present drawback of easily dissolved[2, 7], leading to reduced recovery efficiency and corrosion to equipment.

Membrane separation technique, an environment friendly approach for separating Mg^{2+} and Li^{+}, has drawn more attention in the field of lithium recovery. Nanofiltration

(NF) membranes with no chemical reaction during separation process have been proven to be a promising alternative for lithium extraction [7]. The low-pressure-driven NF membranes can separate monovalent and multivalent ions based on the combined effect of chargeability and unique pore radius of membranes. During the separation process, the separation property of NF membrane has been demonstrated to be determined by both Donnan exclusion effect and steric hindrance effect[20]. Normally, NF membranes possess a pore size less than 2 nm and molecular weight cut-off around 200~1000Da. Therefore, for separating Mg^{2+} and Li^{+} with similar hydrate radius of 0.428 nm and 0.382 nm, respectively, it is difficult to achieve high separation capacity by only adjusting pore size of membrane. In this case, electrostatic interaction between ions and membrane is crucial for separating ions with similar size but different chargeability.

According to the research conducted by Li et al. [20], they first demonstrated that the use of positively charged hollow NF membranes can greatly improve the separation ability of Mg^{2+}/Li^{+} compared with commercial negatively charged NF membrane. After that, another positively charged NF membrane was obtained by interfacial polymerization on the base membrane, which was then modified with ethylenediaminetetraacetic acid (EDTA) to improve the ability to remove Mg^{2+}[21]. The results showed that, compared with pure membrane without EDTA, the addition of divalent cationic chelator EDTA effectively enhanced the remove rate for Mg^{2+}. Guo et al. [22] explored a novel double Janus NF membrane with triple layered composed with carboxylated cellulose nanocrystal negative charged layer and positive charged polyamide layer, and showed a high separation ability for Mg^{2+} and Li^{+} in simulated brine with high Mg^{2+}/Li^{+} mass ratio. In previous study[23], a high positive charged membrane was successfully fabricated, which presented great Mg^{2+}/Li^{+} separation performance for brine with high Mg^{2+}/Li^{+} mass ratio. The resulting membrane showed a high rejection difference between Mg^{2+} and Li^{+} of 76%, while the low permeation flux limited the extraction efficiency for lithium. Zhang et al. [24] mixed piperazine (PIP) grafted hydroxyl-functionalized multi-walled carbon nanotubes (MWCNTs-OH) into polyamide layer of NF membrane, which significantly enhanced the permeation

flux of membrane, while the separation ability needs to be further improved. It is worth noting that, it is difficult to achieve both high separation capacity and high flux due to the "trade-off" effect, which limits the work efficiency and application of NF membrane[20]. In recent years, researches on Mg^{2+} and Li^{+} separation using NF membranes are still scarce, and most studies have focused on modification for polyamide layer, while there is no report on optimizing substrate membranes.

Graphene oxide (GO), a single-atom nanosheet with oxygen-rich functional groups, displays excellent hydrophilicity, mechanical stability, pollution resistance[25-27]. Currently, GO has become a popular material in the field of desalination and water purification membrane[28-32]. Choi et al. coated multi GO layers on polyamide layer of NF membrane by layer-by-layer deposition, thereby increased the hydrophilicity and anti-fouling of final NF membranes[33]. Nan et al. [34] formed a positive charged NF membrane via layer-by-layer assemble between GO and polyethyleneimine (PEI), the crosslink layers of GO and PEI displayed a high separation ability between divalent cations Mg^{2+} and monovalent cations Na^{+}. To improve the hydrophilicity of membrane, Yin et al. [35] incorporated GO into polyamide layer by mixing GO with organic phase trimesoyl chloride (TMC) during the interfacial reaction with aqueous m-phenylenediamine (MPD), and the GO interlayer place was verified to play as a water channel. Wang et al. [36] reported another NF membrane with high water permeation and anti-pollution abilities, they dispersed GO into PIP aqueous phase, followed by interfacial polymerization with TMC organic phase. It has been demonstrated that the hydrophilic oxygen-containing functional groups (-OH, -COOH) in GO can react with $-NH_2$ or -NH groups in aqueous monomer and -COCl in organic monomer TMC during the interfacial polymerization process[32, 36, 37]. Therefore, due to various excellent properties, GO additives have great potential in the field of membrane.

In order to efficiently extracting lithium, both high permeation flux and high separation ability for Mg^{2+} and Li^{+} are necessary. The goal of this work is to synthesis a novel NF membrane with high permeation flux, high separation performance and long-time stability for improving the lithium extraction purity and efficiency. From the

perspective of optimizing the substrate film, we modified polyethersulfone (PES) ultrafiltration substrate membrane with GO nano-additives to improve the mechanism and hydrophilicity performance, followed with interfacial polymerization between PEI and TMC. Several analyze methods were applied to explore the chemical composition, microstructure, separation performance, etc. of the obtained composite membranes. In addition, the synergy effects of GO loading concentration on substrate membrane and polyamide layer were comprehensively studied.

2.2 Experiment

2.2.1 Materials and regents

Graphite powder, polyethylene glycol (PEG), H_2O_2, HNO_3, H_2SO_4, $KMnO_4$, N, N-dimethylacetamide (DMAc), PEI (70000 Da), TMC, $NaCO_3$, sodium dodecyl sulfate (SDS), Na_2SO_4, $MgSO_4$ (heptahydrate), NaCl, LiCl and $MgCl_2$ (hexahydrate) were all provided by Wako Pure Chemical Indus-tries Ltd., Japan. PES (3000P, 62000 g/mol) was bought from Solvay Advanced Polymer (Belgium).

2.2.2 Preparation of GO/PES based composite membrane

GO was synthesized from graphite powder using method of modified Hummers'[38, 39]. The GO modified PES ultrafiltration (UF) substrate membranes were formed through phase inversion method[40, 41], and the detailed compositions of casting solutions are given in Table 2-1. The synthesized GO was firstly ultrasonically dispersed in DMAc for three hours, and then blended with PES and PEG (Mw = 10000 g/mol), and continuously stirred at 50 ^oC for 6 hours to form a homogeneous casting solution. After degassing for 8 h, the casting solution was cast on a glass plate using a casting knife with a gap height of 200 μm and immediately dipped into the deionized water bath. The formed GO/PES substrate primary membranes were immersed in deionized water before next utilize. The GO/PES composite UF membranes with different embedding GO contents (0 wt%, 0.01 wt%, 0.03 wt%, 0.05 wt%, 0.1wt%, 0.3

wt%, 0.5 wt%, 1 wt%) were defined as UF0, UF001, UF003, UF005, UF01 and UF05, respectively.

The NF membranes were synthesized through interfacial polymerization method based on previous report[23]. The aqueous phase solution (0.5 wt% aqueous monomer PEI, 0.1 wt% surfactant SDS and 0.1 wt% acid acceptance agent $NaCO_3$) was firstly dipped on the surface of prepared GO/PES UF membrane for 5 min and then the excess solution was removed by a rubber roller. Next, the membrane was immersed in the 0.1% (w/v) TMC/n-hexane organic solution for 3 min to allow the occurrence of interfacial reaction between PEI and TMC on the membrane surface. Followed with 10 min in oven at 70 ºC for further polymerization. Finally, the obtained NF membranes were washed and stored in the deionized water before performance test. In addition, the obtained NF membranes formed from UF0, UF001, UF003, UF005, UF01 and UF05 substrate membrane were noted as NF0, NF001, NF003, NF005, NF01 and NF05, respectively.

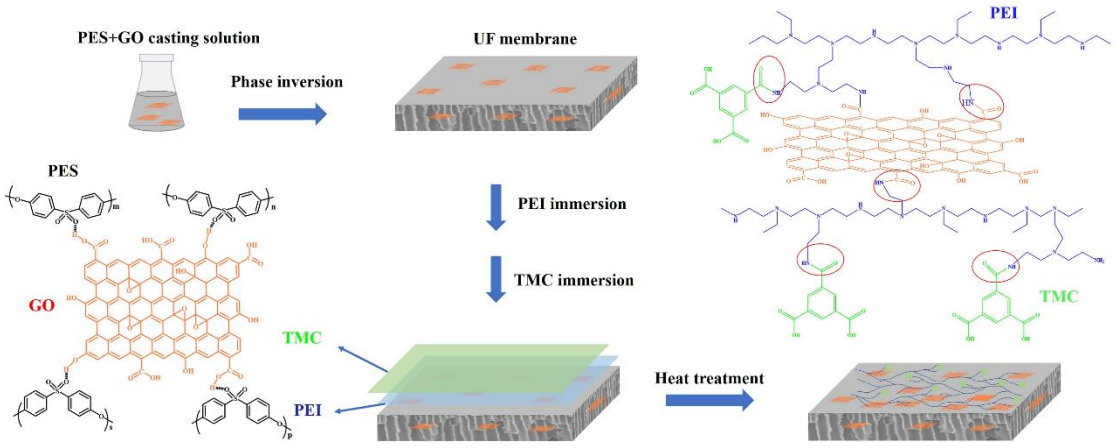

Fig.2-1. Schematic representation of membrane synthesize process.

Table 2-1 Composition of casting solution of UF substrate membrane

Membrane	GO (wt%)	PES (wt%)	PEG (wt%)	DMAc (wt%)
UF0	0	18	10	72
UF001	0.01	18	10	71.99
UF003	0.03	18	10	71.97
UF005	0.05	18	10	71.95
UF01	0.1	18	10	71.9

UF05	0.5	18	10	71.5

2.2.3 Membrane characterization

The morphologies and structure of membranes were characterized by field emission scanning electron microscopy (FESEM, Hitachi S-5000, Japan) and atomic force microscopy (AFM, Shimadzu SPM-9500J3, Japan). Fourier-transform infrared spectroscopy (ATR-FTIR, Shimadzu Co., Ltd., Japan), energy dispersive spectroscopy (EDS, S-3000N, Hitachi, Japan) and X-ray photoelectron spectroscopy (XPS, AXIS-ULTRA DLD, KRATOS) were applied to identify the chemical function groups, element composition and distribution in membranes. The water contact angle (CA, digidrop, GBX, Whitestone way, France) was carried out to analyze the hydrophilicities of membrane surface. In addition, to confirm the chargeability of membranes, the electrokinetic analyzer (Sur-PASS TM3 Anton Paar, GmbH, Austria) was adopted to investigate the zeta potential of membranes at a pH range from 5 to 10. The porosity ε (%) of membrane was determined using gravimetric method, which can be evaluated as the equation[42-46]:

$$\varepsilon = \frac{W_1 - W_0}{S \times D \times \rho} \times 100\% \quad (1)$$

in which, W_1 (g) and W_0 (g) are defined as the weight of wet membrane and dry membrane, respectively. S (cm^{-2}) and D (cm) stand for the area and thickness of membrane, respectively, and ρ stands for the density of water (g/cm^{-3}).

2.2.4 Separation performance testing

The separation performance of membrane was tested using a cross-flow filtration equipment with an effective test area of 12.56 cm^2. In addition, the separation test was conducted at 25 ºC under a low-pressure of 3 bar. The pH of feed solution was around 7. Before separation testing, all membranes to be tested were firstly stabilized at 4 bar for 30 min with pure water and then maintained at 3 bar to stabilize the flow flux. The permeabilities of membranes were assessed by the permeation flux F, which can be

calculated as:

$$F = \frac{Q}{T \times S \times P} \quad (2)$$

In which, Q (L) is defined as the permeate volume, T (h) is the total time for permeation, S (m^2) is the effective area, and P (bar) is defined as the pressure during permeation process. To evaluate the rejection ability of membrane for inorganic salt, the filtration test was carried out using the target solution with a concentration of 2.0 g/L under 3 bar. The rejection rate R was calculated by equation (3):

$$R = \left(1 - \frac{C_p}{C_f}\right) \times 100\% \quad (3)$$

In which, C_p and C_f are defined as concentration of permeate solution and feed solution, respectively. According to previous report[47], the pore size of membrane can be evaluated by the PEG filtration test, as shown in equation (4):

$$r = 0.0397 MWCO^{0.43} \quad (4)$$

The molecular weight cut-off (MWCO) of membrane was denoted as the molecular weight of PEG with a rejection for 90%. The difference in PEG concentration in solution was calculated by the total organic carbon analyzer (TOC-VCSH; Shimadzu Co., Kyoto, Japan).

A 2 g/L simulated solution composed of $MgCl_2$ and LiCl was used to characterize the separation performance of membrane for Mg^{2+} and Li^+. The Mg^{2+}/Li^+ ratio of the simulated solution was maintained at 20. Each test was conducted more than 3 times to calculate an average value. The Mg^{2+}/Li^+ separation ability of membrane can be evaluated by the separation factor $S_{Mg,Li}$, which was calculated by equation (5):

$$S_{Mg,Li} = \frac{P_{Mg/Li}}{F_{Mg/Li}} \quad (5)$$

In which, $P_{Mg,Li}$ and $F_{Mg,Li}$ represent mass ratio of Mg^{2+}/Li^+ in permeate solution and feed solution, respectively. The concentrations of Mg^{2+} or Li^+ in brine solution before and after filtration were quantified using inductively coupled plasma optical emission spectroscopy (ICP-OES, 10000IV, Shimadzu, Japan).

2.3 Result and discussion

2.3.1 Chemical composition analysis

The ATR-FTIR analysis was used to compare and analyze the changes of the functional groups on the surface of membranes before and after GO embedding and interfacial polymerization reaction. It can be seen in Fig.2-2 that each spectrum of UF membrane had characteristic peaks at ~3057cm^{-1} and ~3170cm^{-1}, corresponding to C-H unsaturated bond of PES phenyl ring [22]. Fig.2-2(b) shows that, compared with PES pure membrane, a broad peak around 3668~3355 cm^{-1} appeared on each GO doped UF membrane, which was originated from the -OH stretch of GO nanosheet [37, 47]. In addition, the peak intensity around 3668~3355 cm^{-1} enhanced slightly with the increase of GO doping amount. After polymerization between PEI and TMC, a new peak corresponds to the C=O vibration in amide appeared at 1635 cm^{-1}, which indicated the successful formation of polyamide layer. As shown in Fig.2-2(d), compared with UF005, a stronger broad peak around 3628~3294 cm^{-1} can be observed in NF005, which was attributed to not only -OH but also unreacted -NH from PEI monomer[24, 48, 49]. On the spectrum of each NF membrane, near to the peak at 2864 cm^{-1} (C-H), a new peak at 2960 cm^{-1} appeared due to the existence of -NH_n^+ (n=2, 3)[22].

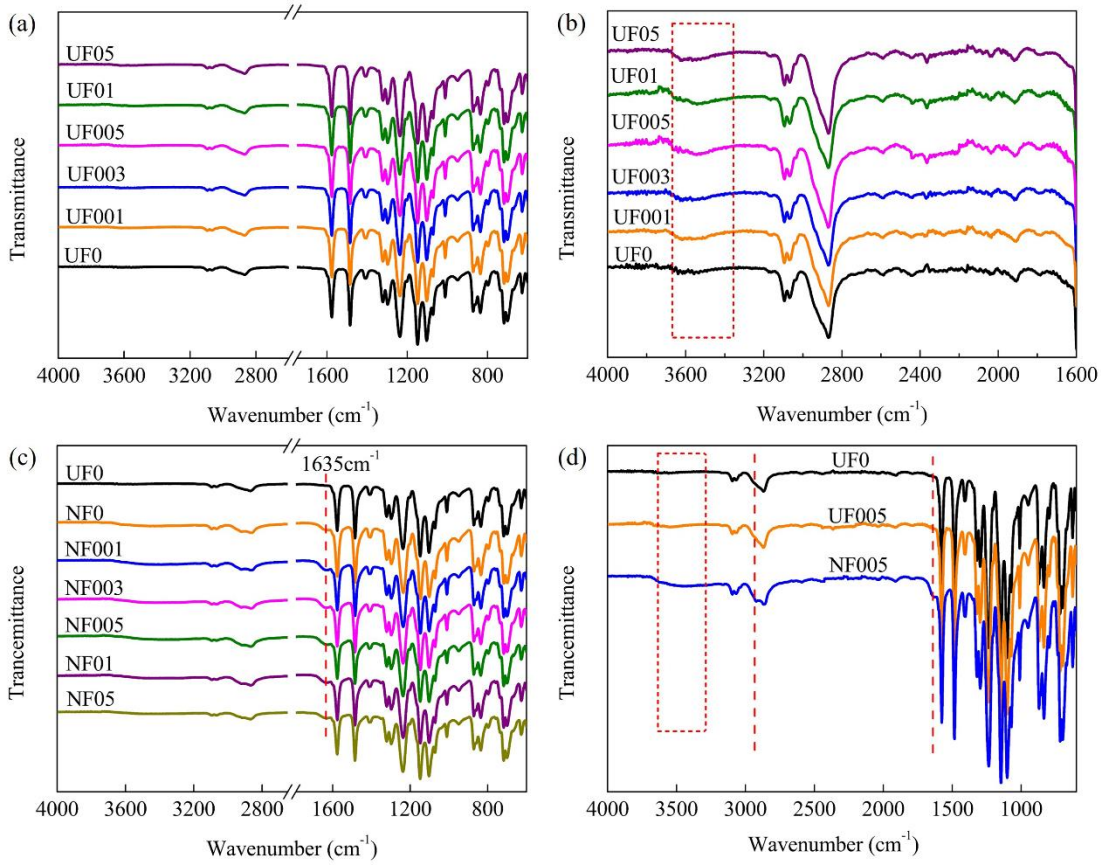

Fig.2-2. ATR-FTIR spectra of membranes: (a-b) UF membranes with different GO contents, (c) pure PES matrix membrane and NF membranes with different GO concentrations and (d) UF0, UF005 and NF005.

Fig.2-4 shows the composition and content of several functional groups, which were quantified by XPS characterization. With some chemical bond determined from C1s and N1s in Fig.2-4, Fig.2-5 and Table 2-2, we evaluated the effect of GO doping on the degree of crosslinking of the polyamide thin layer. For all NF membranes, C1s spectrum can be divided into five status of C-C, C-N, C-O, N-C=O and O-C=O, located respectively at around 284.5, 285.7, 286.3, 287.8 and 288.5 eV.

After immersing UF005 membrane in the PEI aqueous solution for 5 minutes, it is denoted as M005. Compared with NF005, a weaker peak in M005 can be found at the same position of 1635 cm^{-1}, as shown in Fig.2-3. On the other hand, a small content of N-C=O also appeared in the deconvoluted C1s spectrum of M005, which revealed that the cross-link net appeared after the UF005 membrane was immersed in the PEI aqueous solution. Both the results of ATR-FTIR and XPS demonstrated that the group

-COOH of GO in UF membrane will react with amine group -NH_2 of PEI monomer, and the similar phenomenon has also been reported in some reports[32, 37]. In addition, with the increase of GO doping content from 0 wt% to 0.5 wt%, the ratio of C-N in NF membranes decreased from 22.31% to 19.56%, while the ratio of N-C=O increased from 9.15% to 15.13%. The reduced C-N/N-C=O ratio implied an increase in crosslink degree of polyamide layer. This may be due to the reaction between GO and PEI monomer, which enhanced the crosslink of GO and PEI and TMC. Therefore, the more the GO content in the UF membrane, the fewer free amine functional groups remain in the PEI monomer. Due to the cross-linking between GO and PEI, the adhesion between the polyamide layer and the base membrane was enhanced, which is beneficial to improve the stability of the NF membrane. However, when the graphene content was excessive, more amine groups were "anchored" by the GO and could not migrate to the organic phase to react with TMC monomer, resulting in the crosslink of PEI/TMC becoming loose.

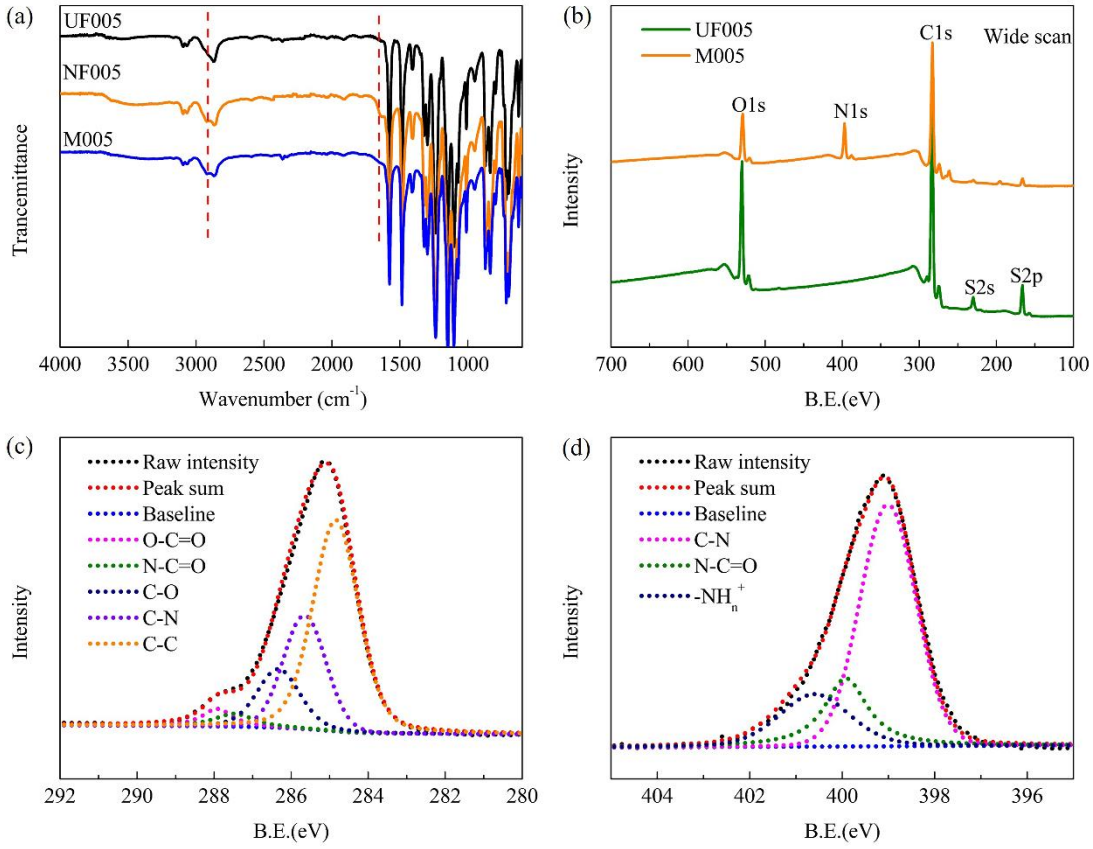

Fig.2-3. (a) ATR-FTIR spectra of UF005, NF005 and M005, (b) XPS wide scan of UF005 and M005, (c) deconvoluted C1s and (d) deconvoluted N1s of membrane M005.

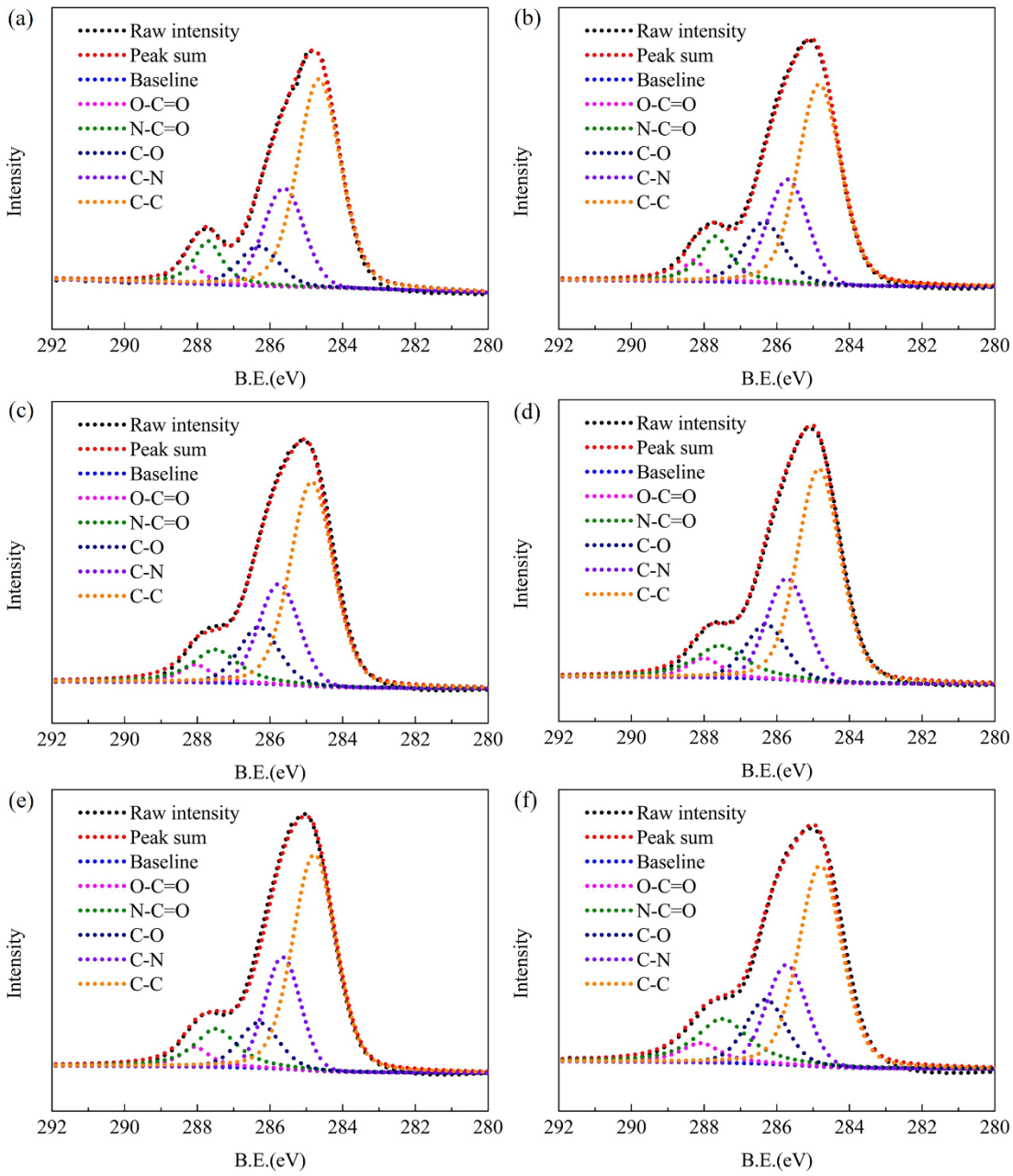

Fig.2-4. Deconvoluted C1s of membranes: (a) NF0, (b) NF001, (c) NF003, (d) NF005, (e) NF01 and (f) NF05.

On the other hand, all NF membranes have three N1s-related peaks at around 398.9, 399.7 and 401.1 eV, corresponding to C-N, N-C=O and $-NH_n^+$ (n=2,3), respectively. Similar trend was found in peaks of N1s spectrum, the ratio of C-N decreased and the ratio of N-C=O increased with the increase of GO doping concentration. In addition, the ratio of $-NH_n^+$ (n=2,3) decreased from 16.35% to 4.69% with the raise of GO concentration from 0 wt% to 0.5 wt%, which was consistent with the result of C1s. The $-NH_n^+$ (n=2,3) is originated from the protonation of unreacted amine groups in PEI

monomer, which is beneficial to improve the positive chargeability of NF membrane surface. After introducing GO nanosheet into PES casting solution, the hydrogen bond interactions are generated among free groups (-OH) and (-COOH) from GO nanosheet and (O=S=O) from PES polymer[49-51]. Therefore, the doped GO additives were "anchored" in UF membrane due to the bonding between GO and PES. On the other hand, the -COOH of GO would react with amine group -NH_2 of PEI monomer. More GO would "anchor" more amine groups, thereby reducing free amine groups remaining in the polyamide layer. The GO additives were "anchored" in PES substrate membrane, and the PEI monomers were "anchored" by GO at the same time. Therefore, the GO additive acted as a bridge between PES substrate membrane and polyamide layer. In summary, the existence of GO in UF membrane promoted the interaction between the UF base membrane and the polyamide thin layer, due to the "anchor effect" between PES, GO and PEI.

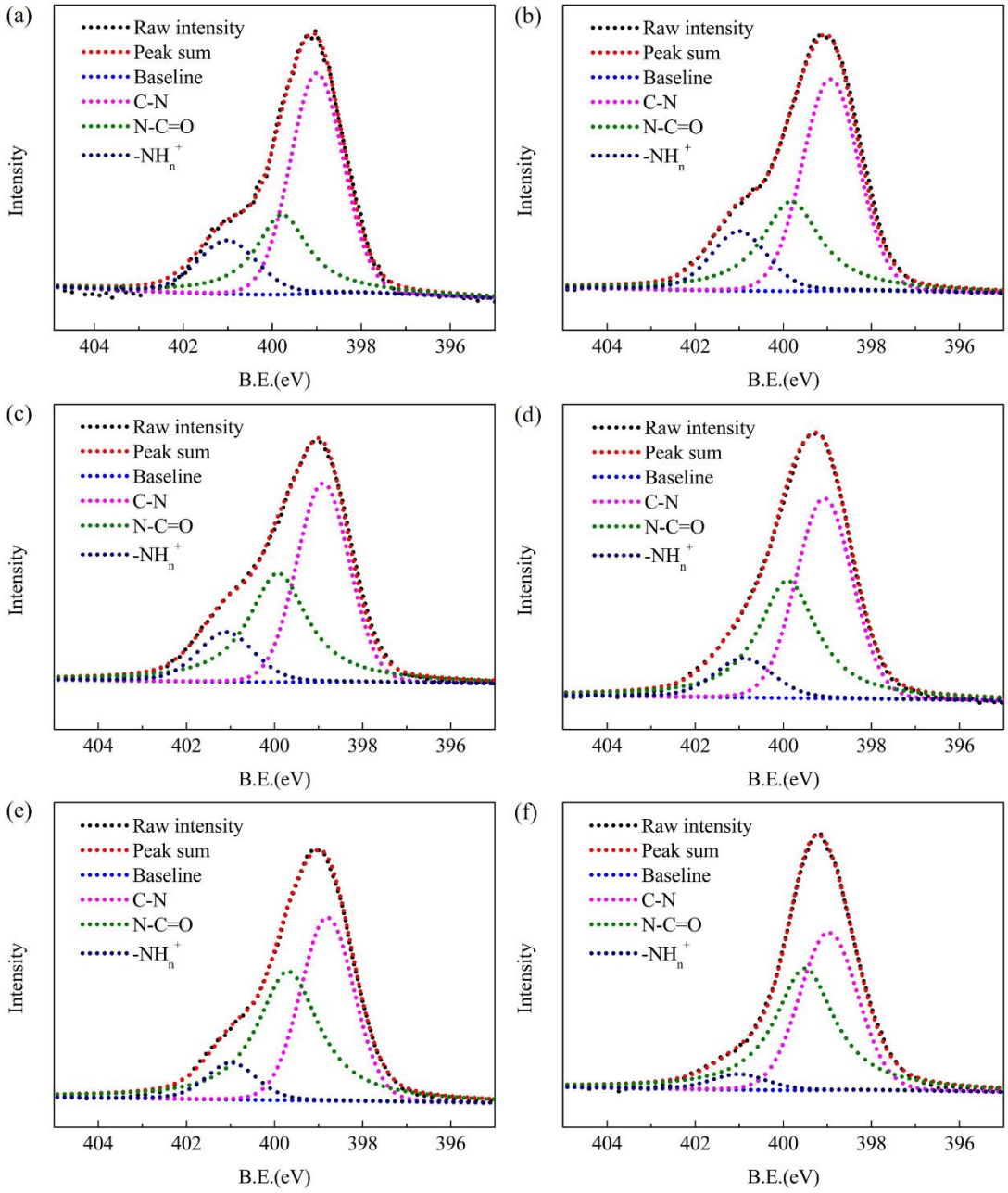

Fig.2-5. Deconvoluted N1s of membranes: (a) NF0, (b) NF001, (4c) NF003, (d) NF005, (e) NF01 and (f) NF05.

Table 2-2 XPS results derived from C1s and N1s spectra.

Membrane	C			N		
	Energy (eV)	Species	(%)	Energy (eV)	Species	(%)
M005	284.5	C-C	54.07	398.9	C-N	62.17
	285.7	C-N	24.78	399.7	N-C=O	19.17
	286.3	C-O	13.95	401.1	$-NH_n^+$	18.65
	287.8	N-C=O	3.49			
	288.5	O-C=O	3.72			
NF0	284.5	C-C	55.54	398.9	C-N	55.34
	285.7	C-N	22.31	399.7	N-C=O	28.3
	286.3	C-O	9.8	401.1	$-NH_n^+$	16.35
	287.8	N-C=O	9.15			
	288.5	O-C=O	3.19			
NF001	284.5	C-C	50.32	398.9	C-N	51.54
	285.7	C-N	22.14	399.7	N-C=O	32.61
	286.3	C-O	14.09	401.1	$-NH_n^+$	15.84
	287.8	N-C=O	10.02			
	288.5	O-C=O	3.42			
NF003	284.5	C-C	50.94	398.9	C-N	46.08
	285.7	C-N	21.28	399.7	N-C=O	40.39
	286.3	C-O	13.03	401.1	$-NH_n^+$	13.51
	287.8	N-C=O	10.84			
	288.5	O-C=O	3.89			
NF005	284.5	C-C	51.53	398.9	C-N	47.97
	285.7	C-N	21.85	399.7	N-C=O	41.31
	286.3	C-O	12.27	401.1	$-NH_n^+$	10.71
	287.8	N-C=O	11.3			
	288.5	O-C=O	4.05			

NF01	284.5	C-C	53.25	398.9	C-N	42.49
	285.7	C-N	20.71	399.7	N-C=O	48.7
	286.3	C-O	10.35	401.1	$-NH_n^+$	8.81
	287.8	N-C=O	11.54			
	288.5	O-C=O	4.14			
NF05	284.5	C-C	46.44	398.9	C-N	44.67
	285.7	C-N	19.56	399.7	N-C=O	50.63
	286.3	C-O	13.77	401.1	$-NH_n^+$	4.69
	287.8	N-C=O	15.13			
	288.5	O-C=O	5.09			

2.3.2 Morphology and structure characterization

The top surface and cross section morphologies of UF005 and NF005 membranes were displayed in Fig.2-6. There were obvious differences in morphology structure between UF substrate membrane and NF membrane. As can be seen in Fig.2-6, UF005 substrate membrane exhibited a smoother top surface with uniformly distributed small pores compared with NF005 membrane. After polymerization reaction on UF substrate membrane surface, a dense and thin polyamide layer, with a thickness less than 100nm, firmly “grown” on the substrate membrane surface. A large amount of small valley-ridge like wrinkle structures with different sizes can be clearly found in top surface of NF005 membrane, which is an evidence of the successful completion of polyamide layer[21, 47]. The PEI branches with numerous amine groups can migrate into the interface of aqueous and organic phase to react with acid chloride groups of TMC monomers to form the dense active thin layer. The PEI applied in this work possessed a large molecular weight of 70000 Da, so the polymerization process of PEI and TMC was not severe as some previous reported aqueous monomers with low molecular weight which can migrate to the organic phase easily and complete reaction quickly[24, 52]. As exhibited in Fig.2-6 (c1-c2), after doping a low content of GO in the substrate UF membrane, the polyamide layer thickness of NF005 was around 59.8nm, which was

slightly lower than the polyamide layer thickness of pure NF membrane NF0 (68.7nm). The incorporated GO in membrane surface may cross-link with some free -NH_2 in PEI monomer, enhancing the interaction between PEI monomer and base membrane. During the interfacial polymerization process, the migration rate of PEI chains slowed down due to some "anchored" PEI chains by GO. As a result, the reaction rate between PEI and TMC decreased to a certain extent, leading to a slightly looser and thinner polyamide layer of NF005. It is worth noting that, with a thinner polyamide layer, the transmission resistance of membrane NF005 to water molecules would be decreased, contributing to a higher water permeability of membrane NF005. According to the result of XPS, the peak of N1s appeared in the spectrum of each NF membrane. From the EDS mapping images in Fig.2-6, the N element from PEI monomer was introduced and evenly distributed on the membrane, indicated that a uniform polyamide active layer occurred on the substrate membrane after interfacial polymerization process.

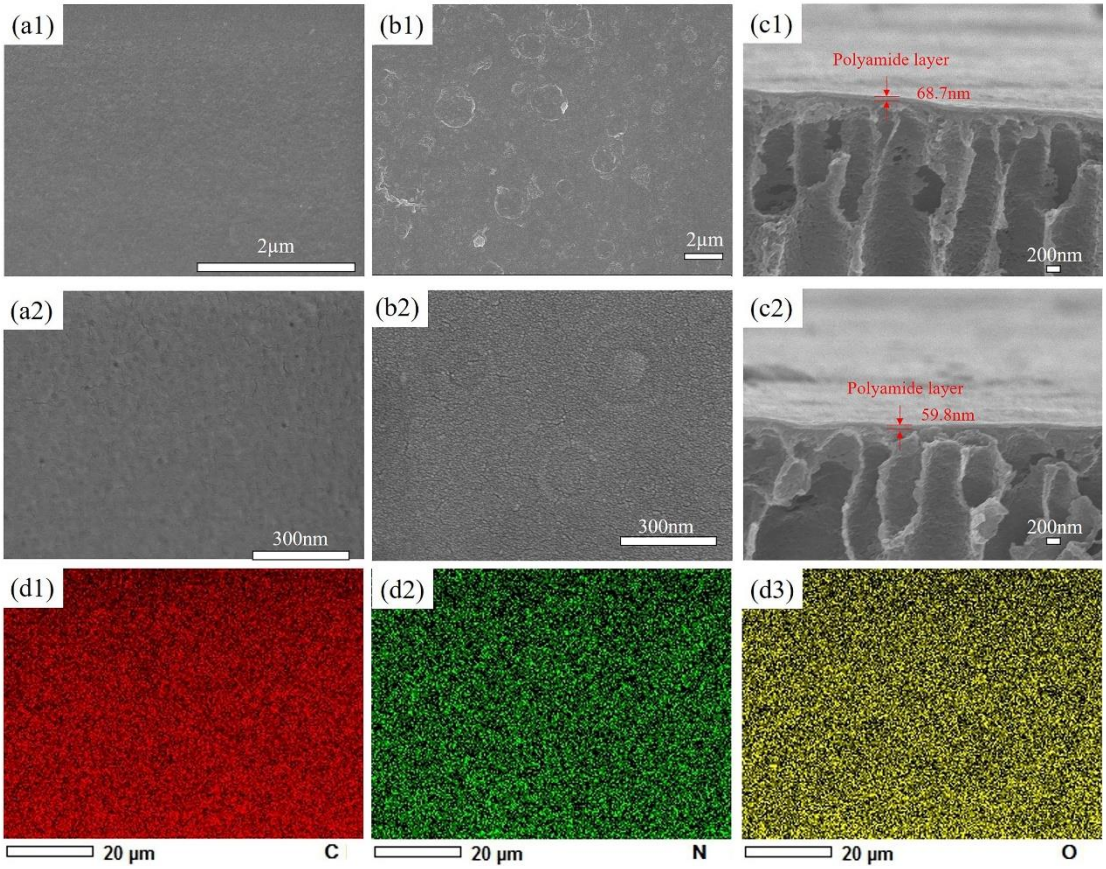

Fig.2-6. SEM images of (a1-a2) top surface of UF005, (b1-b2) top surface of NF005, cross section of (c1) NF0 and (c2) NF005, and (c1-c2-c3) EDS mapping of NF005 membrane.

To further investigate the influence of doped GO on morphology structure of membranes, AFM analysis was carried out to capture topology images of membranes with a scan range of 10μm×10μm. As presented in Fig.2-7 and Table 2-3, UF0 membrane showed a relatively smooth surface with a low roughness (Ra= 14.08nm, Rms=17.85nm). With the raise of GO concentration from 0 wt% to 0.5 wt%, Ra and Rms values of substrate membranes declined slightly from 14.08nm and 17.85nm to 11.78nm and 15.06nm, respectively. However, with further addition of GO concentration in UF membranes from 0.05 wt% to 0.5 wt%, the membrane roughness increased gradually, manifested as raise of Ra and Rms values up to 24.9nm and 31.15nm.

The doped-GO additive was “anchored” in UF membrane due to the bonding between free groups (-OH) and (-COOH) in GO and (O=S=O) in PES polymer. With an ultra-low amount of doped GO, the larger peak-valley structures were filled out by many small peaks and valleys, resulting to a relative smoother surface compared with pure PES substrate membrane. Similar phenomenon has been observed in previous reports[43, 53, 54]. With further increase of GO doping content, the UF substrate membrane showed greater roughness, and larger peaks and “aerolite hole” like valley structure can be observed in UF05 membrane surface. With high GO loading in the casting solution, GO nanosheets are prone to agglomerate together, leading to a rougher surface and may cause defects[42, 53]. After the occurrence of interfacial polymerization on substrate membrane, the surface roughness increased slightly, owing to the formation of valley-ridge like wrinkle structures, which was consistent with the SEM results. Although the roughness values of the membrane increased after interfacial polymerization, the NF005 membrane was still relatively smooth, which is benefit for anti-fouling[54, 55].

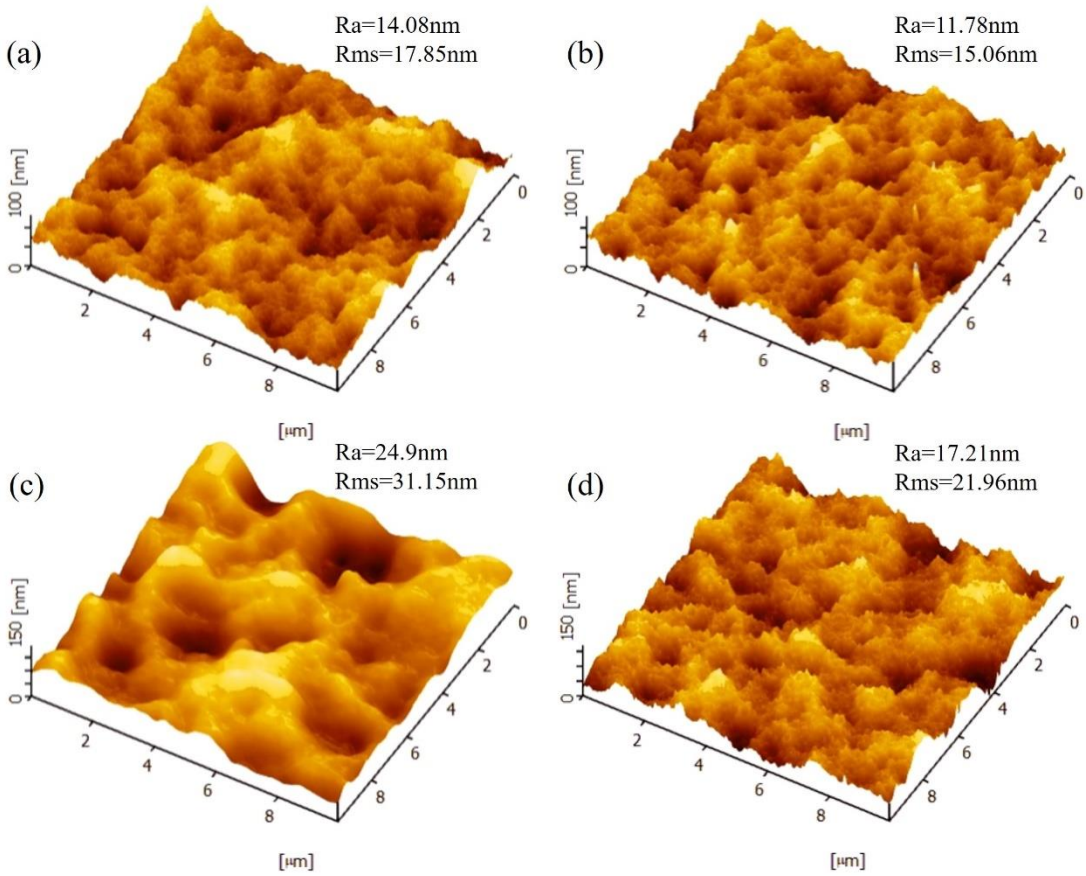

Fig.2-7. AFM topology images of membranes (a) UF0, (b) UF005, (c) UF05 and (d) NF005.

Table 2-3 Roughness values of UF membranes with different GO contents, and NF005 membrane.

Membrane	Ra (nm)	Rms (nm)
UF0	14.08	17.85
UF001	13.98	17.43
UF003	12.03	15.01
UF005	11.78	15.06
UF01	15.42	19.43
UF05	24.9	31.15
NF005	17.21	21.96

As can be seen in Fig.2-8(a), the contact angle of UF membranes declined with the increase of GO doping content, which implied the enhance of hydrophilicity of membranes. During the phase inversion process, GO with many hydrophilic functional

groups (-OH and -COOH) can migrate to the surface and pore walls of the membrane and disperse uniformly, resulting in an increase in the hydrophilicity of the membrane. A layer of hydration can be formed on the surface of the hydrophilic membrane, which prevented the adsorption and aggregation of pollutants, thereby improving the stability of the membrane. The porosity of UF membranes increased from 69.11% to 75.35% when the incorporate content of GO increased from 0 wt% to 0.1 wt%, then declined to 66.78% when the graphene doping content was further increased to 0.5 wt%, as shown in Fig.2-8(b). It can be explained that, during the process of phase inversion, the hydrophilic additive GO worked as a nucleating agent and promoted the exchange between solvent and non-solvent, thereby forming a microporous membrane structure[41, 43]. However, when GO is gradually added from 0.1 wt% to 0.5 wt%, the viscosity of the mixed casting solution would gradually increase, thereby hindering the phase separation process and resulting in a final membrane with a relatively dense structure[56].

2.3.3 Characterization of membrane performance

2.3.3.1 Permeation property of UF membrane

Fig.2-8(c) presents the permeability of PES pure UF membrane and GO incorporated UF membranes, compared with pure PES UF membrane, GO-doped UF membranes showed higher permeability to pure water. In addition, the pure water flux increased largely from 210.19 to 477.7 L/m^2hbar when the GO content increased to 0.1 wt%, then declined to 419.93 L/m^2hbar as the GO content further increased to 0.5 wt%. After doping GO nanosheet in the UF membrane, the increased water flux of final NF membrane was due to the dual effects of GO on the changes in the morphology and hydrophilicity of the final NF membrane. Fig.2-8(d) exhibits the process of water molecules permeating the GO-doped UF membrane. Due to the existence of GO, the hydrophilicity of final UF membranes was significantly improved, which has been demonstrated by the test of contact angle. In addition, after doping GO in PES matrix,

more water channels would be formed between GO and GO and between GO and PES polymer, which is conducive to water molecules pass through the UF membrane during the filtration process. On the other hand, according to the results of porosity characterization, with a low doping content of GO, the porosity of final UF membrane would increase accordingly, which is conducive to improving the water permeability. The decreased pure water flux of UF005 was consistent with the result of AFM image and porosity. Excessive GO content can form agglomeration and reduce membrane porosity, resulting in a decline in membrane permeability. The phenomenon proved that a small amount of doping of GO may significantly enhance the hydrophilicity and permeability of the UF membrane.

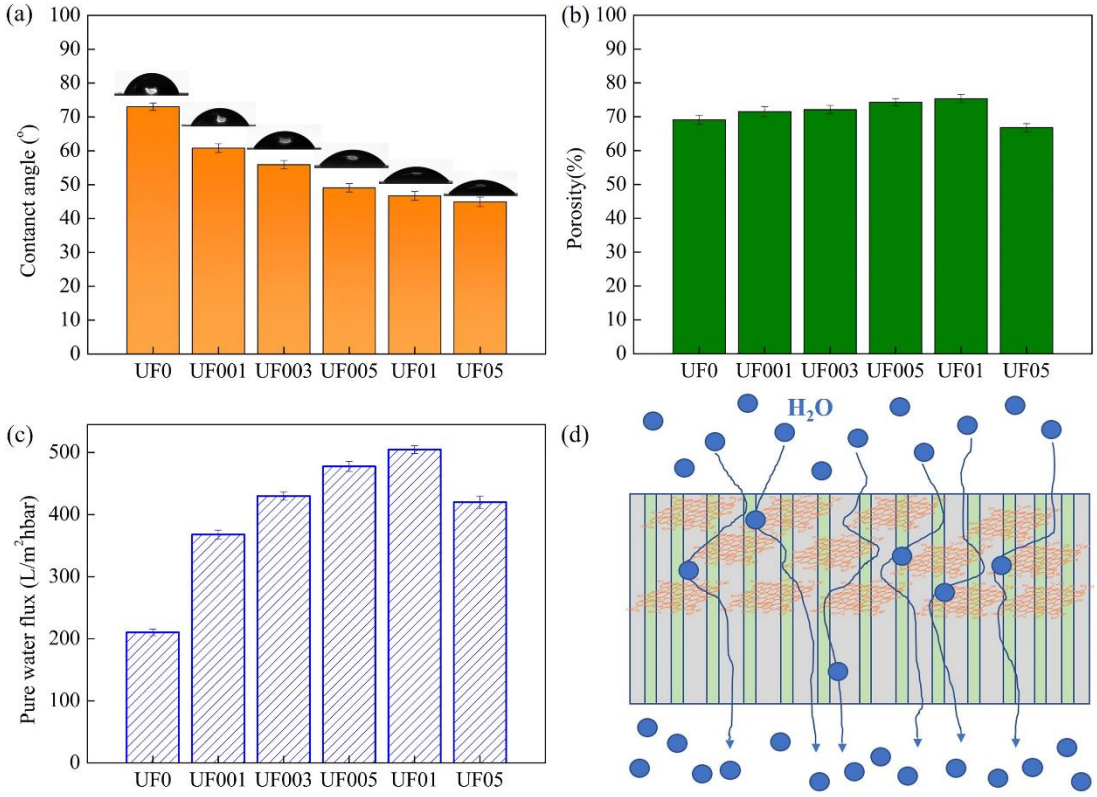

Fig.2-8. (a) Contact angle, (b) porosities and (c) pure water flux of UF membranes with different GO doping amounts, and (d) schematic diagram of water molecules permeating the GO-doped UF membrane.

2.3.3.2 Separation performance of NF membrane

Fig.2-9(a) shows the cut-off molecular weights of the membranes UF0 and UF005,

which can be used to evaluate the pore size changes of the membranes. As mentioned in equation (4), the pore radius of membranes NF0 and NF005 were approximately 0.56nm and 0.66nm, respectively. Compared with the pure NF0 membrane, the increased pore size of NF005 was due to the embedding GO in the PES UF membrane. The GO embedded in the base membrane connected the base membrane with the polyamide layer through cross-linking with PES and PEI, which consumed a part of the amine functional groups in PEI monomers. This would reduce the degree of cross-linking between PEI and TMC to a certain extent, resulting in a relatively loose PEI/TMC interfacial polymerization layer. The difference between the radius values of NF0 and NF005 was about 0.1 nm, indicating that the effect of ultra-low GO doping content has slightly effect om the membrane pore size.

The surface chargeability of membranes in a range of pH from 5 to 10 are shown in Fig.2-9(b). After incorporating a small amount of GO, the negative chargeability of UF005 was enhanced compared with pure PES UF membrane, due to the dissociation of -COOH in GO nanosheets. The isoelectric point of UF0 and UF005 were 9.17 and 8.84, respectively, and both membranes exhibited high positive chargeability under the conditions in this work (pH≈7). The pure NF0 membrane showed high positive charge capacity at pH above the isoelectric point, which was due to the protonation of a large amount of unreacted amine groups in PEI monomer. The slightly weak in the positive charge of NF005 was due to the crosslink between GO and PEI, which reduced the amount of unreacted amine groups.

In order to evaluate the Mg^{2+}/Li^{+} separation performance of the NF membrane, a simulated solution was used as the feed solution, and the filtration test was performed at 3 bar and 25ºC. The simulated solution with a concentration of 2 g/L was composed of $MgCl_2$ and LiCl, and the Mg^{2+}/Li^{+} ratio of the simulated solution was maintained at 20. The difference in permeability and rejection ability of Mg^{2+} and Li^{+} of a series of NF membranes with different GO doping contents in UF membrane is shown in Fig.2-9(c). Compared with pure NF0 membrane, the separation performance hardly changed with a slightly addition of GO contents in UF membrane from 0.01 wt% to 0.05 wt%,

while the flux increased largely from around 5 to 11.15 L/m^{2}hbar. When the embedded content of GO was further increased, both the flux and rejection of Mg^{2+} and Li^+ declined significantly. Among these membranes prepared in this work, membrane NF005 exhibited optimal properties for Mg^{2+}/Li^+ separation and permeability ($R(Mg^{2+})$= 95.14%, $R(Li^+)$=20.93% and F=11.15 L/m^{2}hbar), which was attributed to the ultra-low content of GO doping. It has been reported that the synergistic effect of steric hindrance effect and Donnan electrostatic repulsion effect determined the separation capacity of membrane. Owing to the similar hydraulic radius of Li^+(0.382nm) and Mg^{2+}(0.428nm), the electrostatic repulsion effect played a dominant role in the selective separation of Mg^{2+} and Li^+. The Zeta potential result shows that membrane NF005 also exhibited high positive chargeability at pH=7 compared with the pure NF0 membrane. This can be explained as the ultra-low doping of GO in UF membrane only consume a small amount of amine groups, so it had little effect on the positive chargeability of the final NF membrane. That was why membrane NF005 have high separation performance for Mg^{2+} and Li^+. Compared with the divalent cations Mg^{2+}, low valence cations Li^+ carries less positive charge. In addition, the hydrate radius of Li^+ is 0.382 nm, which is relatively smaller than the hydrate radius of Mg^{2+} (0.428 nm). During the filtration process, positive charged UF005 membrane surface showed weaker exclusive effect and steric hindrance effect to Li^+ than Mg^{2+}, leading to lower rejection to Li^+. Subsequently, after passing through the positive charged polyamide layer, the Li^+ would be “attracted” through the UF005 membrane easily. Due to the higher negative charged obtained by GO modification, the electrostatic attraction effect between Li^+ and the UF substrate membrane was enhanced, accelerating the penetration of Li^+ through substrate membrane into the permeate solution. In short, the doping of a small amount of GO can cause changes in the structure and properties of both UF substrate membrane and the final NF membrane, which helps to achieve high separation performance.

On the other hand, with the increase of GO content from 0 wt% to 0.05 wt%, the large increase in flux about 119% was the result of several factors, including the

decreased thickness of polyamide layer, the increased pore size of NF membrane, improved hydrophilicity by GO modification, the increased porosity of UF membrane and the water channel formed by GO nanosheets. However, as mentioned in above results, excess loading content of GO may aggregate and lead to a denser UF membrane surface with low porosity, which had a negative impact on permeability. What's more, more GO may consume more amine groups in PEI monomer, leading to a reduction in unreacted amine groups and loose cross-linking between PEI and TMC. As a result, both flux and separation performance decreased when further increase the GO loading content in UF membrane.

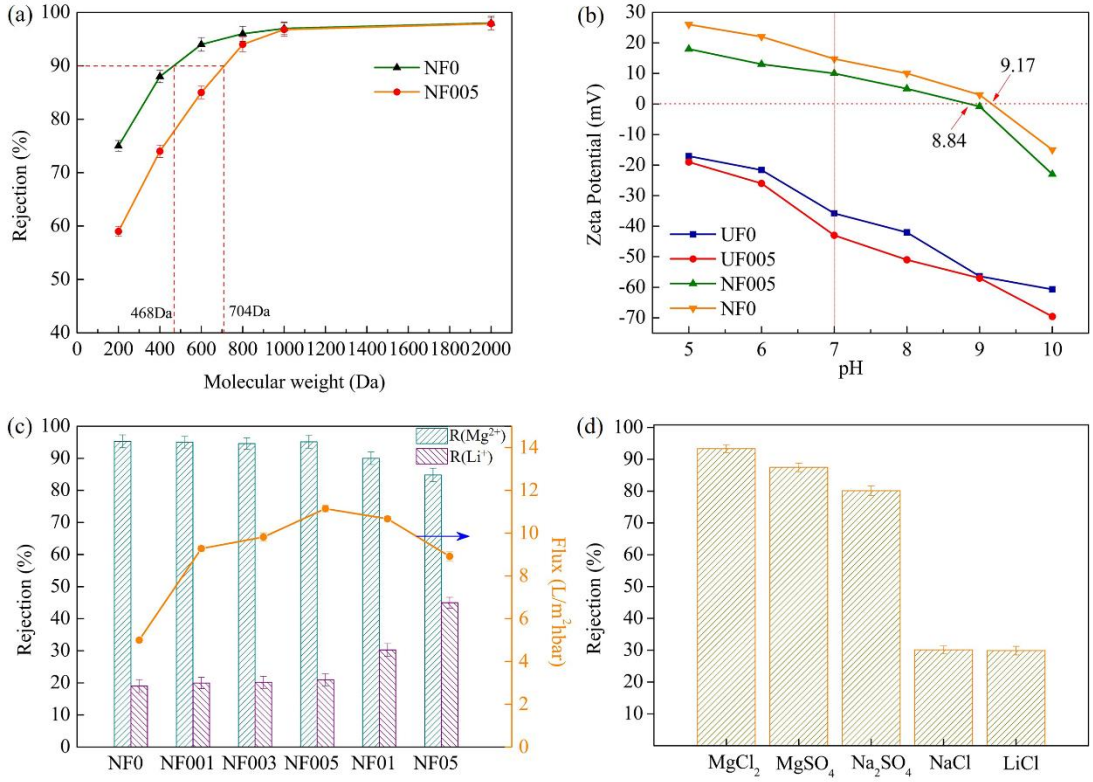

Fig.2-9. (a) MWCO of NF0 and NF005 membranes, (b)the Zeta potential of membranes UF0, UF005, NF0 and NF005, (c) the Mg/Li separation and flux properties of NF membrane with different GO doping contents, and (d) the rejection ability of NF005 for several different inorganic salts.

Fig.2-9(d) presents the separation performance of NF005 to inorganic salts, and the rejection ability followed as: $MgCl_2$ > Mg_2SO_4 > Na_2SO_4 > NaCl≈LiCl. Due to the high positive chargeability of NF005, the electrostatic repulsion effect between

membrane and divalent cations (Mg^{2+}) was higher than that between membrane and monovalent cation (Li^+ and Na^+). In addition, the higher rejection of Na_2SO_4 than NaCl and LiCl may be due to the larger radius of SO_4^{2-} (0.379nm) than Cl^-(0.332nm), which indicated the cooperation of steric hindrance effect and Donnan electrostatic repulsion effect.

2.3.3.3. Stability of NF membrane

A 7-day long-time cycle filtration test was carried out to evaluate the stability of the obtained membrane NF005. Firstly, a 20 h separation test was conducted using the simulated solution (2g/L, Mg^{2+}/Li^+ mass ratio = 20). After the first 20h filtration, the membrane was cleaned and immersed in the deionized water before the next cycle test. According to the results in Fig.2-10, in the first 20 hours cycle testing, the Mg^{2+}/Li^+ separation performance and flux were basically maintained. And both the separation performance and flux declined slightly after a 7-day cycle test, indicating the high stability of membrane. The GO incorporated in UF membrane acted as a “bridge” between UF substrate membrane and polyamide layer, which strengthened the bond between the polyamide layer and the UF base membrane. Therefore, even in a long-term filtration experiment, the polyamide layer was not easily detached from the UF base membrane. On the other hand, hydrophilic GO has been proved to enhance the anti-fouling property of membrane[41, 43, 57], and carbon nanomaterials GO additive can improve the mechanical properties of the membrane[58, 59], which is beneficial to improve the stability of final membrane to a certain extent. In summary, it was the synergy of structure and surface properties of membrane that provided the final membrane excellent stability during the long-time filtration process.

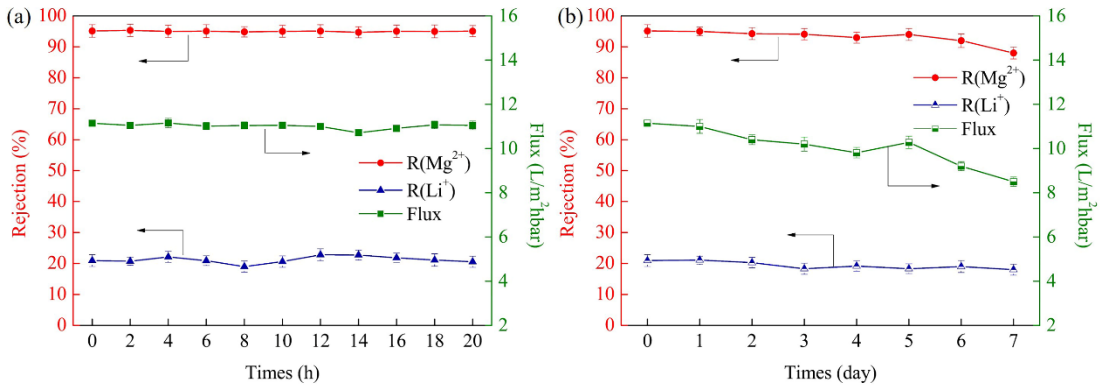

Fig.2-10. (a) The first 20 h filtration test of membrane NF005 and (b) 7-day long-time filtration test of membrane NF005.

A separation factor $S_{Mg,Li}$ of 1 means that there is no change in the Mg^{2+}/Li^{+} mass ratio before and after separation, indicating that the membrane has no separation effect on Mg^{2+} and Li^{+}. However, when separation factor $S_{Mg,Li}$ is less than 1, it reveals that the mass ratio of Mg^{2+}/Li^{+} is reduced and the target Li^{+} is enriched in the permeate solution. Additionally, the smaller the separation factor $S_{Mg,Li}$, the better the separation effect of membrane on Mg^{2+} and Li^{+}. Table 2-4 summarized a series of reported NF membrane applied for Mg^{2+}/Li^{+} separation. It can be seen that, the $S_{Mg,Li}$ values of all reported membranes in Table 2-4 were less than 0.5, indicating that all of these NF membrane had good separation performance for Mg^{2+} and Li^{+}. The $S_{Mg,Li}$ value of NF005 membrane prepared in this work was around 0.062, which was less than most NF membranes in Table 2-4. The low $S_{Mg,Li}$ value of NF005 membrane indicated an excellent separation ability for Mg^{2+} and Li^{+}. Besides, it is surprised that the NF005 membrane prepared in this study exhibited a highest flux under a low operation pressure of 3 bar. During the filtration process, the high flux indicates the high work efficiency of membrane. The results demonstrated that a low amount of GO additives in UF substrate membrane may greatly improve the flux while maintaining a high separation performance of NF membrane during the separation process. In summary, the structure and property of substrate membrane may significantly determine the performance of final NF membrane, and the conclusion of this work can provide a reference direction for NF membrane modification in the future.

Table 2-4 Comparison of several reported NF membranes and NF membrane prepared in this work.

Membrane	Conditions	Separation properties	Flux (L/m^2hbar)	Reference
PAN/DAPP/TMC	3 bar 2000 mg/L Mg^{2+}/Li^+ ratio (20)	$S_{Mg,Li}$=0.384	-	[20]
NF90	3 bar 2000 mg/L Mg^{2+}/Li^+ ratio (20)	$S_{Mg,Li}$=0.476	-	[20]
Polyetherimide/TMC/ BPEI/EDTA	10 bar Mg^{2+}/Li^+ ratio (24)	$S_{Mg,Li}$=0.108	0.6	[21]
PES/(PIP-PHF)/TMC	6 bar 2000 mg/L Mg^{2+}/Li^+ ratio (21.4)	$S_{Mg,Li}$=0.076	6.7	[60]
PES/CNC-COOH/ PEI/TMC	8 bar 2000 mg/L Mg^{2+}/Li^+ ratio (30)	$S_{Mg,Li}$=0.082	4.17	[22]
PES/(CNC-COOH)/ PEI/TMC	8 bar 2000 mg/L Mg^{2+}/Li^+ ratio (60)	$S_{Mg,Li}$=0.171	3.4	[22]
PES/PEI/TMC	8 bar 2000 mg/L Mg^{2+}/Li^+ ratio (20)	$S_{Mg,Li}$=0.05	5.02	[23]
DL-2540	20 bar Mg^{2+}/Li^+ ratio (60)	$S_{Mg,Li}$=0.35	-	[61]
DK	16 bar Mg^{2+}/Li^+ ratio (18~24)	$S_{Mg,Li}$=0.34	-	[62]

(PES-GO)/PEI/TMC	3 bar 2000 mg/L Mg^{2+}/Li^{+} ratio (20)	$S_{Mg,Li}$≈0.062	11.15	This work

2.4 Conclusion

In this work, we successfully optimized the Mg^{2+}/Li^{+} separation efficiency of NF membrane by doping a small amount of GO additives in the PES UF substrate membrane. The polyamide thin layer was formed through polymerization between PEI and TMC on the GO-doped UF membrane surface. Several characterization methods (SEM, AFM, ATR-FTIR, XPS, etc.) were applied to evaluate and analyze the properties of the membrane.

A large amount of unreacted protonated amine groups ($-NH_3^+$ and $-NH_2^+$) in the polyamide layer gave the membrane surface high positive chargeability. The "bridge" GO linked with both the O=S=O groups in PES matrix and amine groups $-NH_2$ in PEI monomer, which greatly enhanced the interaction between substrate membrane and polyamide layer. On the other hand, a small increase of the hydrophilic GO additives (from 0 wt% to 0.05 wt%) greatly improved the porosity and permeability of UF membrane, and the pore size of final NF membrane was enlarged slightly, and the thickness of polyamide layer was decreased slightly, which correspondingly improved the flux of the prepared NF membrane during the filtration process. However, a large loading amount of GO may aggregate and consume too many amine groups in PEI monomer, resulting in reduced separation and permeation capabilities. Under the combined effect of the above reasons, the final NF005 membrane exhibited an optimal Mg^{2+}/Li^{+} separation performance and efficiency, the rejection for Mg^{2+} and Li^{+} and the flux were 95.14%, 20.93%, and 11.15 L/m^2hbar, respectively. In addition, the final NF005 membrane performed a high stability after a 7-day long-time filtration, which may be due to the improved hydrophilicity and mechanical properties by GO modification. This work successfully optimized the performance of the NF membrane by modifying the substrate membrane with ultra-low content of GO, which provides a

reference direction for future NF membrane optimization research. It is obviously that the improved flux may greatly accelerate the lithium extraction efficiency of NF membrane during the Mg^{2+}/Li^{+} separation process. The membrane NF005 prepared in this work showed excellent separation performance and high permeation flux under a low operation pressure, which greatly improved the Mg^{2+}/Li^{+} separation efficiency and reduced energy consumption, indicating that it has application potential in the field of lithium extraction.

Reference

[1] L. Kavanagh, J. Keohane, G. Garcia Cabellos, A. Lloyd, J. Cleary, Global lithium sources—industrial use and future in the electric vehicle industry: a review, Resources, 7 (2018) 57.

[2] G. Liu, Z. Zhao, A. Ghahreman, Novel approaches for lithium extraction from salt-lake brines: A review, Hydrometallurgy, 187 (2019) 81-100.

[3] Q.-B. Chen, Z.-Y. Ji, J. Liu, Y.-Y. Zhao, S.-Z. Wang, J.-S. Yuan, Development of recovering lithium from brines by selective-electrodialysis: Effect of coexisting cations on the migration of lithium, Journal of Membrane Science, 548 (2018) 408-420.

[4] B. Swain, Recovery and recycling of lithium: A review, Separation and Purification Technology, 172 (2017) 388-403.

[5] X. Li, Y. Mo, W. Qing, S. Shao, C.Y. Tang, J. Li, Membrane-based technologies for lithium recovery from water lithium resources: A review, Journal of Membrane Science, 591 (2019) 117317.

[6] X. Zhao, H. Yang, Y. Wang, Z. Sha, Review on the electrochemical extraction of lithium from seawater/brine, Journal of Electroanalytical Chemistry, 850 (2019) 113389.

[7] Y. Zhang, L. Wang, W. Sun, Y. Hu, H. Tang, Membrane technologies for Li^{+}/Mg^{2+} separation from salt-lake brines and seawater: A comprehensive review, Journal of Industrial and Engineering Chemistry, 81 (2020) 7-23.

[8] K.T. Tran, T. Van Luong, J.-W. An, D.-J. Kang, M.-J. Kim, T. Tran, Recovery of

magnesium from Uyuni salar brine as high purity magnesium oxalate, Hydrometallurgy, 138 (2013) 93-99.

[9] X. Liu, M. Zhong, X. Chen, Z. Zhao, Separating lithium and magnesium in brine by aluminum-based materials, Hydrometallurgy, 176 (2018) 73-77.

[10] Y. Zhang, Y. Hu, L. Wang, W. Sun, Systematic review of lithium extraction from salt-lake brines via precipitation approaches, Minerals Engineering, 139 (2019) 105868.

[11] B. Swain, Separation and purification of lithium by solvent extraction and supported liquid membrane, analysis of their mechanism: a review, Journal of Chemical Technology & Biotechnology, 91 (2016) 2549-2562.

[12] S. Chen, D. Gao, X. Yu, Y. Guo, T. Deng, Thermokinetics of lithium extraction with the novel extraction systems (tri-isobutyl phosphate + ionic liquid + kerosene), The Journal of Chemical Thermodynamics, 123 (2018) 79-85.

[13] R.E.C. Torrejos, G.M. Nisola, M.J. Park, A.B. Beltran, J.G. Seo, S.-P. Lee, W.-J. Chung, Liquid–liquid extraction of Li^{+}using mixed ion carrier system at room temperature ionic liquid, Desalination and Water Treatment, 53 (2014) 2774-2781.

[14] L. Zhang, D. Shi, L. Li, X. Peng, F. Song, H. Rui, Solvent extraction of lithium from ammoniacal solution using thenoyltrifluoroacetone and neutral ligands, Journal of Molecular Liquids, 274 (2019) 746-751.

[15] X. Xu, Y. Chen, P. Wan, K. Gasem, K. Wang, T. He, H. Adidharma, M. Fan, Extraction of lithium with functionalized lithium ion-sieves, Progress in Materials Science, 84 (2016) 276-313.

[16] F. Xue, B. Wang, M. Chen, C. Yi, S. Ju, W. Xing, Fe_3O_4-doped lithium ion-sieves for lithium adsorption and magnetic separation, Separation and Purification Technology, 228 (2019) 115750.

[17] M. Chen, R. Wu, S. Ju, X. Zhang, F. Xue, W. Xing, Improved performance of Al-doped $LiMn_2O_4$ ion-sieves for Li_+ adsorption, Microporous and Mesoporous Materials, 261 (2018) 29-34.

[18] S. Wang, P. Li, X. Zhang, S. Zheng, Y. Zhang, Selective adsorption of lithium from high Mg-containing brines using H_xTiO_3 ion sieve, Hydrometallurgy, 174 (2017) 21-

28.

[19] G. Liu, Z. Zhao, L. He, Highly selective lithium recovery from high Mg/Li ratio brines, Desalination, 474 (2020) 114185.

[20] X. Li, C. Zhang, S. Zhang, J. Li, B. He, Z. Cui, Preparation and characterization of positively charged polyamide composite nanofiltration hollow fiber membrane for lithium and magnesium separation, Desalination, 369 (2015) 26-36.

[21] W. Li, C. Shi, A. Zhou, X. He, Y. Sun, J. Zhang, A positively charged composite nanofiltration membrane modified by EDTA for LiCl/$MgCl_2$ separation, Separation and Purification Technology, 186 (2017) 233-242.

[22] C. Guo, N. Li, X. Qian, J. Shi, M. Jing, K. Teng, Z. Xu, Ultra-thin double Janus nanofiltration membrane for separation of Li^+ and Mg^{2+}: "Drag" effect from carboxyl-containing negative interlayer, Separation and Purification Technology, 230 (2020) 115567.

[23] P. Xu, W. Wang, X. Qian, H. Wang, C. Guo, N. Li, Z. Xu, K. Teng, Z. Wang, Positive charged PEI-TMC composite nanofiltration membrane for separation of Li^+ and Mg^{2+} from brine with high Mg^{2+}/Li^+ ratio, Desalination, 449 (2019) 57-68.

[24] H.-Z. Zhang, Z.-L. Xu, H. Ding, Y.-J. Tang, Positively charged capillary nanofiltration membrane with high rejection for Mg^{2+} and Ca^{2+} and good separation for Mg^{2+} and Li^+, Desalination, 420 (2017) 158-166.

[25] J. Lyu, X. Wen, U. Kumar, Y. You, V. Chen, R.K. Joshi, Separation and purification using GO and r-GO membranes, RSC Advances, 8 (2018) 23130-23151.

[26] C. Cheng, G. Jiang, C.J. Garvey, Y. Wang, G.P. Simon, Jefferson Z. Liu, D. Li, Ion transport in complex layered graphene-based membranes with tuneable interlayer spacing, Science Advances, 2 (2016) e1501272-e1501272.

[27] P. Zhang, J.-L. Gong, G.-M. Zeng, B. Song, S. Fang, M. Zhang, H.-Y. Liu, S.-Y. Huan, P. Peng, Q.-Y. Niu, D.-B. Wang, J. Ye, Enhanced permeability of rGO/S-GO layered membranes with tunable inter-structure for effective rejection of salts and dyes, Separation and Purification Technology, 220 (2019) 309-319.

[28] F. Pan, Y. Li, Y. Song, M. Wang, Y. Zhang, H. Yang, H. Wang, Z. Jiang, Graphene

oxide membranes with fixed interlayer distance via dual crosslinkers for efficient liquid molecular separations, Journal of Membrane Science, 595 (2020) 117486.

[29] R.R. Nair, H.A. Wu, P.N. Jayaram, V. Grigorieva, A.K. Geim, Unimpeded permeation of water through helium-leak–tight graphene-based membranes, Science, 335 (2012) 442-444.

[30] N. Song, X. Gao, Z. Ma, X. Wang, Y. Wei, C. Gao, A review of graphene-based separation membrane: Materials, characteristics, preparation and applications, Desalination, 437 (2018) 59-72.

[31] A. Anand, B. Unnikrishnan, J.-Y. Mao, H.-J. Lin, C.-C. Huang, Graphene-based nanofiltration membranes for improving salt rejection, water flux and antifouling–A review, Desalination, 429 (2018) 119-133.

[32] M. Shan, H. Kang, Z. Xu, N. Li, M. Jing, Y. Hu, K. Teng, X. Qian, J. Shi, L. Liu, Decreased cross-linking in interfacial polymerization and heteromorphic support between nanoparticles: Towards high-water and low-solute flux of hybrid forward osmosis membrane, J Colloid Interface Sci, 548 (2019) 170-183.

[33] W. Choi, J. Choi, J. Bang, J.H. Lee, Layer-by-layer assembly of graphene oxide nanosheets on polyamide membranes for durable reverse-osmosis applications, ACS Appl Mater Interfaces, 5 (2013) 12510-12519.

[34] Q. Nan, P. Li, B. Cao, Fabrication of positively charged nanofiltration membrane via the layer-by-layer assembly of graphene oxide and polyethylenimine for desalination, Applied Surface Science, 387 (2016) 521-528.

[35] J. Yin, G. Zhu, B. Deng, Graphene oxide (GO) enhanced polyamide (PA) thin-film nanocomposite (TFN) membrane for water purification, Desalination, 379 (2016) 93-101.

[36] J. Wang, C. Zhao, T. Wang, Z. Wu, X. Li, J. Li, Graphene oxide polypiperazine-amide nanofiltration membrane for improving flux and anti-fouling in water purification, RSC Adv., 6 (2016) 82174-82185.

[37] S. Bano, A. Mahmood, S.-J. Kim, K.-H. Lee, Graphene oxide modified polyamide nanofiltration membrane with improved flux and antifouling properties, Journal of

Materials Chemistry A, 3 (2015) 2065-2071.

[38] T. Wu, B. Zhou, T. Zhu, J. Shi, Z. Xu, C. Hu, J. Wang, Facile and low-cost approach towards a PVDF ultrafiltration membrane with enhanced hydrophilicity and antifouling performance via graphene oxide/water-bath coagulation, RSC Advances, 5 (2015) 7880-7889.

[39] Z. Xu, T. Wu, J. Shi, W. Wang, K. Teng, X. Qian, M. Shan, H. Deng, X. Tian, C. Li, F. Li, Manipulating Migration Behavior of Magnetic Graphene Oxide via Magnetic Field Induced Casting and Phase Separation toward High-Performance Hybrid Ultrafiltration Membranes, ACS Appl Mater Interfaces, 8 (2016) 18418-18429.

[40] Z. Xu, T. Wu, J. Shi, K. Teng, W. Wang, M. Ma, J. Li, X. Qian, C. Li, J. Fan, Photocatalytic antifouling PVDF ultrafiltration membranes based on synergy of graphene oxide and TiO_2 for water treatment, Journal of Membrane Science, 520 (2016) 281-293.

[41] M. Hu, Z. Cui, J. Li, L. Zhang, Y. Mo, D.S. Dlamini, H. Wang, B. He, J. Li, H. Matsuyama, Ultra-low graphene oxide loading for water permeability, antifouling and antibacterial improvement of polyethersulfone/sulfonated polysulfone ultrafiltration membranes, J Colloid Interface Sci, 552 (2019) 319-331.

[42] N.N. Gumbi, M. Hu, B.B. Mamba, J. Li, E.N. Nxumalo, Macrovoid-free PES/SPSf/O-MWCNT ultrafiltration membranes with improved mechanical strength, antifouling and antibacterial properties, Journal of Membrane Science, 566 (2018) 288-300.

[43] S. Zinadini, A.A. Zinatizadeh, M. Rahimi, V. Vatanpour, H. Zangeneh, Preparation of a novel antifouling mixed matrix PES membrane by embedding graphene oxide nanoplates, Journal of Membrane Science, 453 (2014) 292-301.

[44] L. Yu, Y. Zhang, B. Zhang, J. Liu, H. Zhang, C. Song, Preparation and characterization of HPEI-GO/PES ultrafiltration membrane with antifouling and antibacterial properties, Journal of Membrane Science, 447 (2013) 452-462.

[45] L. Zhang, Z. Cui, M. Hu, Y. Mo, S. Li, B. He, J. Li, Preparation of PES/SPSf blend ultrafiltration membranes with high performance via H2O-induced gelation phase

separation, Journal of Membrane Science, 540 (2017) 136-145.

[46] G. Zhao, R. Hu, J. Li, H. Zhu, Graphene oxide quantum dots embedded polysulfone membranes with enhanced hydrophilicity, permeability and antifouling performance, Science China Materials, 62 (2019) 1177-1187.

[47] G.S. Lai, W.J. Lau, P.S. Goh, A.F. Ismail, N. Yusof, Y.H. Tan, Graphene oxide incorporated thin film nanocomposite nanofiltration membrane for enhanced salt removal performance, Desalination, 387 (2016) 14-24.

[48] Y.C. Xu, Z.X. Wang, X.Q. Cheng, Y.C. Xiao, L. Shao, Positively charged nanofiltration membranes via economically mussel-substance-simulated co-deposition for textile wastewater treatment, Chemical Engineering Journal, 303 (2016) 555-564.

[49] M. Kumar, Z. Gholamvand, A. Morrissey, K. Nolan, M. Ulbricht, J. Lawler, Preparation and characterization of low fouling novel hybrid ultrafiltration membranes based on the blends of GO-TiO_2 nanocomposite and polysulfone for humic acid removal, Journal of Membrane Science, 506 (2016) 38-49.

[50] S. Aditya Kiran, Y. Lukka Thuyavan, G. Arthanareeswaran, T. Matsuura, A.F. Ismail, Impact of graphene oxide embedded polyethersulfone membranes for the effective treatment of distillery effluent, Chemical Engineering Journal, 286 (2016) 528-537.

[51] A. Abdel-Karim, S. Leaper, M. Alberto, A. Vijayaraghavan, X. Fan, S.M. Holmes, E.R. Souaya, M.I. Badawy, P. Gorgojo, High flux and fouling resistant flat sheet polyethersulfone membranes incorporated with graphene oxide for ultrafiltration applications, Chemical Engineering Journal, 334 (2018) 789-799.

[52] W. Fang, L. Shi, R. Wang, Mixed polyamide-based composite nanofiltration hollow fiber membranes with improved low-pressure water softening capability, Journal of Membrane Science, 468 (2014) 52-61.

[53] N. Meng, R.C.E. Priestley, Y. Zhang, H. Wang, X. Zhang, The effect of reduction degree of GO nanosheets on microstructure and performance of PVDF/GO hybrid membranes, Journal of Membrane Science, 501 (2016) 169-178.

[54] C. Zhao, X. Xu, J. Chen, F. Yang, Effect of graphene oxide concentration on the

morphologies and antifouling properties of PVDF ultrafiltration membranes, Journal of Environmental Chemical Engineering, 1 (2013) 349-354.

[55] H.-R. Chae, J. Lee, C.-H. Lee, I.-C. Kim, P.-K. Park, Graphene oxide-embedded thin-film composite reverse osmosis membrane with high flux, anti-biofouling, and chlorine resistance, Journal of Membrane Science, 483 (2015) 128-135.

[56] Z. Wang, H. Yu, J. Xia, F. Zhang, F. Li, Y. Xia, Y. Li, Novel GO-blended PVDF ultrafiltration membranes, Desalination, 299 (2012) 50-54.

[57] J. Lee, H.-R. Chae, Y.J. Won, K. Lee, C.-H. Lee, H.H. Lee, I.-C. Kim, J.-m. Lee, Graphene oxide nanoplatelets composite membrane with hydrophilic and antifouling properties for wastewater treatment, Journal of Membrane Science, 448 (2013) 223-230.

[58] M. Ionita, A.M. Pandele, L. Crica, L. Pilan, Improving the thermal and mechanical properties of polysulfone by incorporation of graphene oxide, Composites Part B: Engineering, 59 (2014) 133-139.

[59] U.R. Farooqui, A.L. Ahmad, N.A. Hamid, Graphene oxide: A promising membrane material for fuel cells, Renewable and Sustainable Energy Reviews, 82 (2018) 714-733.

[60] Q. Shen, S.J. Xu, Z.L. Xu, H.Z. Zhang, Z.Q. Dong, Novel thin-film nanocomposite membrane with water-soluble polyhydroxylated fullerene for the separation of Mg^{2+}/Li^{+} aqueous solution, Journal of Applied Polymer Science, 136 (2019) 48029.

[61] S.-Y. Sun, L.-J. Cai, X.-Y. Nie, X. Song, J.-G. Yu, Separation of magnesium and lithium from brine using a Desal nanofiltration membrane, Journal of Water Process Engineering, 7 (2015) 210-217.

[62] G. YANG, H. SHI, W. LIU, W. XINGN, a. XU, Investigation of Mg^{2+}/Li^{+} Separation by Nanofiltration, Chinese Journal of Chemical Engineering, 19 (2011) 586-591.

Chapter 3

✵✵✵✵✵✵✵✵✵✵✵✵✵✵✵✵✵✵✵✵✵✵✵✵✵✵✵✵

Novel aminated graphene quantum dots (GQDs-NH_2)-engineered nanofiltration membrane with high Mg^{2+}/Li^{+} separation efficiency

✵✵✵✵✵✵✵✵✵✵✵✵✵✵✵✵✵✵✵✵✵✵✵✵✵✵✵✵

3 Novel aminated graphene quantum dots (GQDs-NH_2)-engineered nanofiltration membrane with high Mg^{2+}/Li^+ separation efficiency

3.1 Introduction

In order to further improve the lithium extraction of the membrane, we optimized the properties of the nanofiltration (NF) membrane by modify the structure of the formed polyamide layer. The NF membranes have outstanding performance for water treatment [1-4] due to its specific characteristics [5-7]. To effectively enrich lithium from salt-lakes, it is critical to resolving the issue of Mg^{2+}/Li^+ separation [8-14].

The NF membrane has been verified as a feasible method for separating divalent Mg^{2+} and monovalent Li^+ [15-17], especially the positively charged NF membranes [5, 10, 18, 19]. The NF membrane is commonly composed of the base-membrane and selective thin layer. The dual-effect of membrane chargeability and structure determines the separation capacity of divalent and monovalent ions. Xu et al. fabricated a highly positively charged NF membrane on the polyethersulfone (PES) ultrafiltration (UF) film surface via interfacial polymerization between polyethyleneimine (PEI) and TMC [20]. The final membrane was endowed with a high positive chargeability due to a significant amount of protonated $-NH_n^+$ (n=2, 3) and performed outstandingly during Mg^{2+}/Li^+ separation. Due to the existence of the "trade-off" effect, it is hard to simultaneously control both high separation ability and permeability of the NF membrane. The low permeation flux of NF membrane may significantly limit its work efficiency and practical applications.

During the synthesis process, carbon-based nano-additives, such as carbon nanotube and its derivatives [4, 21-23] as well as graphene oxide (GO) and its

derivatives, have been embedded into the membrane to improve the permeation flux of membrane [24-27]. After doping with such additives, the final membrane is endowed with superior properties of both polymer materials and carbon-based nanomaterials. Due to the unique structure and large quantities of oxygen-bearing functional groups (e.g., carboxyl, epoxy, and hydroxyl) at the edge of the GO nanosheet, the incorporated GO additives can optimize the properties of membrane (e.g., mechanical, antifouling, and hydrophilicity). Graphene oxide quantum dots (GQDs) are zero-dimensional carbon-based nanomaterial [28] that considered as the GO with small size of 3~20 nm [29]. GQDs inherit most of the excellent characteristics of GO, whereas GQDs have an edge-volume ratio higher than that of GO nanosheet [30-32]. The smaller size and oxygen-bearing functional groups of GQDs make GQDs a better substitute for GO, these features have garnered increased interest in GQDs. Bi et al. introduced GQDs into the selective thin layer during polymerization between PIP and TMC [33]. Due to the presence of GQDs in the selective layer, the flux of the modified NF membrane reached 6.8 times that of the pure membrane. Similarly, Seyedpoura et al. added GQDs into the interfacial polymerization layer formed by 1,3-phenylendiamine (MPD) and TMC [29]. They surprisingly found that the antifouling and permeation performance of the final composite membranes were significantly improved after GQDs were incorporated into the selective layer. The small size endows GQDs with more edges and oxygen-bearing functional groups, making it easier to uniformly disperse in the membrane. Therefore, the hydrophilicity of the membrane was improved, making it effective to inhibit pollutants.

However, incorporation of GQDs into the polyamide layer will weaken the positive charge density of membrane to a certain degree due to the hydrolysis of -COOH in GQDs. Recently, researchers have reported some functionalized GQDs (e.g., PEI-functionalized GQDs, fluorine-functionalized GQDs, and amino-functionalized GQDs (GQDs-NH_2)) [34-36], which have significantly expanded the application of GQDs in various fields. By grafting amine groups (-NH_2) at the edge of GQDs, the obtained GQDs-NH_2 can not only inherit the advantage of GQDs but also carry some amine

groups (-NH_2). The GQDs-NH_2 additives can act as aqueous monomers to introduce more -NH_2 and -OH groups during interfacial polymerization, thereby improving the properties of NF membranes (e.g., morphologies, hydrophilicity, and chargeability). Till now, no one has reported the research on Mg^{2+}/Li^{+} separation using NF membrane modified with nano-sized GQDs-NH_2. In this study, we embedded GQDs-NH_2 into the aqueous phase during polymerization to prepare a novel GQDs-NH_2 incorporated NF membrane with high Mg^{2+}/Li^{+} separation efficiency. The structure and properties of NF membranes with different incorporating content of GQDs-NH_2 were analyzed by several characterization methods. In addition, the effect of doped GQDs-NH_2 on the Mg^{2+}/Li^{+} separation capability, permeation efficiency and antifouling performance of the final NF membrane was extensively discussed.

3.2 Experimental

3.2.1 Materials and regents

PES (3000P, 62000 g/mol) was supplied by Solvay Advanced Polymer (Belgium). Polyethylene glycol (PEG), N, N-dimethylacetamide (DMAc), PEI, sodium dodecyl sulfate (SDS), TMC, n-hexane, $NaCO_3$, NaCl, LiCl, $MgCl_2$, $CaCl_2$, $MgSO_4$, and Na_2SO_4 were all purchased from Wako Pure Chemical Industries Ltd., Japan. GQDs-NH_2 was provided by Nanjing XFNANO Materials Tech. Co. Ltd.

3.2.2 Formation of GQDs-NH_2 modified membranes

The PES UF substrate film was formed via the phase inversion method [37, 38]. The pristine PES base membrane was first immersed in the aqueous solution comprising PEI (5 wt%), GQDs-NH_2, SDS (0.1 wt%, surfactant) and Na_2CO_3 (0.1 wt%, acid acceptance agent) [20]. After immersion in the aqueous phase solution for 5 min, the aqueous solution was removed using a rubber roller. Next, the obtained amine-saturated membrane was covered by the organic phase solution comprising 0.1% (w/v) TMC and n-hexane. After 3 min, the organic solution was removed, and then, the

membrane was heat-treated in an oven at 70 °C for 10 min. Finally, the obtained NF membranes were stored in deionized water before performance characterization. The obtained NF membranes with different incorporating content of GQDs-NH_2 (0 wt%, 0.005 wt%, 0.01 wt%, 0.03 wt%, 0.05 wt%, and 0.1 wt%) were named as NF-0, NF-0.005, NF-0.01, NF-0.03, NF-0.05, and NF-0.1, respectively.

3.2.3 Characterization of GQDs-NH_2 incorporated NF membrane

The surface topology and microstructure images of membranes were described using the atomic force microscopy (AFM, Shimadzu SPM-9500J3, Japan) and the field emission scanning electron microscopy (FESEM, Hitachi S-5000, Japan). The characterization of chemical functional groups in membranes was analyzed by fourier-transform infrared spectroscopy (ATR-FTIR, Shimadzu Co., Ltd., Japan). X-ray photoelectron spectroscopy (XPS, AXIS-ULTRA DLD, KRATOS) was used to measure element compositions of membranes. The water contact angle (CA, digidrop, GBX, Whitestone way, France) was adopted for assessing the impact of GQDs-NH_2 dosage on the hydrophilicity of the NF membrane surface. In addition, the electrokinetic analyzer (Sur-PASS TM3 Anton Paar, GmbH, Austria) was applied to test the chargeability of membrane surface. Furthermore, the particle size and morphology of GQDs-NH_2 were captured by the high-resolution transmission electron microscopy (HRTEM, JEOL JEM 2010).

3.2.4 NF performance test for GQDs-NH_2 incorporated NF membrane

NF performance was characterized via a cross-flow filtration equipment with an effective test area of 12.56 cm^2 under a pressure of 3 bar. Each membrane was pre-performed for 0.5 h at 4 bar to stabilize the flux with the pure water, and then, the pressure was adjusted to 3 bar to start the test. Each test was conducted at least five times to get an average value. The permeation flux F (L/m^2hbar) was calculated using

equation (1):

$$\mathrm{F} = \frac{V}{S \times T \times P} \quad (1)$$

In which, V (L), S (m^2), T (h), and P (bar) denote the permeate volume, effective test area, filtration time, and operation pressure during the test process, respectively. The rejection R of membrane was evaluated using equation (2):

$$\mathrm{R} = (1 - \frac{C_2}{C_1}) \times \% \quad (2)$$

In which, C_1 and C_2 denote the concentrations of feed and permeation solutions, respectively. The molecular weight cut-off (MWCO) of membrane was evaluated by filtering 50 mg/L PEG aqueous with various molecular weight. The total organic carbon analyzer (TOC-VCSH; Shimadzu Co., Kyoto, Japan) was used to measure the concentration of PEG in feed and permeate solution. The MWCO of membrane was denoted as the molecular weight of PEG with a rejection for 90%. The pore radius of membrane can be calculated using equation (3) [39]:

$$r = 0.0397 MWCO^{0.43} \quad (3)$$

Additionally, the separation performance of the NF membrane for Mg^{2+} and Li^{+} was evaluated by a separation factor SF, which can be calculated using equation (4):

$$\mathrm{SF} = \frac{R^2_{Mg/Li}}{R^1_{Mg/Li}} \quad (4)$$

In which, $R^1_{Mg/Li}$ and $R^2_{Mg/Li}$ denote the Mg^{2+}/Li^{+} in the feed and permeation solution, respectively. The feed solution (2g/L) is a mixed solution comprising $MgCl_2$ and LiCl, in which the initial value of Mg^{2+}/Li^{+} is 20.

To evaluate the anti-fouling ability of membranes, the membrane was first tested for 12 h with the pure water to obtain the stable flux F_1. The simulated BSA fouling solution (0.1g/L) was then filtered through the membrane for 12 h. Finally, the membrane was washed for 1 h with pure water and filtered for another 12h with pure water to get the stable flux F_2. The flux recovery rate FRR after cleaning was calculated as follows:

$$\mathrm{FRR} = \frac{F_2}{F_1} \times 100\% \quad (5)$$

3.3 Result and discussion

3.3.1 Characterization of membrane chemical structures

According to the wide scan result of XPS in Fig.3-1 (a), each membrane displayed two sharp emission peaks near 285.1 and 531.2 eV, corresponding to C1s and O1s, respectively. Obviously, a new major emission peak at around 399.5 eV appeared in the spectra of each NF membrane, indicating the successful introduction of N element. Moreover, compared to the PES base film , two peaks at 168.21 eV (S2p) and 229.45 eV (S2s) can barely be observed on the spectra of NF membranes due to the new polymerization layer covering the PES substrate surface [20].

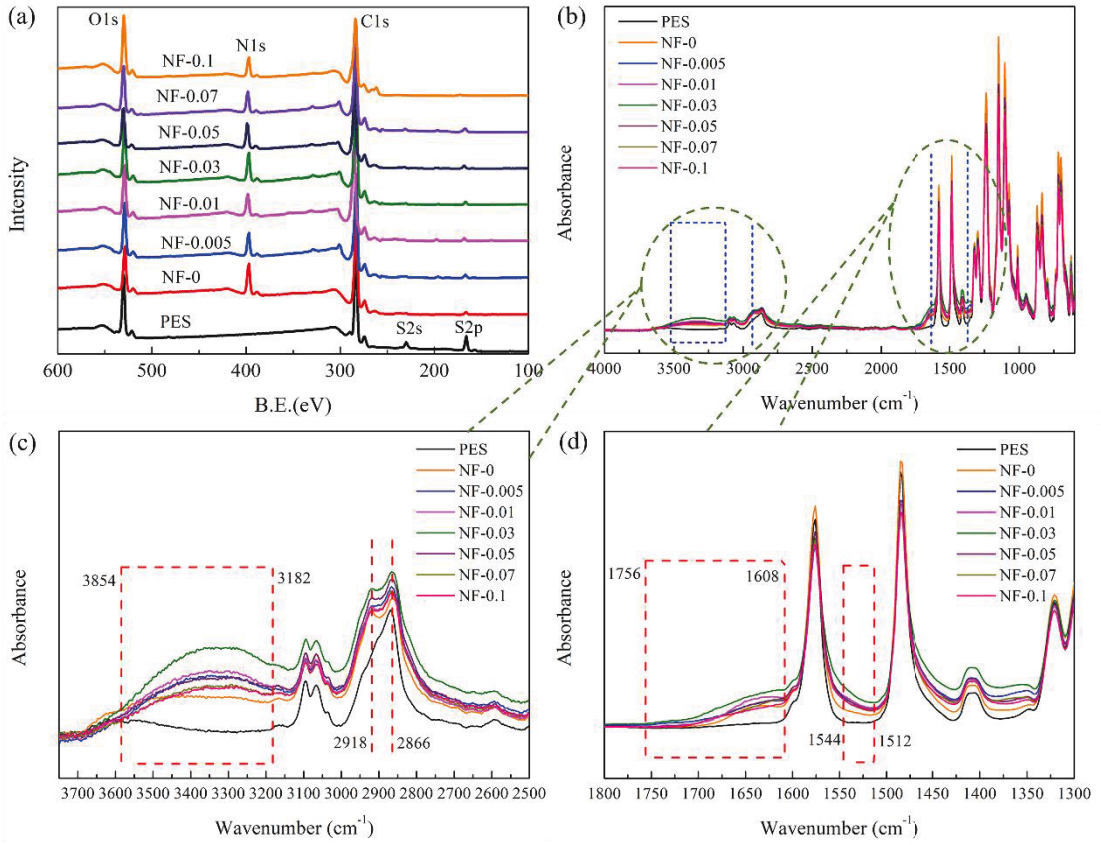

Fig.3-1. (a) XPS wide scan, ATR-FTIR spectra range from (b) 4000 cm^{-1} to 600 cm^{-1}, (c) 3750 cm^{-1} to 2500 cm^{-1}, and (d) 1800 cm^{-1} to 1300 cm^{-1} of all membranes

As shown in Figs.3-1b, 3-1c, and 3-1d, ATR-FTIR results were applied to further analyze changes in the membrane functional groups. A new broad peak in the range of 3182 ~ 3854 cm^{-1} appeared after interfacial polymerization, which corresponds to the

stretching vibration of both -OH and residual -NH_2 [21, 40]. The findings can be explained as the high molecular weight PEI monomers carry a significant number of amine groups -NH_2. The unreacted-NH_2 will remain on the polyamide thin layer after interfacial polymerization [19, 41]. Compared to the pure NF-0 membrane, the GQDs-NH_2 incorporated NF membrane showed a stronger peak at 3182 ~ 3854 cm^{-1}. The doped GQDs-NH_2 monomers introduce a large amount of -OH and -NH_2 into the interfacial polymerization system, resulting in more unreacted -OH and -NH_2 remaining in the thin polyamide layer. Similarly, a new peak at 2918 cm^{-1} consistent with NH_n^+ (n=2, 3) appeared on each NF membrane spectrum, and the peak intensity of GQDs-NH_2 incorporated NF membrane was higher than that of the pure NF-0 membrane. According to Fig.3-1(d), the typical amide stretching vibration bands at 1608 ~ 1756 cm^{-1} (C=O, amide-I) and 1512 ~ 1544 cm^{-1} (N-H, amide-II) appeared on each NF membrane, which confirms the success of polymerization and formation of the thin polyamide layer [42, 43]. Note that in each GQDs-NH_2 incorporated NF membrane, the stretching vibration intensity of amide groups was significantly higher than that in the pure NF-0 membrane, which reflected the polymerization among PEI, GQDs-NH_2, and TMC. The -OH and -NH_2 groups in the monomer GQDs-NH_2 can react with TMC during interfacial polymerization.

Fig.3-2 and Table 3-1 show the deconvolution results of C1s and N1s XPS spectra of NF membranes with different GQDs-NH_2 embedding contents, which can be used to further measure and analyze the effect of GQDs-NH_2 dosage on the chemical structure of NF membranes. The C1s spectra can be divided into five statuses, including C-C, C-N, C-O, N-C=O, and O-C=O, which are located at about 284.5, 285.7, 286.3, 287.8, and 288.5 eV, respectively. According to the results, with the increase of GQDs-NH_2 embedding content from 0% to 0.03%, the percent of N-C=O and O-C=O changed significantly from 9.15% to 12.58% and from 3.18% to 2.13%, respectively. However, with a further addition of GQDs-NH_2 content from 0.03% to 0.1%, the percent of N-C=O and O-C=O slightly changed from 12.58% to 12.11% and from 2.13% to 2.48%, respectively.

The N-C=O and O-C=O mainly originated from amide -CONH- and carboxyl -COOH hydrolyzed by acid chloride -COCl, respectively. -NH_2 at the edge of nano-sized GQDs-NH_2 can polymerize with acid chloride -COCl in TMC monomers during interfacial polymerization [36], producing more amide -CONH-. Moreover, the higher the GQDs-NH_2 content, the more the acid chloride -COCl in TMC will be consumed, resulting in less -COOH in the polyamide layer [43]. Compared to the pure NF-0 membrane, the GQDs-NH_2 incorporated NF membrane had a higher ratio value of N-C=O/O-C=O, indicating the enhanced crosslinking degree between GQDs-NH_2 and TMC. GQDs-NH_2 monomer participated in the polymerization process, strengthening the interaction of PEI/ GQDs-NH_2/TMC and stabilizing the distribution of GQDs-NH_2 in the thin polyamide layer. However, with a high GQDs-NH_2 content of more than 0.03%, the ratio value of N-C=O/O-C=O slightly decreased. For high incorporating content, GQDs-NH_2 may unevenly distribute and aggregate in the membrane surface, causing lower interaction among PEI, GQDs-NH_2, and TMC.

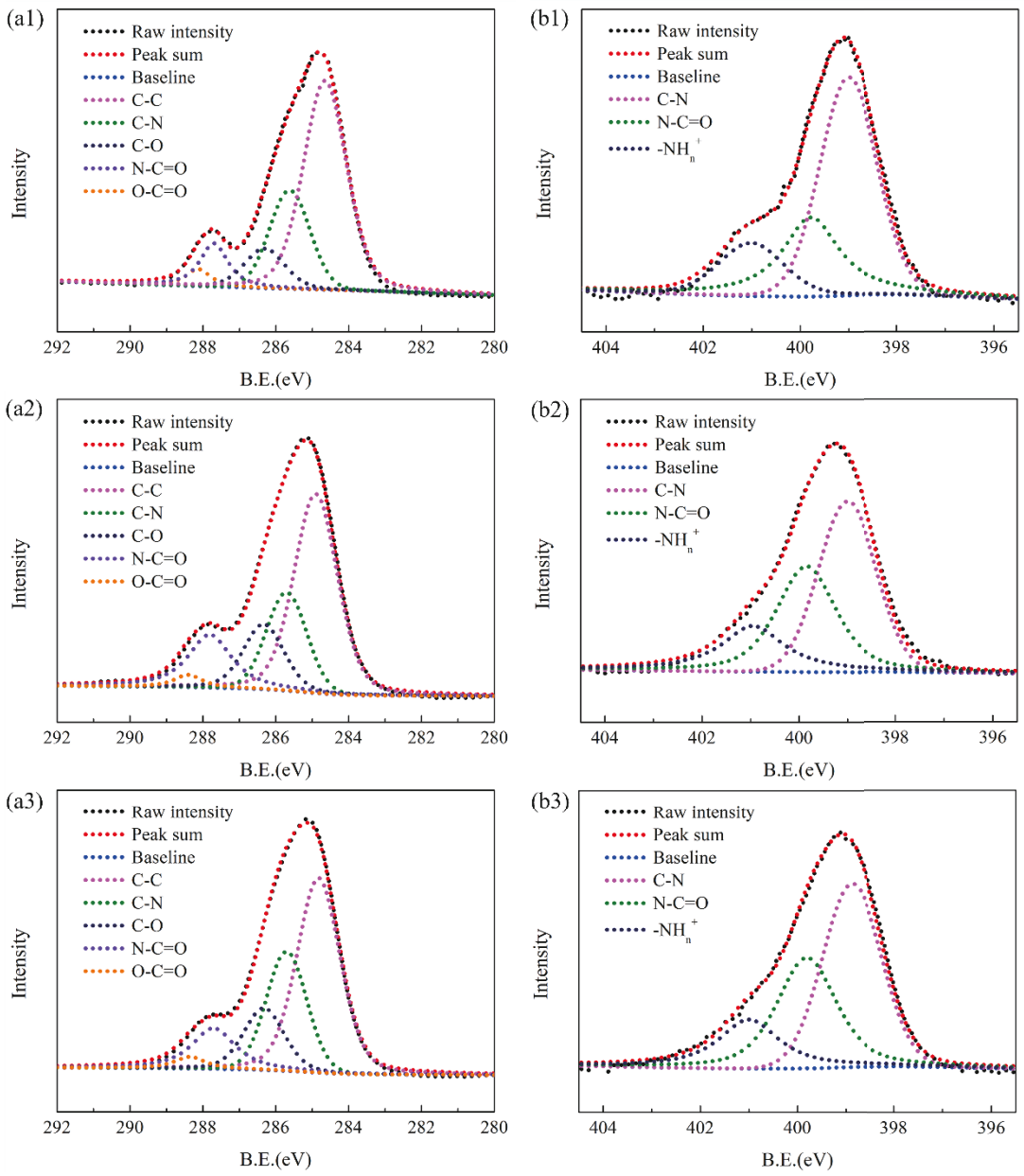

Fig.3-2. Deconvolution of (a) C1s and (b) N1s spectra of NF membranes incorporated with different contents of GQDs-NH_2: (1) NF-0, (2) NF-0.03, and (3) NF-0.1.

The N1s spectra can be divided into three peaks, located at 398.9, 399.7, and 401.1 eV, corresponding to nitrogen species C-N, N-C=O, and -NH_n^+ (n=2, 3), respectively. As more amide groups were formed by GQDs-NH_2 and TMC, the ratio of N-C=O in the GQDs-NH_2 incorporated NF membrane was higher than that of the pure membrane NF-0. Furthermore, a similar trend can be found in the change of -NH_n^+ (n=2, 3) species. By doping GQDs-NH_2, more free amine groups will be introduced into the interfacial polymerization system. Therefore, more residua amine groups will be present in the

thin polyamide layer, leading to more protonated -NH_n^+ (n=2, 3) on the membrane surface. In summary, a suitable incorporation content of GQDs-NH_2 in the thin polyamide layer may promote the crosslinking of PEI/GQDs-NH_2/TMC and establish a stable interaction between GQDs-NH_2 and polyamide layer.

Table 3-1 XPS results originated from C1s and N1s spectra.

Membrane	C 1s		N 1s	
	Species	Percent (%)	Species	Percent (%)
NF-0	C-C	55.55	C-N	55.34
	C-N	22.31	O-C=N	28.3
	C-O	9.8	NH_n^+	16.35
	N-C=O	9.15		
	O-C=O	3.18		
NF-0.03	C-C	46.46	C-N	45.27
	C-N	23.23	O-C=N	35.18
	C-O	12.41	NH_n^+	19.55
	N-C=O	15.58		
	O-C=O	2.31		
NF-0.1	C-C	47.01	C-N	46.72
	C-N	24.52	O-C=N	34.75
	C-O	13.87	NH_n^+	18.52
	N-C=O	12.11		
	O-C=O	2.48		

3.3.2 Morphology structure characterization of membrane

FESEM and AFM analysis characterized the effect of embedded GQDs-NH_2 on the morphology structure of the NF membrane. As shown in Fig.3-3, due to the polymerization between high molecular weight monomer PEI and TMC, typical valley-ridge like wrinkle structures appeared on the surface of pure NF-0 membrane. Due to the crosslinking between GQDs-NH_2 and TMC, we found that many small valley-

ridges were filled in the large valley-ridge wrinkle structure after the incorporation of the nano-sized monomer GQDs-NH_2. As stated in the chemical structure characterization section, the incorporated GQDs-NH_2 can promote crosslinking and interaction among PEI, GQDs-NH_2, and TMC. Compared to the highly branched macromolecules PEI, the nano-sized GQDs-NH_2 monomers with excellent water solubility can evenly distribute in the aqueous phase and can quickly react with TMC monomer to form the small valley-ridge structures. Furthermore, Figs.5(c1) and 5(c2) show that, with a high incorporation content of GQDs-NH_2, a few nodular structures appeared on the NF membrane surface, which can be illustrated by the agglomeration of excessive GQDs-NH_2 monomers [44].

As shown in Fig.3-3, all NF membranes shared a thin polyamide layer of less than 100 nm. The polymerization process between TMC and PEI was not severe as that between TMC and other small monomers due to the high-branched macromolecules of PEI, which led to a relatively thin polyamide layer compared to that obtained from other reported interfacial polymerization systems (e.g., PIP/TMC and MPD/TMC) [5, 21, 45]. The thickness of polyamide layer decreased slightly with the incorporation of GQDs-NH_2. To some extent, in the presence of GQDs-NH_2 on the surface of membrane, the steric hindrance may occur between GQDs-NH_2 and PEI, which will hinder the distribution of the PEI. On the other hand, the electrostatic repulsion effect between the cationic amine groups -NH_2 in monomer GQDs-NH_2 and PEI may also hinder the diffusion of PEI monomer and retard the polymerization between PEI and TMC, resulting in a thinner polyamide layer [35, 36]. However, the effect of GQDs-NH_2 on the thickness of polyamide layer was relatively low due to the nano size of GQDs-NH_2. In addition, a thin polyamide layer is considered to have lower transmission resistance during filtration, which helps to improve the permeation flux of membrane.

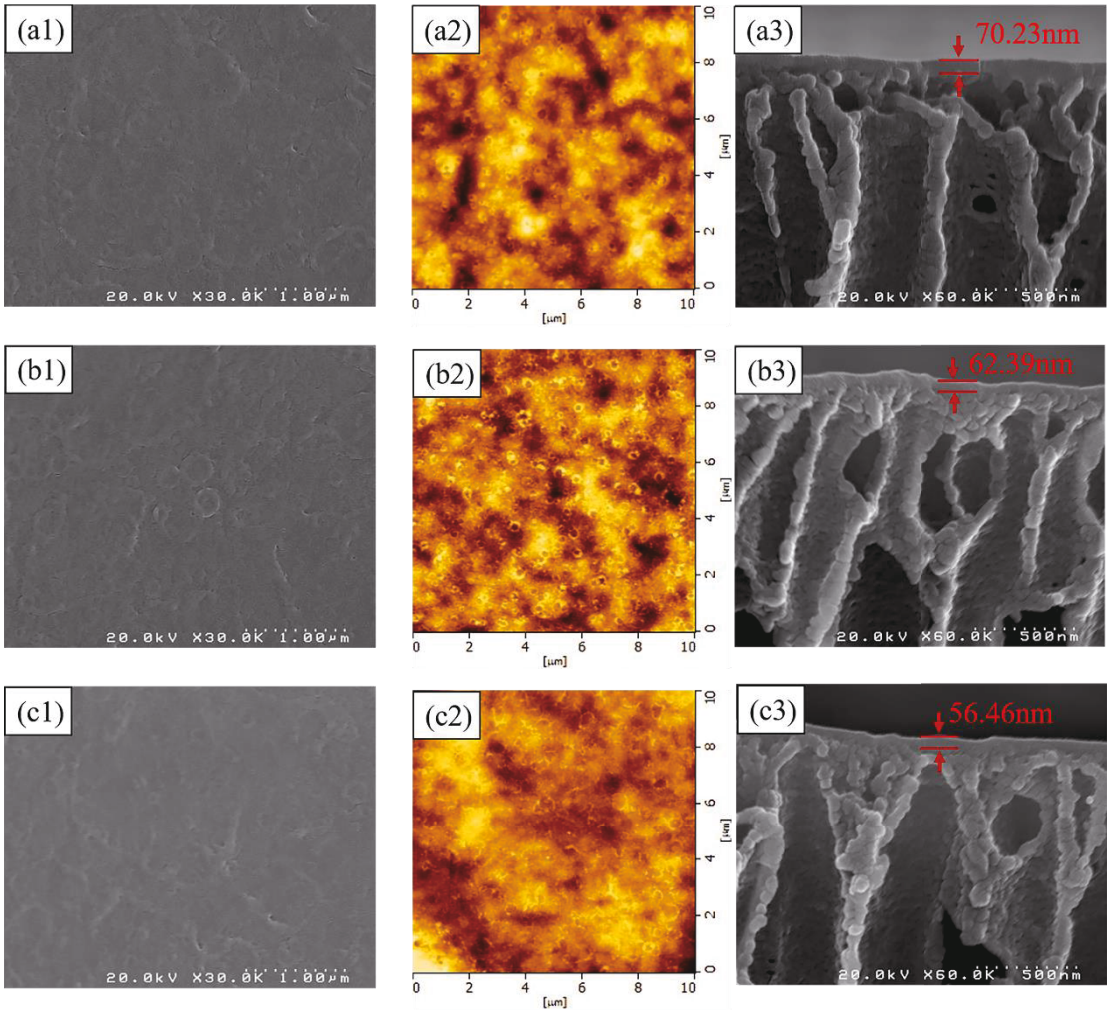

Fig.3-3. Morphology structure images of (a) NF-0, (b) NF-0.03, and (c) NF-0.1: (1) FESEM surface images, (2) AFM surface images and (3) FESEM cross section images

The average roughness (Ra) and root-mean square roughness (Rms) of each membrane were evaluated by the AFM analysis. As shown in Fig.3-4 and Table 3-2, the membrane NF-0 exhibited a rougher surface compared to the pristine PES substrate membrane due to the presence of the thin polyamide layer. In contrast, after incorporating GQDs-NH_2, the final NF membrane presented a smoother topography surface. As mentioned in the discussion of FESEM results, some small valley-ridge structures can be formed by GQDs-NH_2 and TMC, filling in the larger valley-ridge structures formed by PEI and TMC. In addition, the evenly distributed nano-sized GQDs-NH_2 monomer will occupy the valleys of the polyamide crosslinking layer, leading to a smoother surface to a certain extent.

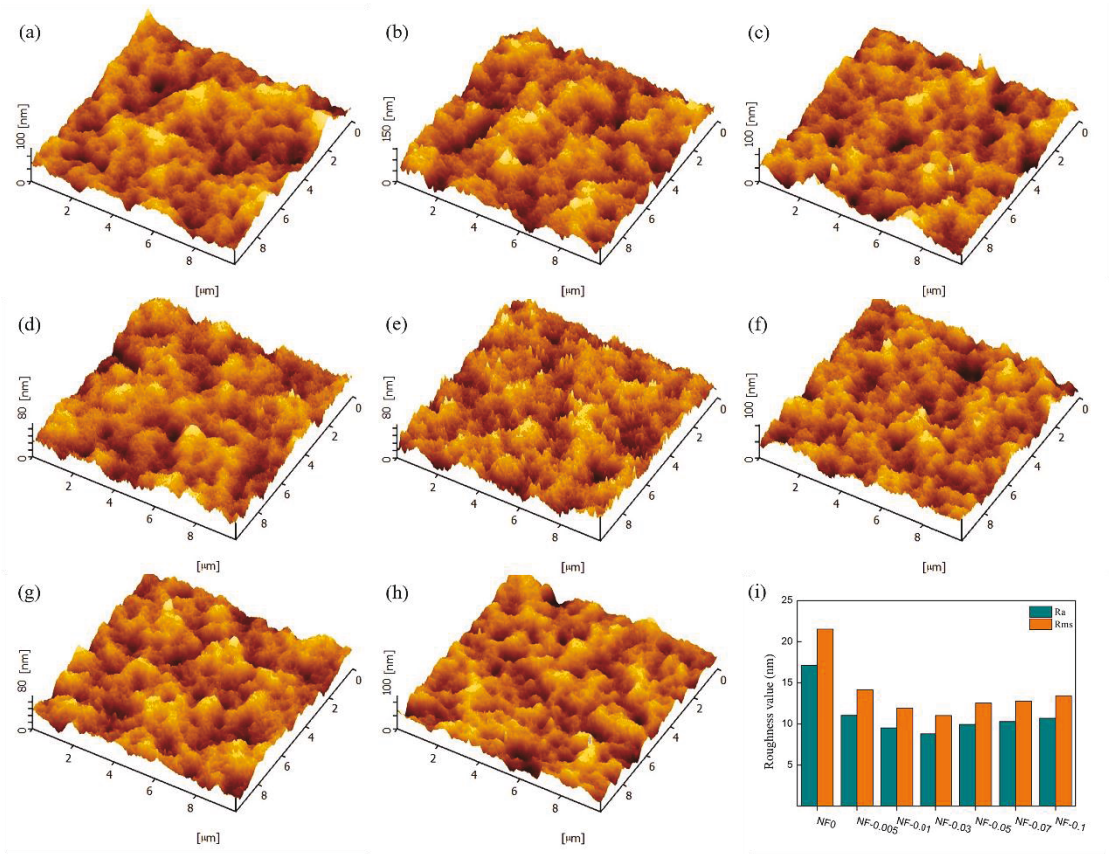

Fig.3-4. AFM topology images of membranes (a) PES pristine membrane, NF membrane with different GQDs-NH_2 doping contents (b) 0%, (c) 0.005%, (d) 0.01%, (e) 0.03%, (f) 0.05%, (g) 0.07%, and (h) 0.1%, and (i) roughness comparison of all NF membranes.

According to the AFM results, the roughness of the NF membrane surface slightly increased when the doping content of GQDs-NH_2 was higher than 0.03%. With a high incorporation content of the GQDs-NH_2 monomer, the electrostatic interaction between amine groups -NH_2 in GQDs-NH_2 and PEI may enhance accordingly, leading to a slightly looser interfacial polymerization crosslinking net between TMC and PEI [33, 46]. On the other hand, excessive GQDs-NH_2 cannot be evenly distributed in the membrane surface and may cause nano-agglomeration between GQDs-NH_2 monomers [47], resulting in a slightly rougher membrane surface. In summary, after the incorporation of the nano-sized GQDs-NH_2 monomers, the surface of the final NF membrane becomes smoother than that of the pure NF-0 membrane, and the roughness value of the membrane NF-0.03 was lowest compared to other NF membrane. It is worth noting that, the smoother membrane surface was associated with fewer adhesion

site of pollutants on the membrane surface, so that the final NF composite membrane can be endowed with a higher antifouling capacity [31, 48, 49].

Table 3-2 Roughness values of PES substrate membrane and NF membranes incorporated with different content of GQDs-NH_2

Membrane	Ra (nm)	Rms (nm)
PES	14.08	17.85
NF-0	17.13	21.52
NF-0.005	11.04	14.17
NF-0.01	9.52	11.92
NF-0.03	8.79	11.02
NF-0.05	9.94	12.54
NF-0.07	10.28	12.77
NF-0.1	10.69	13.42

3.3.3 Permeation characterization of membranes

Fig. 3-6(a-b) shows the surface hydrophilicity results of the PES substrate membrane and NF membranes, which were characterized by the CA tests. The PES substrate membrane has a contact angle of 73°. After interfacial polymerization, the contact angle of pure NF0 membrane significantly reduced to 55.9° due to the higher hydrophilicity of membrane surface. Hydrophilic amine and carboxyl groups on the membrane surface enhanced the hydrophilicity of the NF membrane. Moreover, Fig.3-6 shows that after the incorporation of GQDs-NH_2, the contact angle of the obtained NF membrane gradually decreased to 15.7° with the increase of GQDs-NH_2 content from 0 wt% to 0.1 wt%, which is much lower than that of the pure NF-0 membrane. The more GQDs-NH_2 incorporated in the polyamide layer, the more hydrophilic amine and hydroxyl groups will be introduced in the polyamide layer [36, 43], resulting in a more hydrophilic membrane surface. The improved hydrophilicity of the NF membrane helps increase the permeation flux of the membrane during filtration. The hydrated

layer formed on the hydrophilic NF membrane surface, is therefore, effective for inhibiting the adsorption and aggregation of pollutants, thereby stabilizing the NF performance of the membrane.

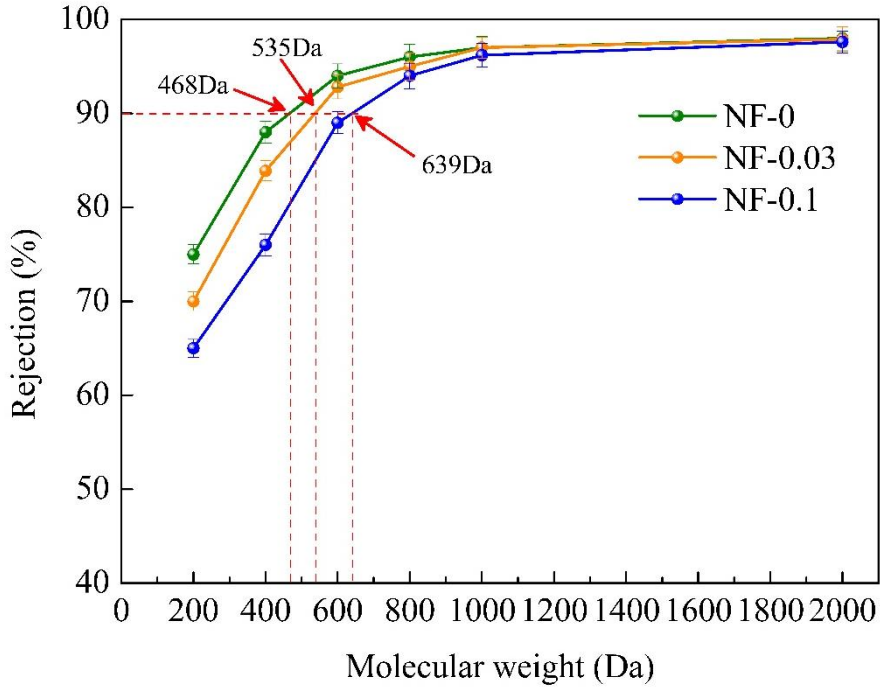

Fig. 3-5 MWCO of membrane NF-0, NF-0.03 and NF-0.1.

Fig.3-6 (c) shows the permeation flux of each NF membrane fabricated in this work. The results show that, with the increase of GQDs-NH_2 incorporation content in the polyamide layer from 0 wt% to 0.1 wt%, the permeation flux of the corresponding NF membrane was accordingly increased from 5.02 to 14.01 L/m^2hbar. After the incorporation of GQDs-NH_2, the improved hydrophilicity of the polyamide layer enhanced the water permeability of the final NF membrane. On the other hand, Fig. 3-5 shows the MWCO of membranes NF-0, NF-0.03, and NF-0.1, which can be applied to evaluate the changes in membrane pore size before and after GQDs-NH_2.embedding. According to Eq. (3), the pore radius of NF-0, NF-0.03, and NF-0.1 were approximately 0.558nm, 0.591nm, and 0.638nm, respectively, which demonstrated the slightly increased pore size of membrane after GQDs-NH_2 embedding. Based on the above discussion of the morphological structure of membranes, the incorporated GQDs-NH_2 can promote the formation of a relatively looser polyamide layer with thinner thickness, reducing the transport resistance during filtration. Fig.3-7 (e-f) show the distribution of

GQDs-NH_2 in the polyamide layer, with a low incorporation content, the GQDs-NH_2 may evenly distribute in the polyamide layer. However, Fig.3-7 (f) shows that under a high content of GQDs-NH_2, GQDs-NH_2 may stick together and form aggregated nanoparticles in the polyamide layer [44], reducing the degree of crosslinking of the polyamide layer. And the higher the content of the embedded GQDs-NH_2, the greater the interference and the competition between GQDs-NH_2 and PEI, which will result in a looser polyamide layer. Thereby, the transmission resistance will be reduced to a certain extent, which is beneficial for the water molecules for penetrating the membrane.

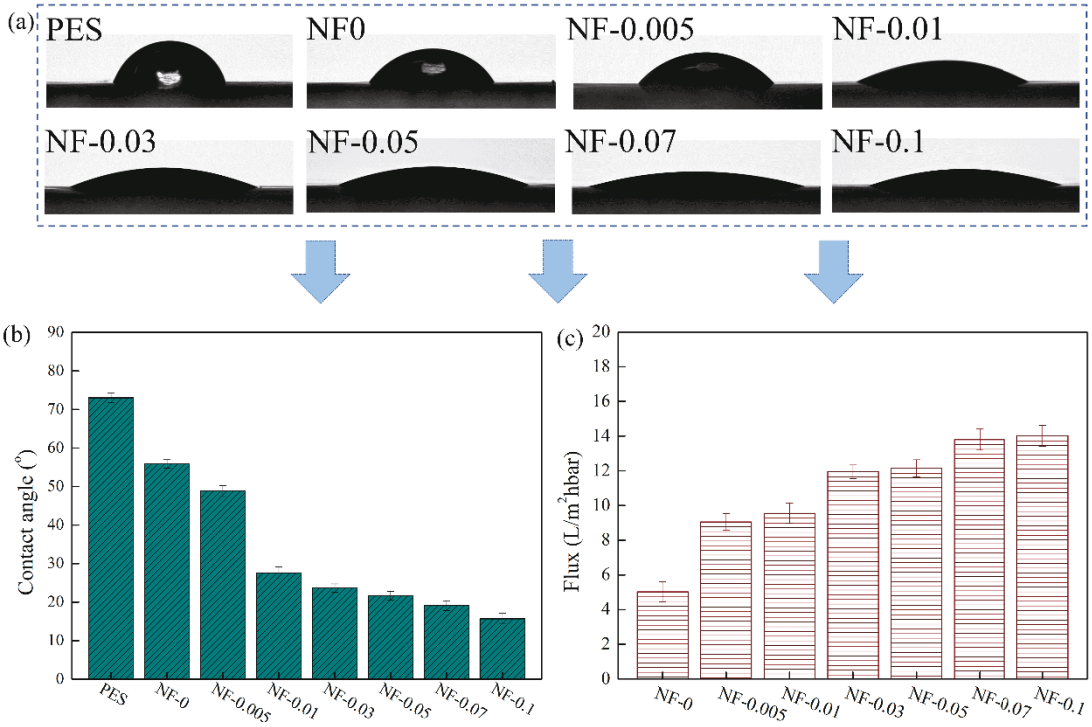

Fig.3-6. The hydrophilicity of membranes: (a) digital photos of water penetrating on membranes, (b) water contact angle of membranes, and (c) permeation flux of membranes.

In addition, the water channels formed between GQDs-NH_2 and GQDs-NH_2 and between GQDs-NH_2 and the polyamide layer can facilitate the passage of water molecules through the membrane [29, 43, 50]. As shown in Fig.3-7(b), the GO nanosheets with larger aspect ratio and lateral size tend to be horizontally distributed in the polyamide layer, thereby making the transmission path longer and more tortuous [47]. Fig.3-7(a1-a2) shows that the GQDs-NH_2 monomers used in this work have a nano-size around 30nm. As shown in Fig.3-7(c), the nano-sized GQDs-NH_2 doped in

the polyamide layer may result in a relatively shorter route with weaker transfer resistance for water molecules to pass through the membrane. Therefore, the above-mentioned multiple factors synergistically determine the water permeability of the final NF membrane. In summary, the incorporation of the nano-sized monomer GQDs-NH_2 in the polyamide layer can effectively improve the hydrophilicity and permeation flux of the final NF membrane.

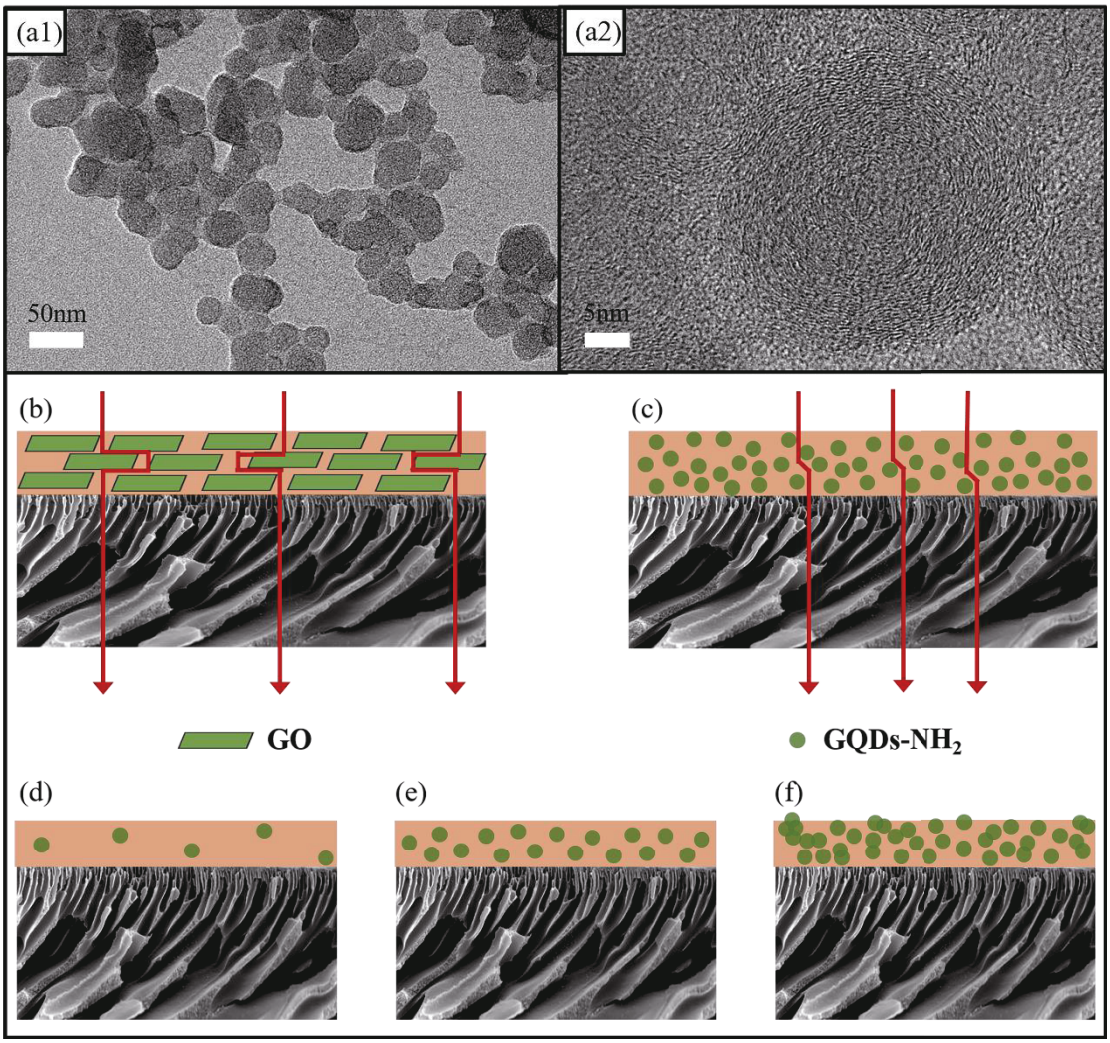

Fig.3-7. (a) TEM image of GQDs-NH_2, schematic diagrams of (b) molecular permeation in GO-doped composite membrane and (c) molecular permeation in GQDs-NH_2-incorporated composite membrane, and (d, e, f) incorporation of GQDs-NH_2, with different content.

3.3.4 Separation characterization of membranes

Fig.3-8(a) shows the charge characteristics of the membrane surface in the pH

range of 5~10, which were tested via the streaming potential method. The results show that the negatively charged PES substrate membrane has an isoelectric point lower than pH=5, while membrane NF0 showed an isoelectric point of pH=8.8. A positively charged polyamide layer was formed on the substrate membrane after interfacial polymerization between PEI and TMC on the surface of the PES substrate membrane. When the pH value in the solution is below the isoelectric point, the membrane surface is positively charged due to the protonation of the unreacted amine groups in PEI [51, 52]. Moreover, the membrane surface will exhibit negative chargeability when the pH value in the solution is higher than the isoelectric point, which is due to the deprotonated carboxyl groups hydrolyzed from unreacted acyl chloride groups in TMC [53]. In addition, it can be found that, after the incorporation of GQDs-NH_2 in the polyamide layer, the isoelectric point values of membranes NF-0.03 and NF-0.1 were slightly higher than that of the pure NF0 membrane. Besides, the isoelectric point values of membrane NF-0.1 was slightly higher than that of NF-0.03, which is corresponding with the deconvolution result of N1s XPS spectra. As discussed in the section of chemical structure characterization of the membrane, the incorporated GQDs-NH_2 during interfacial polymerization may introduce more -NH_2 into the polyamide layer and consume more acyl chloride groups in TMC, thereby leading to higher positive chargeability of the final NF membrane. In summary, the GQDs-NH_2 incorporated membrane NF-0.03 showed high positive chargeability in the feed solution used in this work (pH≈7).

Fig.3-8(b-c) illustrate the Mg^{2+}/Li^{+} separation performance of the GQDs-NH_2 incorporated NF membrane. The separation performance of the NF membrane for Mg^{2+} and Li^{+} can be evaluated by the separation factor *SF*. An *SF* value of less than 1 indicates that the NF membrane achieves separation of Mg^{2+} and Li^{+} to a certain extent. The smaller the *SF* value, the better the Mg^{2+}/Li^{+} separation ability of the NF membrane. The *SF* value of each NF membrane prepared in this work was less than 0.15, indicating that Mg^{2+} and Li^{+} can be effectively separate by these NF membranes. When the incorporation content of GQDs-NH_2 increased from 0 wt% to 0.03 wt%, the value of

SF of the NF membrane decreased from 0.05 to 0.0359, and the mass ratio of Mg^{2+}/Li^{+} in the permeation solution decreased from 1.3 to 0.7. The results indicate that the Mg^{2+}/Li^{+} separation ability of the NF membrane improved with the increase in GQDs-NH_2 content in the membrane. However, with further addition of the GQDs-NH_2 content to 0.1 wt%, the *SF* value increased significantly to 0.13, and the Mg^{2+}/Li^{+} in the permeation solution increased to 2.65. According to the results, membrane NF-0.03 had the lowest *SF* value of 0.0359, and the rejections of NF-0.03 for Mg^{2+} and Li^{+} were 97.16 % and 20.02%, respectively. In addition, after the filtration test using membrane NF-0.03, the Mg^{2+}/Li^{+} significantly decreased from an initial 20 to 0.7.

Monovalent cations Li^{+} carry less positive charge than divalent cations Mg^{2+}, and the hydraulic radius of Li^{+}(0.382 nm) is slightly smaller than Mg^{2+}(0.428 nm). During separation, Mg^{2+} faces stronger electrostatic repulsion and steric hindrance from the positive charged NF membrane, thereby leading to higher rejection for Mg^{2+} than Li^{+}. According to the results shown in Fig.3-8(a), after the incorporation of GQDs-NH_2 in the polyamide layer, the positive chargeability of the membrane NF-0.03 was higher than that of the pure NF-0 membrane under the conditions of this work (pH≈7). Due to the higher positive chargeability of membrane NF-0.03, the electrostatic repulsion between Mg^{2+} and membrane NF-0.03 will be enhanced, resulting in a higher rejection for divalent cations Mg^{2+} [36]. However, as mentioned in the section of chemical structure characterization, the high content of doped GQDs-NH_2 will form nano-agglomerates and result in a slightly looser polyamide layer. Thereby, the transmission resistance will be reduced, resulting in a reduction in the rejection of both Mg^{2+} and Li^{+}. In summary, the membrane NF-0.03 exhibited an excellent Mg^{2+}/Li^{+} separation ability and a high permeation flux under an optimal GQDs-NH_2 incorporation content of 0.03 wt%.

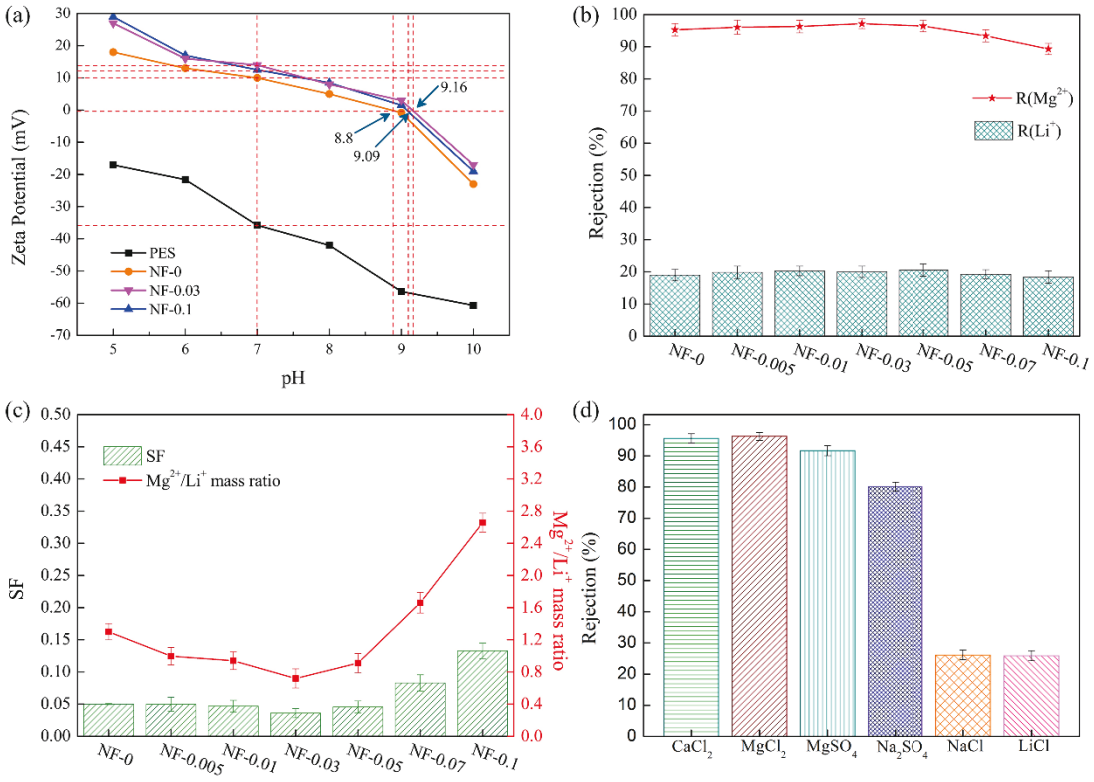

Fig.3-8. (a) Zeta potential of PES substrate membrane and membranes NF-0, NF-0.03, and NF-0.1, (b) the rejection of each NF membrane for Mg^{2+} and Li^{+}, (c) the Mg^{2+}/Li^{+} separation performance of each NF membrane and (d) the rejection of membrane NF-0.03 for several different inorganic salts.

Fig.3-8(d) shows the rejection performance of the membrane NF-0.03 for several inorganic salts. The membrane NF-0.03 showed high rejections for both $CaCl_2$ and $MgCl_2$, which were over 95%, and the rejections for $MgSO_4$ and Na_2SO_4 were slightly lower. However, the rejections for monovalent inorganic salts NaCl and LiCl were less than 30%. Similar phenomenon has been found in several reported articles [19, 21, 40, 54, 55]. Compared to monovalent cations Li^{+} and Na^{+}, divalent cations Mg^{2+} and Ca^{2+} carry more positive charge and have larger hydrate radius. As a result, divalent cations Mg^{2+} and Ca^{2+} will face higher transmission resistance than monovalent cations Li^{+} and Na^{+} when passing through the positively charged NF membrane. As a result, the duel-effect of electrostatic repulsion and steric hindrance determined the final rejection result for various salts. The rejection difference between $MgCl_2$ and LiCl was over 70%. In addition, the positively charged membrane NF-0.03 prepared in this work performed

excellently for removing $MgCl_2$ and $CaCl_2$, which is also promising for of water-softening applications.

3.3.5 Stability and antifouling characterization of membrane

Fig. 3-9(a) shows that during the continuous filtration of the feed solution for 24 h using the membrane NF-0.03, the permeation flux and the rejection of Mg^{2+} and Li^{+} were well maintained, reflecting the stable performance of the membrane NF-0.03. Fouling is a fatal and unavoidable problem during filtration, which can greatly decrease the separation performance of NF membranes [7]. In this work, we adopted BSA (0.1g/L) as a simulated pollutant to evaluate the anti-fouling property of NF membranes. Fig. 3-9(b) shows the water flux of NF membranes before and after the fouling process. After the fouling process, the water flux F_2 of each NF membrane was lower than the initial water flux F_1. The *FRR* values of membranes NF-0 and NF-0.03 were 69% and 85.6%, respectively, which were calculated using Eq. (4). The results indicated that the incorporated GQDs-NH_2 in the polyamide layer could improve the anti-fouling property of the final NF membrane. As shown in Fig .7, due to the introduction of GQDs-NH_2, the hydrophilicity of the final NF membrane can be significantly improved. The hydrated layer will be formed on the hydrophilic NF membrane surface during filtration, which is sufficient for inhibiting the adsorption and aggregation of pollutants, thereby stabilizing the separation performance of the NF membrane [36]. On the other hand, according to the AFM results, after the incorporation of the nano-sized GQDs-NH_2 in the polyamide layer, the roughness value of the final NF membrane was slightly lower than that of the pure NF0 membrane. The smoother the surface of the NF membrane, the fewer the adhesion site of pollutants on the membrane surface [33]. In summary, the incorporated GQDs-NH_2 endowed the NF membrane with a smoother surface and higher hydrophilicity, thereby improving the anti-fouling ability and stability of the NF membrane.

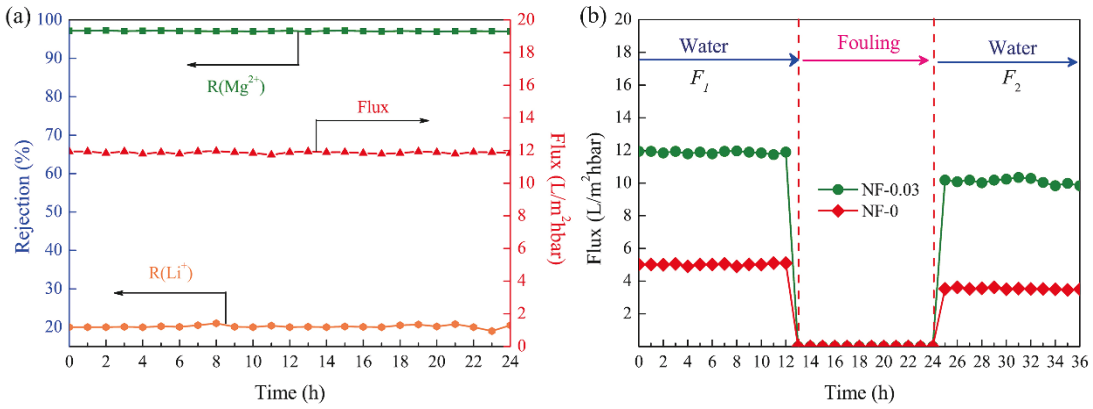

Fig.3-9(a) A long-time filtration test for membrane NF-0.03 and (b) fouling resistance of BSA for membrane NF-0 and NF-0.03: filtering pure water for 12 h; filtering BSA solution for 12 h; and filtering pure water for 12 h after cleaning for 1h using pure water (test condition: the feed solution (2g/L) is composed of $MgCl_2$ and LiCl, $Mg^{2+}/Li^+ = 20$).

Table 3-3 listed several reported composite NF membranes used for Mg^{2+}/Li^+ separation. Each NF membrane in Table 3-3 shows a low separation factor *SF* value less than 0.5, which indicated that each membrane has a high Mg^{2+}/Li^+ separation ability. However, some NF membranes have low flux, which is the bottleneck of their industrial application for lithium extraction. Compared to these reported NF membranes, membrane NF-0.03 prepared in this work shows a lowest SF value of 0.0359 and a highest flux of 11.94 L/m^2hbar under a low operation pressure of 3 bar, which indicated an excellent Mg^{2+}/Li^+ separation efficiency of membrane. The results demonstrate that nano-sized GQDs-NH_2 is a promising additive for regulating the structure and performance of NF membranes in Mg^{2+}/Li^+ separation applications.

Table 3-3 Performance comparison of reported NF membranes and NF membrane prepared in this work

Membrane materials	Test condition	Mg^{2+}/Li^+ separation ability	Flux (L/m^2hbar)	Ref
DL-2540 commercial membrane	Mg^{2+}/Li^+=60 (20 bar)	*SF* = 0.35	-	[12]
DK commercial membrane	Mg^{2+}/Li^+=18-24 (16 bar)	*SF* = 0.34	-	[15]

NF90 commercial membrane	Mg^{2+}/Li^{+}=20 2000ppm (3 bar)	*SF* = 0.476	-	[19]
DAPP/TMC	Mg^{2+}/Li^{+}=20 2000ppm (3 bar)	*SF* = 0.384	-	[19]
TMC/BPEI/EDTA	Mg^{2+}/Li^{+}=24 2000ppm (4 bar)	*SF* = 0.108	0.6	[18]
PIP-MWCNTs/PEI/TMC	Mg^{2+}/Li^{+}=21.4 2000ppm (4 bar)	*SF* = 0.06	8.5	[21]
PES/(PIP-PHF)/TMC	Mg^{2+}/Li^{+}=21.4 2000ppm (6 bar)	*SF* =0.076	6.7	[56]
PEI/TMC	Mg^{2+}/Li^{+}=20 2000ppm (8 bar)	*SF* =0.05	5.02	[20]
CNC-COOH/ PEI/TMC	Mg^{2+}/Li^{+}=30 2000ppm (8 bar)	*SF* = 0.082	4.17	[53]
CNC-COOH/ PEI/TMC	Mg^{2+}/Li^{+}=60 2000ppm (8 bar)	*SF* = 0.171	3.4	[53]
PES-GO/PEI/TMC	Mg^{2+}/Li^{+}=20 2000ppm (3 bar)	*SF* = 0.062	11.15	[5]
PEI/GQDs-NH_2/TMC	Mg^{2+}/Li^{+}=20 2000ppm (3 bar)	*SF* = 0.0359	11.94	This work

3.4 Conclusion

Till now, it is still challenging to achieve both high separation ability and high flux, which is the bottleneck of the industrial application of NF membrane for lithium extraction. In this work, a novel high positively charged NF membrane containing GQDs-NH_2 was synthesized by interfacial polymerization on the PSE base membrane.

Due to the multi-effect caused by GQDs-NH_2, the final obtained NF membranes were endowed with thinner and smoother polyamide layer, enhanced positively chargeability and improved hydrophilicity, and shorter path water channel formed

between GQDs-NH_2 monomers and polyamide layer. Membrane NF-0.03 with a GQDs-NH_2 content of 0.03 wt% performed best for separating Mg^{2+}/Li^+ among all NF membranes fabricated in this work. After filtering the feed solution using membrane NF-0.03, the mass ratio of Mg^{2+}/Li^+ decreased from an initial 20 to 0.7, and rejections of membrane for Mg^{2+} and Li^+ were 97.16 % and 20.02%, respectively. Note that the permeation flux of membrane NF-0.03 improved to 11.94 L/m^2hbar, which was 137.8 % more than that of pure NF-0 membrane. The improved permeation flux of membrane can significantly accelerate the Mg^{2+}/Li^+ separation process and improve the efficiency of lithium extraction. Additionally, the improved hydrophilicity and smoother surface endowed membrane NF-0.03 with higher anti-fouling performance, allowing it to work stably for a long time in practical applications. In summary, the membrane NF-0.03 incorporated with GQDs-NH_2 is effective for enrich and extract lithium from salt-lake brines with a high mass ratio of Mg^{2+}/Li^+.

Reference

[1] S. Tul Muntha, A. Kausar, M. Siddiq, Advances in polymeric nanofiltration membrane: A review, Polymer-Plastics Technology and Engineering, 56 (2016) 841-856.

[2] D.L. Oatley-Radcliffe, M. Walters, T.J. Ainscough, P.M. Williams, A.W. Mohammad, N. Hilal, Nanofiltration membranes and processes: A review of research trends over the past decade, Journal of Water Process Engineering, 19 (2017) 164-171.

[3] A.W. Mohammad, Y.H. Teow, W.L. Ang, Y.T. Chung, D.L. Oatley-Radcliffe, N. Hilal, Nanofiltration membranes review: Recent advances and future prospects, Desalination, 356 (2015) 226-254.

[4] V. Vatanpour, M. Esmaeili, M.H.D.A. Farahani, Fouling reduction and retention increment of polyethersulfone nanofiltration membranes embedded by amine-functionalized multi-walled carbon nanotubes, Journal of Membrane Science, 466 (2014) 70-81.

[5] P. Xu, J. Hong, X. Qian, Z. Xu, H. Xia, Q.-Q. Ni, “Bridge” graphene oxide modified

positive charged nanofiltration thin membrane with high efficiency for Mg^{2+}/Li^{+} separation, Desalination, 488 (2020) 114522.

[6] Y. Zhang, L. Wang, W. Sun, Y. Hu, H. Tang, Membrane technologies for Li^{+}/Mg^{2+} separation from salt-lake brines and seawater: A comprehensive review, Journal of Industrial and Engineering Chemistry, 81 (2020) 7-23.

[7] X. Li, Y. Mo, W. Qing, S. Shao, C.Y. Tang, J. Li, Membrane-based technologies for lithium recovery from water lithium resources: A review, Journal of Membrane Science, 591 (2019) 117317.

[8] B. Swain, Recovery and recycling of lithium: A review, Separation and Purification Technology, 172 (2017) 388-403.

[9] V. Flexer, C.F. Baspineiro, C.I. Galli, Lithium recovery from brines: A vital raw material for green energies with a potential environmental impact in its mining and processing, Sci Total Environ, 639 (2018) 1188-1204.

[10] H. Wu, Y. Lin, W. Feng, T. Liu, L. Wang, H. Yao, X. Wang, A novel nanofiltration membrane with [MimAP][Tf_2N] ionic liquid for utilization of lithium from brines with high Mg^{2+}/Li^{+} ratio, Journal of Membrane Science, 603 (2020) 117997.

[11] L. Kavanagh, J. Keohane, G. Garcia Cabellos, A. Lloyd, J. Cleary, Global lithium sources—industrial use and future in the electric vehicle Industry: A review, Resources, 7 (2018) 57.

[12] S.-Y. Sun, L.-J. Cai, X.-Y. Nie, X. Song, J.-G. Yu, Separation of magnesium and lithium from brine using a Desal nanofiltration membrane, Journal of Water Process Engineering, 7 (2015) 210-217.

[13] X. Wen, P. Ma, C. Zhu, Q. He, X. Deng, Preliminary study on recovering lithium chloride from lithium-containing waters by nanofiltration, Separation and Purification Technology, 49 (2006) 230-236.

[14] G. Liu, Z. Zhao, L. He, Highly selective lithium recovery from high Mg/Li ratio brines, Desalination, 474 (2020) 114185.

[15] G. YANG, H. SHI, W. LIU, W. XING, N. XU, Investigation of Mg^{2+}/Li^{+} separation by nanofiltration, Chinese Journal of Chemical Engineering, 19 (2011) 586-591.

[16] A. Somrani, A.H. Hamzaoui, M. Pontie, Study on lithium separation from salt lake brines by nanofiltration (NF) and low pressure reverse osmosis (LPRO), Desalination, 317 (2013) 184-192.

[17] Q. Bi, Z. Zhang, C. Zhao, Z. Tao, Study on the recovery of lithium from high Mg^{2+}/Li^{+} ratio brine by nanofiltration, Water Science & Technology, 70 (2014) 1690-1694.

[18] W. Li, C. Shi, A. Zhou, X. He, Y. Sun, J. Zhang, A positively charged composite nanofiltration membrane modified by EDTA for LiCl/$MgCl_2$ separation, Separation and Purification Technology, 186 (2017) 233-242.

[19] X. Li, C. Zhang, S. Zhang, J. Li, B. He, Z. Cui, Preparation and characterization of positively charged polyamide composite nanofiltration hollow fiber membrane for lithium and magnesium separation, Desalination, 369 (2015) 26-36.

[20] P. Xu, W. Wang, X. Qian, H. Wang, C. Guo, N. Li, Z. Xu, K. Teng, Z. Wang, Positive charged PEI-TMC composite nanofiltration membrane for separation of Li^{+} and Mg^{2+} from brine with high Mg^{2+}/Li^{+} ratio, Desalination, 449 (2019) 57-68.

[21] H.-Z. Zhang, Z.-L. Xu, H. Ding, Y.-J. Tang, Positively charged capillary nanofiltration membrane with high rejection for Mg^{2+} and Ca^{2+} and good separation for Mg^{2+} and Li^{+}, Desalination, 420 (2017) 158-166.

[22] S.M. Xue, Z.L. Xu, Y.J. Tang, C.H. Ji, Polypiperazine-amide nanofiltration membrane modified by different functionalized multiwalled carbon Nnanotubes (MWCNTs), ACS Appl Mater Interfaces, 8 (2016) 19135-19144.

[23] H. Zarrabi, M.E. Yekavalangi, V. Vatanpour, A. Shockravi, M. Safarpour, Improvement in desalination performance of thin film nanocomposite nanofiltration membrane using amine-functionalized multiwalled carbon nanotube, Desalination, 394 (2016) 83-90.

[24] H.M. Hegab, L. Zou, Graphene oxide-assisted membranes: Fabrication and potential applications in desalination and water purification, Journal of Membrane Science, 484 (2015) 95-106.

[25] Q. Nan, P. Li, B. Cao, Fabrication of positively charged nanofiltration membrane

via the layer-by-layer assembly of graphene oxide and polyethylenimine for desalination, Applied Surface Science, 387 (2016) 521-528.

[26] P. Wen, Y. Chen, X. Hu, B. Cheng, D. Liu, Y. Zhang, S. Nair, Polyamide thin film composite nanofiltration membrane modified with acyl chlorided graphene oxide, Journal of Membrane Science, 535 (2017) 208-220.

[27] J. Zhu, J. Wang, J. Hou, Y. Zhang, J. Liu, B. Van der Bruggen, Graphene-based antimicrobial polymeric membranes: a review, Journal of Materials Chemistry A, 5 (2017) 6776-6793.

[28] X. Liu, H.J. Liu, F. Cheng, Y. Chen, Preparation and characterization of multi stimuli-responsive photoluminescent nanocomposites of graphene quantum dots with hyperbranched polyethylenimine derivatives, Nanoscale, 6 (2014) 7453-7460.

[29] S.F. Seyedpour, A. Rahimpour, A.A. Shamsabadi, M. Soroush, Improved performance and antifouling properties of thin-film composite polyamide membranes modified with nano-sized bactericidal graphene quantum dots for forward osmosis, Chemical Engineering Research and Design, 139 (2018) 321-334.

[30] G. Zhao, R. Hu, J. Li, H. Zhu, Graphene oxide quantum dots embedded polysulfone membranes with enhanced hydrophilicity, permeability and antifouling performance, Science China Materials, 62 (2019) 1177-1187.

[31] C. Zhang, K. Wei, W. Zhang, Y. Bai, Y. Sun, J. Gu, Graphene oxide quantum dots incorporated into a thin film nanocomposite membrane with high flux and antifouling properties for low-pressure nanofiltration, ACS Applied Materials & Interfaces, 9 (2017) 11082-11094.

[32] S. Li, C. Li, X. Song, B. Su, B. Mandal, B. Prasad, X. Gao, C. Gao, Graphene quantum dots-doped thin film nanocomposite polyimide membranes with enhanced solvent resistance for solvent-resistant nanofiltration, ACS Appl Mater Interfaces, 11 (2019) 6527-6540.

[33] R. Bi, Q. Zhang, R. Zhang, Y. Su, Z. Jiang, Thin film nanocomposite membranes incorporated with graphene quantum dots for high flux and antifouling property, Journal of Membrane Science, 553 (2018) 17-24.

[34] Q. Feng, Q. Cao, M. Li, F. Liu, N. Tang, Y. Du, Synthesis and photoluminescence of fluorinated graphene quantum dots, Applied Physics Letters, 102 (2013) 013111.
[35] S. Li, C. Li, B. Su, M.Z. Hu, X. Gao, C. Gao, Amino-functionalized graphene quantum dots (aGQDs)-embedded thin film nanocomposites for solvent resistant nanofiltration (SRNF) membranes based on covalence interactions, Journal of Membrane Science, 588 (2019) 117212.
[36] H. Sun, P. Wu, Tuning the functional groups of carbon quantum dots in thin film nanocomposite membranes for nanofiltration, Journal of Membrane Science, 564 (2018) 394-403.
[37] M. Hu, Z. Cui, J. Li, L. Zhang, Y. Mo, D.S. Dlamini, H. Wang, B. He, J. Li, H. Matsuyama, Ultra-low graphene oxide loading for water permeability, antifouling and antibacterial improvement of polyethersulfone/sulfonated polysulfone ultrafiltration membranes, J Colloid Interface Sci, 552 (2019) 319-331.
[38] Z. Xu, T. Wu, J. Shi, K. Teng, W. Wang, M. Ma, J. Li, X. Qian, C. Li, J. Fan, Photocatalytic antifouling PVDF ultrafiltration membranes based on synergy of graphene oxide and TiO2 for water treatment, Journal of Membrane Science, 520 (2016) 281-293.
[39] G.S. Lai, W.J. Lau, P.S. Goh, A.F. Ismail, N. Yusof, Y.H. Tan, Graphene oxide incorporated thin film nanocomposite nanofiltration membrane for enhanced salt removal performance, Desalination, 387 (2016) 14-24.
[40] Y.C. Xu, Z.X. Wang, X.Q. Cheng, Y.C. Xiao, L. Shao, Positively charged nanofiltration membranes via economically mussel-substance-simulated co-deposition for textile wastewater treatment, Chemical Engineering Journal, 303 (2016) 555-564.
[41] W. Fang, L. Shi, R. Wang, Interfacially polymerized composite nanofiltration hollow fiber membranes for low-pressure water softening, Journal of Membrane Science, 430 (2013) 129-139.
[42] M. Amini, M. Jahanshahi, A. Rahimpour, Synthesis of novel thin film nanocomposite (TFN) forward osmosis membranes using functionalized multi-walled carbon nanotubes, Journal of Membrane Science, 435 (2013) 233-241.

[43] S. Xu, F. Li, B. Su, M.Z. Hu, X. Gao, C. Gao, Novel graphene quantum dots (GQDs)-incorporated thin film composite (TFC) membranes for forward osmosis (FO) desalination, Desalination, 451 (2019) 219-230.

[44] M. Fathizadeh, H.N. Tien, K. Khivantsev, Z. Song, F. Zhou, M. Yu, Polyamide/nitrogen-doped graphene oxide quantum dots (N-GOQD) thin film nanocomposite reverse osmosis membranes for high flux desalination, Desalination, 451 (2019) 125-132.

[45] D. Wu, S. Yu, D. Lawless, X. Feng, Thin film composite nanofiltration membranes fabricated from polymeric amine polyethylenimine imbedded with monomeric amine piperazine for enhanced salt separations, Reactive and Functional Polymers, 86 (2015) 168-183.

[46] G.S. Lai, W.J. Lau, S.R. Gray, T. Matsuura, R.J. Gohari, M.N. Subramanian, S.O. Lai, C.S. Ong, A.F. Ismail, D. Emazadah, M. Ghanbari, A practical approach to synthesize polyamide thin film nanocomposite (TFN) membranes with improved separation properties for water/wastewater treatment, Journal of Materials Chemistry A, 4 (2016) 4134-4144.

[47] M. Wang, F. Pan, L. Yang, Y. Song, H. Wu, X. Cheng, G. Liu, H. Yang, H. Wang, Z. Jiang, X. Cao, Graphene oxide quantum dots incorporated nanocomposite membranes with high water flux for pervaporative dehydration, Journal of Membrane Science, 563 (2018) 903-913.

[48] H.-R. Chae, J. Lee, C.-H. Lee, I.-C. Kim, P.-K. Park, Graphene oxide-embedded thin-film composite reverse osmosis membrane with high flux, anti-biofouling, and chlorine resistance, Journal of Membrane Science, 483 (2015) 128-135.

[49] C. Zhao, X. Xu, J. Chen, F. Yang, Effect of graphene oxide concentration on the morphologies and antifouling properties of PVDF ultrafiltration membranes, Journal of Environmental Chemical Engineering, 1 (2013) 349-354.

[50] S. Roy, S.A. Ntim, S. Mitra, K.K. Sirkar, Facile fabrication of superior nanofiltration membranes from interfacially polymerized CNT-polymer composites, Journal of Membrane Science, 375 (2011) 81-87.

[51] K.P. Lee, G. Bargeman, R. de Rooij, A.J.B. Kemperman, N.E. Benes, Interfacial polymerization of cyanuric chloride and monomeric amines: pH resistant thin film composite polyamine nanofiltration membranes, Journal of Membrane Science, 523 (2017) 487-496.

[52] X.-D. Weng, X.-J. Bao, H.-D. Jiang, L. Chen, Y.-L. Ji, Q.-F. An, C.-J. Gao, pH-responsive nanofiltration membranes containing carboxybetaine with tunable ion selectivity for charge-based separations, Journal of Membrane Science, 520 (2016) 294-302.

[53] C. Guo, N. Li, X. Qian, J. Shi, M. Jing, K. Teng, Z. Xu, Ultra-thin double Janus nanofiltration membrane for separation of Li^+ and Mg^{2+}: "Drag" effect from carboxyl-containing negative interlayer, Separation and Purification Technology, 230 (2020) 115567.

[54] W. Fang, L. Shi, R. Wang, Mixed polyamide-based composite nanofiltration hollow fiber membranes with improved low-pressure water softening capability, Journal of Membrane Science, 468 (2014) 52-61.

[55] S. Zhao, Z. Wang, A loose nano-filtration membrane prepared by coating HPAN UF membrane with modified PEI for dye reuse and desalination, Journal of Membrane Science, 524 (2017) 214-224.

[56] Q. Shen, S.J. Xu, Z.L. Xu, H.Z. Zhang, Z.Q. Dong, Novel thin-film nanocomposite membrane with water-soluble polyhydroxylated fullerene for the separation of Mg^{2+}/Li^+ aqueous solution, Journal of Applied Polymer Science, 136 (2019) 48029.

Chapter 4

✵✵✵✵✵✵✵✵✵✵✵✵✵✵✵✵✵✵✵✵✵✵✵✵✵✵✵✵

MWCNTs-COOK-assisted high positively charged composite membrane: Accelerating Li^+ enrichment and Mg^{2+} removal

✵✵✵✵✵✵✵✵✵✵✵✵✵✵✵✵✵✵✵✵✵✵✵✵✵✵✵✵

4 MWCNTs-COOK-assisted high positively charged composite membrane: Accelerating Li^+ enrichment and Mg^{2+} removal

4.1 Introduction

Effectively separate Li^+ and the co-exist Mg^{2+} is critical for enriching and extracting high purity lithium products from salt-lake brines[1-12]. The synthesis effect of steric hindrance and Donnan exclusion make Nanofiltration (NF) membrane a promising approach for enriching high purity Li^+ [13-19]. In addition, for separating Li^+ and Mg^{2+}, the NF membrane with a positively charged surface is a better choice than the commonly applied negatively charged NF membrane [20-24]. Various previously reports verified the perm-selectivity of positively charged membrane for Li^+ and Mg^{2+} in brines. However, these membranes still face the low flux difficulty, which is a fatal problem that can cause low work efficiency during separation process.

Great efforts have been made to enhance the permeate flux of composite membranes. Nano-additives, such as TiO_2 [25-27], graphene oxide [28-31], and carbon nanotubes (CNTs) [32-36], have emerged as a promising alternative to enhance the water flux of membranes. Shen et al. embedded the water-soluble polyhydroxylated fullerene (PHF) into the NF membrane surface during interfacial polymerization [37]. They found that the additive PHF endowed the NF membrane with an enhanced flux and anti-fouling ability when separating Li^+ and Mg^{2+}. Zhang et al. grafted piperazine on hydroxyl-functionalized multi-wall CNTs and embedded it as an additive during NF membrane fabrication [38]. The resultant NF membrane showed an improved flux of 8.5 L/m^2hbar, and the separation factor was 16.46. Recently, Yang et al. coated single-walled CNTs on the microfiltration substrate, followed by interfacial polymerization and PEI grafting [39]. They surprisingly found that the prepared positively charged NF

membrane with dual-layer exhibited simultaneously improved flux and separation factor of 12 L/m^2hbar and 33.4, respectively.

Among these commonly applied nano-additives, the nanomaterial CNTs have special smooth cylindrical nanostructure, large specific surface area, high biocidal and antioxidant ability, and high thermal and mechanical characteristics [40-45], which make it attractive in membrane optimization. In addition, the hollow structure of CNTs and inter-gaps between CNTs and polymer matrix can provide more nano-channels for water to pass through the membrane, which can greatly enhance the permeate flux of the membrane. However, CNTs tend to cluster and cannot be evenly dispersed in commonly used solvent before functionalization. Commonly, CNTs are functionalized by oxidation to "grow" hydrophilic functional groups on CNTs, thereby endowing CNTs with higher water solubility [46-51]. However, during the oxidation process, a large amount of acid solutions (e.g., H_2SO_4 and HNO_3) will be consumed, which does not conform to the advocated environmental protection concept. In this work, we proposed an easy-to-operate and environmentally friendly functionalization method to synthesize a new class of potassium carboxylate functionalized multi-wall CNTs (MWCNTs-COOK) with high hydrophilicity. Compared to the MWCNTs-COOH, -COOK on MWCNTs-COOK surface is more easily ionize in water. Besides, the charged -COOK makes MWCNTs-COOK repel from each other. Therefore, MWCNTs-COOK exhibits higher water solubility and can be more uniformly dispersed in water, which makes them promising materials for optimizing membrane properties.

Further improving the separation efficiency of the NF membrane for Li^+ and Mg^{2+}, especially the permeate flux during filtration, is essential for accelerating the lithium extraction process. Herein, we designed a new class of positively charged NF membrane with high permeate flux for effectively enriching Li^+ and separating Mg^{2+}. The prepared MWCNTs-COOK were synthesized as nano-additives to regulate the interfacial polymerization process between PEI and TMC on the ultrafiltration substrate, thereby fine-tuning the microstructure and optimizing the performance of the final NF membrane. How the MWCNTs-COOK nano-additives improve the Li^+/Mg^{2+}

separation efficiency of NF membrane was comprehensively investigated and evaluated from multiple aspects (e.g., morphology, structure, surface properties, and rejection ability) by using various characterization methods.

4.2 Experiments

4.2.1 Regents and materials

Polyethersulfone (PES, 62000 g/mol) was applied as the polymer of ultrafiltration substrate and was purchased from Solvay Advanced Polymer (Belgium). MWCNTs (10-20nm in diameter, 0.5-2μm in length) were supplied by Nanjing XFNANO Materials Tech. Co. Ltd. Polyethylene glycol (PEG), n-hexane, N, N-dimethylacetamide (DMAc), PEI, sodium dodecyl sulfate (SDS), TMC, potassium persulfate ($K_2S_2O_8$), KOH, $NaCO_3$, LiCl, and $MgCl_2$ were all purchased from Wako Pure Chemical Industries Ltd., Japan.

4.2.2 Synthesis of MWCNTs-COOK

First, we pre-dispersed 40mg pristine MWCNTs powder in 50ml deionized water by probe-sonication at room temperature for 10 min. Next, 0.45g $K_2S_2O_8$ and 50ml KOH solution (1 wt%) were added into the solution, and then strongly stirred at 80 ℃ for 3 h. After that, the mixture was diluted with deionized water and dispersed with probe-sonication, and then centrifuged at 3000 rmp for 20min to eliminate residues. Finally, the potassium carboxylate functionalized MWCNTs-COOK powder was collected via filtering the supernatant though the membrane (47 mm/0.2μm) and dried at 50 ℃ for 24h.

4.2.3 Preparation of MWCNTs-COOK doped NF membrane

The PES ultrafiltration substrate was fabricated through the commonly utilized method non-solvent phase inversion [52, 53]. PES (18%) and PEG (10%) were

dispersed in DMAc and stirred at 50 °C for 6 h to obtain a homogeneous casting solution. After full degassing, the casting solution was cast on a clean glass plate using a casting knife with a gap height of 200 μm and immediately immersed into the pure water bath to form the primary membranes. The obtained PES ultrafiltration membrane presented a pore size around 30nm, a porosity of 69.11%, and a permeate flux of 210.19 L/m^2hbar.

The polyamide layer of the composite membrane was formed through the interfacial polymerization process. The aqueous solution was composed of 0.5 wt% PEI, 0.1 wt% surfactant SDS, 0.1 wt% $NaCO_3$, and nano-additives MWCNTs-COOK with different content. The aqueous phase solution involved MWCNTs-COOK was poured on the PES substrate surface. After 5 min, the excess solution was removed. Followed by immersing the membrane surface in the organic phase solution (0.1 w/v% TMC in n-hexane) for 3 min to let the polymerization occur. Next, the membrane was cured at 70 ℃ for 10 min. Finally, the obtained membranes were washed and immersed in the deionized water before utilizing. The obtained NF membranes doped with MWCNTs-COOK concentration of 0ppm, 30ppm, 100ppm,150ppm, 300ppm, and 1000ppm were named NF1, NF2, NF3, NF4, NF5, and NF6, respectively.

4.2.4 Membrane characterization

The field emission scanning electron microscopy (FESEM, Hitachi S-5000, Japan) and atomic force microscopy (AFM, Shimadzu SPM-9500 J3, Japan) were adopted to visualize the morphologies and topography and evaluate the roughness of obtained membranes surface. The Fourier-transform infrared spectroscopy (FTIR, Shimadzu Co., Ltd., Japan) and X-ray photoelectron spectroscopy (XPS, AXIS-ULTRA DLD, KRATOS) were applied to observe and examine functional groups and chemical composition of the synthesized MWCNTs-COOK and membranes. The effect of MWCNTs-COOK dosage on the NF membrane hydrophilicities was evaluated using the contact angle (CA, digidrop, GBX, Whitestone way, France). The CA test of each sample was conducted more than 5 times to minimize the error. The chargeability of

membrane surface was assessed by the electrokinetic analyzer (Sur-PASS TM3 Anton Paar, GmbH, Austria). The spectra of MWCNTs before and after potassium carboxylate functionalization was estimated by the Raman spectroscope (Kaiser Optical Systems, Inc.).

4.2.5 NF performance test of membrane

The separation performance of the obtained NF membranes was evaluated using a cross-flow filtration system with an effective test area of 12.56 cm^2 at 25℃. A 2000 ppm mixture consists of $MgCl_2$ and LiCl was applied as the simulated brine to measure the separation performance of the prepared NF membranes. And the mass ratio of Mg^{2+}/Li^+ in the simulated brine was 20. Each membrane sample was pre-filtered at 4 bar for 1 h with deionized water to obtain the stabilize permeate flux. Then adjusting the operating pressure to 3 bar to start the filtration testing. The water permeability of NF membranes was assessed by the flux F (L/m^2hbar) during filtration, which can be calculated by the following Eq.(1):

$$F = \frac{V}{A \times T \times P} \tag{1}$$

In which, the V (L), A (m^2), T (h), and P (bar) refer to volume of permeate, membrane area, time and operation pressure during filtration test, respectively. The separation ability of NF membranes for ions was evaluated by the rejection rate R (%), which can be calculated by Eq.(2):

$$R = (1 - \frac{C_2}{C_1}) \times 100\% \tag{2}$$

In which, C_1 (ppm) and C_2 (ppm) refer to the ion concentration in feed and permeate solutions, respectively. The concentration of ions in solution was evaluated by the inductively coupled plasma optical emission spectroscopy (ICPOES,10000IV, Shimadzu, Japan). The separation ability of NF membrane for Li^+ and Mg^{2+} was evaluated by the separation factor $S_{Li,Mg}$, which was calculated by the following Eq.(3):

$$S_{Li,Mg} = \frac{C_{1,Mg}/C_{1,Li}}{C_{2,Mg}/C_{2,Li}} \tag{3}$$

In which, the $C_{1,Mg}$ (ppm) and $C_{2,Mg}$ (ppm) refer to the concentration of Mg^{2+} in

feed and permeate solutions, respectively. Similarly, $C_{1,Li}$ (ppm) and $C_{2,Li}$ (ppm) represent the concentrations of Li^+ in the permeate solution and feed solution, respectively. The molecular weight cut-off (MWCO) of NF membranes was evaluated by a filtration test using 50 mg/L PEG aqueous with different molecular weights. The MWCO value of the NF membrane was considered as the minimum molecular weight of PEG that shares a rejection of 90% [14, 23]. The concentration of PEG in aqueous solution was quantified using the total organic carbon analyzer (TOCVCSH; Shimadzu Co., Kyoto, Japan).

4.3 Results and discussion

4.3.1 Characterization of MWCNTs-COOK

The Raman spectroscopy was applied to evaluate the structural integrity of the MWCNTs before and after potassium carboxylate functionalization. As shown in Fig.4-1(a), there are two distinct peaks at 1351cm^{-1} and 1583cm^{-1} on each spectrum, which were related to the disorder mode (D band) and tangential mode (G band), respectively. The intensity ratio of D band/ G band (I_D/I_G) is commonly considered to be related to the disorder degree of the MWCNTs and the amount of sp^2-hybridized carbons [54, 55]. The result showed that the I_D/I_G value of MWCNTs increased from an initial 0.89 to 1.25 after functionalization, which verified the success of confirmed the successful introduction of functional groups on the MWCNT surface. The chemical composition changes of MWCNTs before and after modification was further evaluated by the XPS spectra. As illustrated in Fig.4-1(b), after oxidation, new peaks located at 292.8 eV, 377.5 eV, and 531.5eV can be deserved on the spectrum of MWCNTs-COOK, which corresponded to K2s, K2p, and O1s, respectively. The C1s of MWCNTs-COOK consists of three carbon statues of C-C, C-O, and O-C=O. And the O1s spectrum of MWCNTs-COOK consists of two main oxygen status of O-C=O and C-O. These results revealed the success grafting of functional groups -COOK and -OH on the MWCNTs, which would lead to the high solubility of the obtained MWCNTs-COOK.

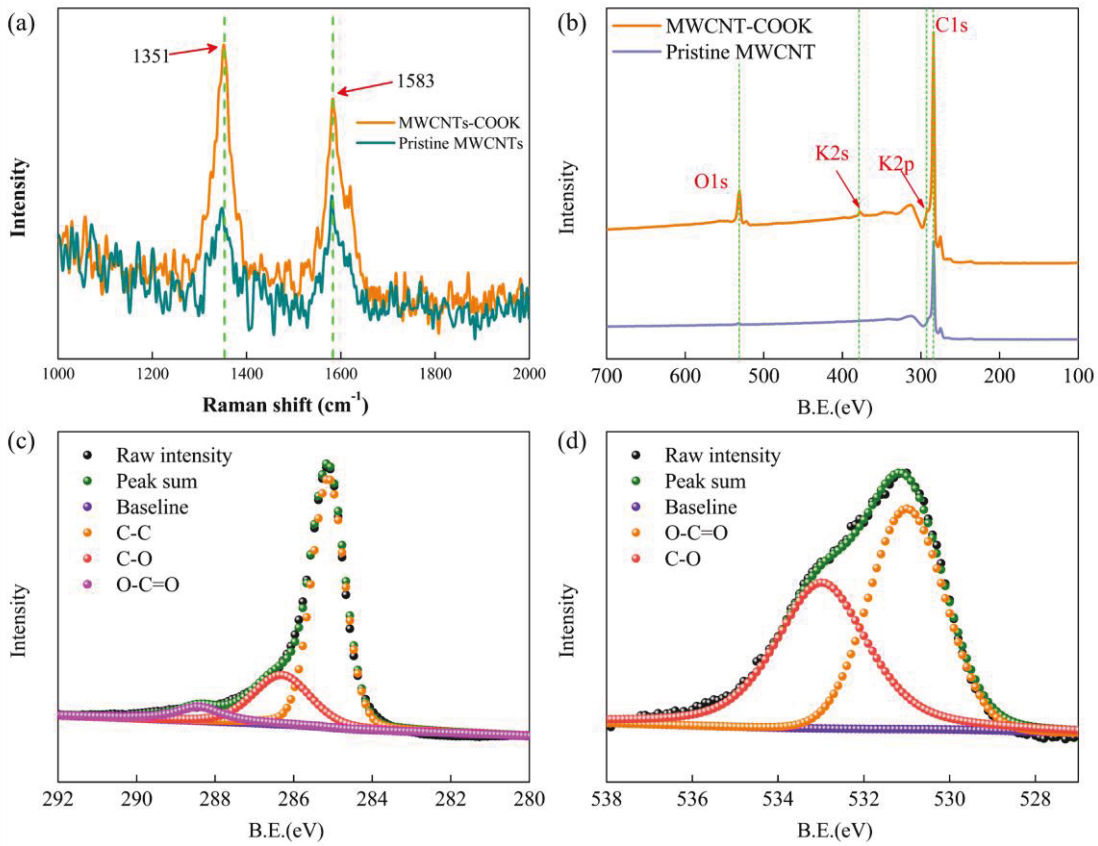

Fig. 4-1 (a) Raman spectra and (b) XPS spectra of MWCNTs before and after modification, (c) deconvolution of C1s (d) deconvolution of O1s of MWCNTs-COOK.

4.3.2 Chemical and morphology structure characterization

The FTIR analysis was adopted to confirm the cross-linking reaction during interfacial polymerization. As displayed in Fig.4-2, compared to the PES substrate, newly developed peaks around 1613 ~ 1710 cm^{-1} and 1518 ~ 1554 cm^{-1} appeared on each NF membrane spectrum, which were originated from the emerged amide-I (C=O) and amid-II (N-H), respectively [56, 57]. The emerged amide groups verified the appearance of the newly polyamide layer. Besides, in the range of 3187 ~ 3690 cm^{-1}, a strong peak emerged after interfacial polymerization, which was ascribed to the aggregate stretching vibration of -OH and N-H [38, 43, 58]. The results revealed that a lot of unreacted amine groups from PEI amine monomer and hydroxyl groups from MWCNTs-COOK nano-additives were remained on the final NF membrane surface. Another newly emerged peak located at 2920 cm^{-1} can be clearly found on each

spectrum of NF membrane, which corresponds to -NH_n^+ (n = 2, 3) that protonated from the residual amine groups [24].

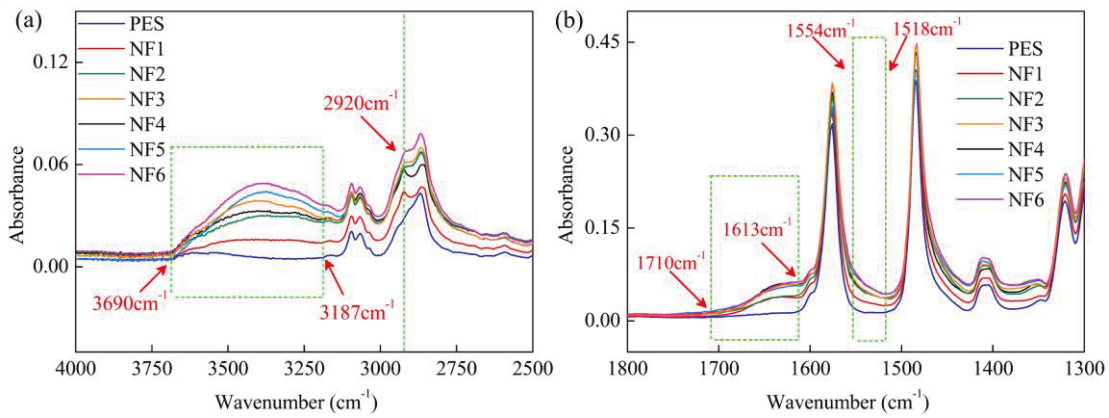

Fig.4-2 FTIR analysis of membranes range from: (a) 2500 to 4000 cm^{-1} and (b) 1300 to 1800 cm^{-1}.

The adjustment of MWCNTs-COOK nano-additives on the chemical bond composition of the membrane surface was further measured by XPS analysis. As presented in Fig.4-3 (a) and Table 4-1, the C1s spectrum of each NF membrane contains five carbon statues of C-C, C-N, C-O, N-C=O, and O-C=O located around 284.8, 285.7, 286.3, 287.8, and 288.5 eV, respectively. As can be found in the deconvolution results, both the chemical bonds N-C=O and O-C=O show an increasing trend with the increasing dosage of MWCNTs-COOK nano-additives in NF membranes. The more MWCNTs-COOK nano-additives, the more functional groups -COOK and -OH would be introduced into the interfacial polymerization process. A higher dosage of MWCNTs-COOK lead to a higher content of chemical bond O-C=O. On the other hand, these functional groups carried by MWCNTs-COOK would crosslink with amine groups on PEI and acyl chloride groups on TMC, thereby leading to more chemical bonds -N-C=O and O-C=O. The crosslinking greatly enhanced the connection between MWCNTs-COOK, PEI, and TMC, resulting in firmer growth of MWCNTs-COOK in NF membrane. In addition, higher MWCNTs-COOK dosage led to an increase of -N-C=O/O-C=O ratio, which indicated more connection between MWCNTs-COOK, PEI, and TMC.

Fig.4-4 presents the deconvolution results of N1s spectra of these prepared NF membranes with different MWCNTs-COOK dosage. Each N1s spectrum can be

divided into three species of C-N, N-C=O, and -NH_n^+ located around 398.8, 399.8, and 401.1 eV, respectively. Among these N species, -NH_n^+ was originated from the residual amine groups on the membrane. According to the deconvolution results in Fig.4-4 and Table 4-1, a slight decrease of -NH_n^+ content can be observed when gradually increasing the MWCNTs-COOK dosage in the membrane. The functional groups on MWCNTs-COOK would crosslink with PEI and consume a part of amine groups, leading to a slight decrease in free amine groups. In summary, the above results verified that the introduced MWCNTs-COOK could affect the interfacial polymerization process, and the chemical composition and formation of the emerged polyamide layer can be adjusted by controlling the MWCNTs-COOK dosage in the membrane.

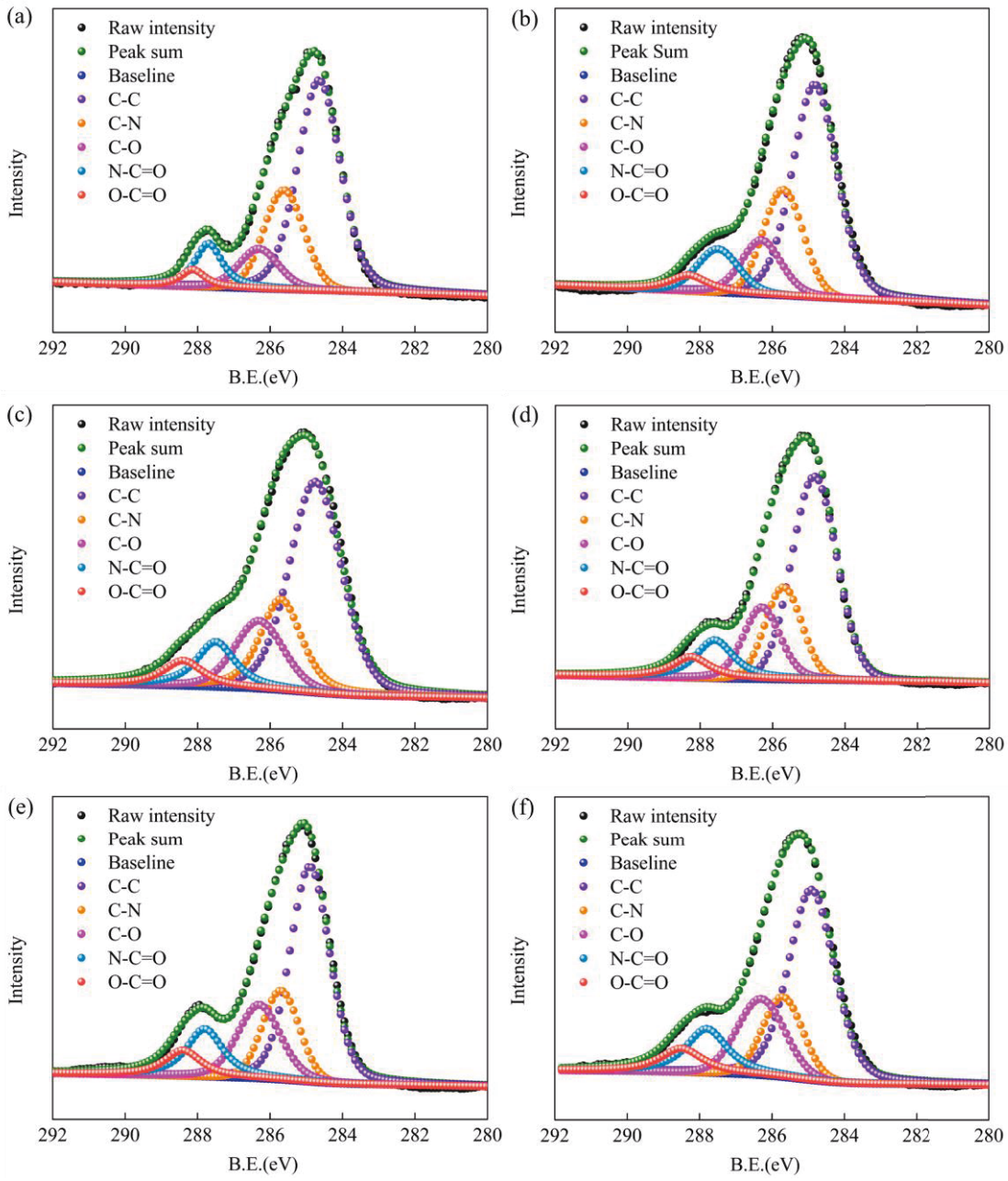

Fig.4-3 Deconvolution results of C1s spectra: (a) NF1, (b) NF2, (c) NF3, (d) NF4, (e) NF5, and (f) NF6.

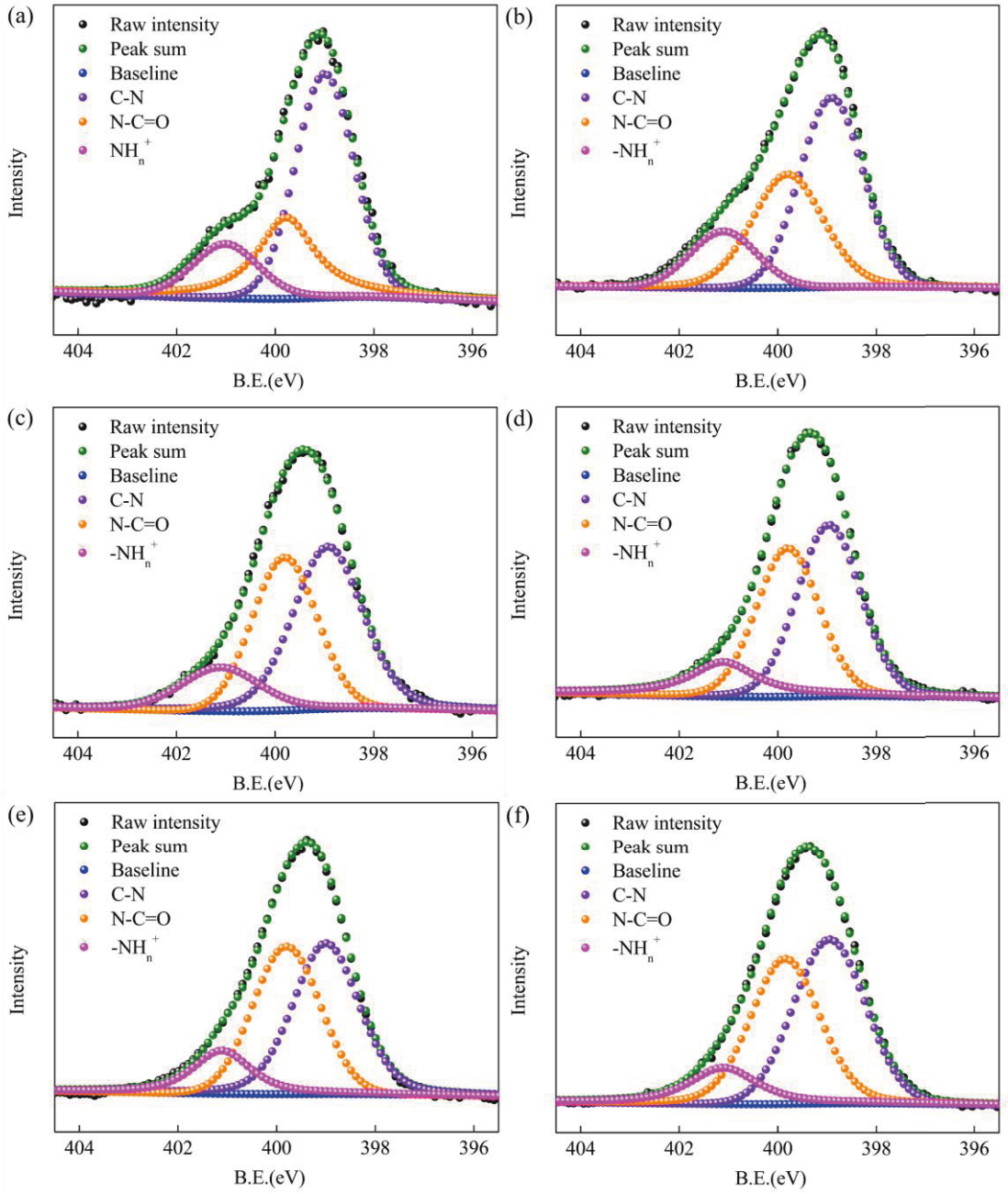

Fig.4-4 Deconvolution results of N1s spectra: (a) NF1, (b) NF2, (c) NF3, (d) NF4, (e) NF5, and (f) NF6.

Table 4-1 Deconvolution results of XPS analysis originated from C1s and N1s spectra

Membrane	C		N	
	Species	Percent (%)	Species	Percent (%)
NF1	O-C=O	3.19	$-NH_n^+$	16.35
	N-C=O	9.15	N-C=O	28.3
	C-O	9.8	C-N	55.34
	C-N	22.31		
	C-C	55.54		
NF2	O-C=O	4.18	$-NH_n^+$	15.49
	N-C=O	9.76	N-C=O	35.21
	C-O	12.09	C-N	49.29
	C-N	21.16		
	C-C	52.19		
NF3	O-C=O	5.70	$-NH_n^+$	14.7
	N-C=O	9.88	N-C=O	38.11
	C-O	15.21	C-N	47.18
	C-N	19.01		
	C-C	50.19		
NF4	O-C=O	6.25	$-NH_n^+$	14.16
	N-C=O	10.72	N-C=O	39.82
	C-O	15.62	C-N	46.01
	C-N	18.30		
	C-C	49.11		
NF5	O-C=O	6.45	$-NH_n^+$	13.4
	N-C=O	11.98	N-C=O	41.02
	C-O	17.51	C-N	45.57
	C-N	16.59		
	C-C	47.46		
NF6	O-C=O	6.73	$-NH_n^+$	12.61

N-C=O	12.10	N-C=O	41.54
C-O	17.92	C-N	45.84
C-N	15.73		
C-C	47.51		

Fig.4-5 presents the FESEM images, which were adopted to observe the microstructure changes of prepared membranes. Compared to the substrate membrane in Fig.4-5(a), the typical valley and ridge wrinkle structures can be found on the NF membrane surface in Fig.4-5(b), which was due to the active crosslinking between PEI and TMC. After incorporating 150ppm MWCNTs-COOK nano-additives, the NF membrane showed a close mesh structure. The incorporated MWCNTs-COOK can connect with both monomers PEI and TMC, leading to a tightly crosslinked network among PEI, MWCNTs-COOK, and TMC. However, when the content of MWCNTs-COOK rose to 1000ppm, the loose tubular-nodular crumpled structures can be observed on the obtained NF membrane surface. On the one hand, excessive MWCNTs-COOK nano-additives in aqueous tend to cluster together. Besides, more MWCNTs-COOK in the aqueous solution will fix more PEI, limiting the penetration of more PEI branches to the two-phase interface. Moreover, more MWCNTs-COOK will compete with PEI to react with TMC during interfacial polymerization, reducing the interaction between PEI and TMC and even resulting in a looser defective polyamide layer.

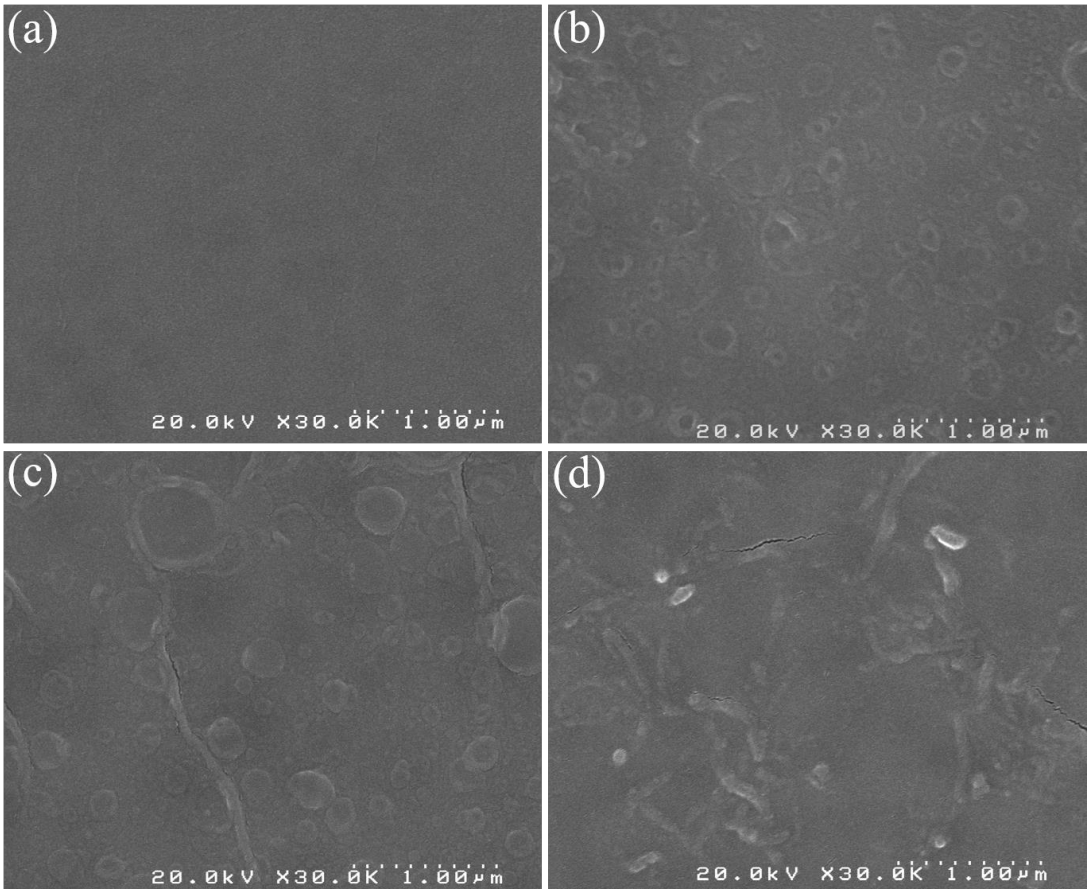

Fig.4-5 FESEM images of (a) PES substrate and NF membranes with MWCNTs-COOK dosage of: (b) 0ppm, (c) 150ppm, and (d) 1000ppm.

The regulation of MWCNTs-COOK on the topology and roughness of the final NF membrane was further measured by AFM analysis. As displayed in Fig.4-6 and Table 4-2, with a small increase of MWCNTs-COOK from 0ppm to 150ppm, the NF membrane surface tended to be smoother, accompanied by a gradual decrease roughness of membrane surface. With a small amount of MWCNTs-COOK, the nano-additives were evenly distributed and crosslinked in the emerged polyamide layer, filling the valley and ridge structure and leading to a smoother membrane surface. However, with a further addition of MWCNTs-COOK to 1000ppm, the resultant NF membrane exhibited a prominent ridged surface with significantly increased surface roughness. The AFM topology matches well with the FESEM measurement results. Incorporating excessive MWCNTs-COOK will significantly interfere with the interfacial polymerization process, leading to a lower crosslink degree of the formed polyamide layer. The unevenly distributed MWCNTs-COOK were in-suit firmed on

the polyamide layer due to excessive content, resulting in a loose and bumpy membrane surface. In summary, the microstructure and topology of the NF membrane can be slightly regulated by controlling the content of MWCNTs-COOK nano-additives. Note that low-dose MWCNTs-COOK would evenly distribute and crosslink with PEI and TMC, contributing to a relatively dense crosslinked network and smooth membrane surface.

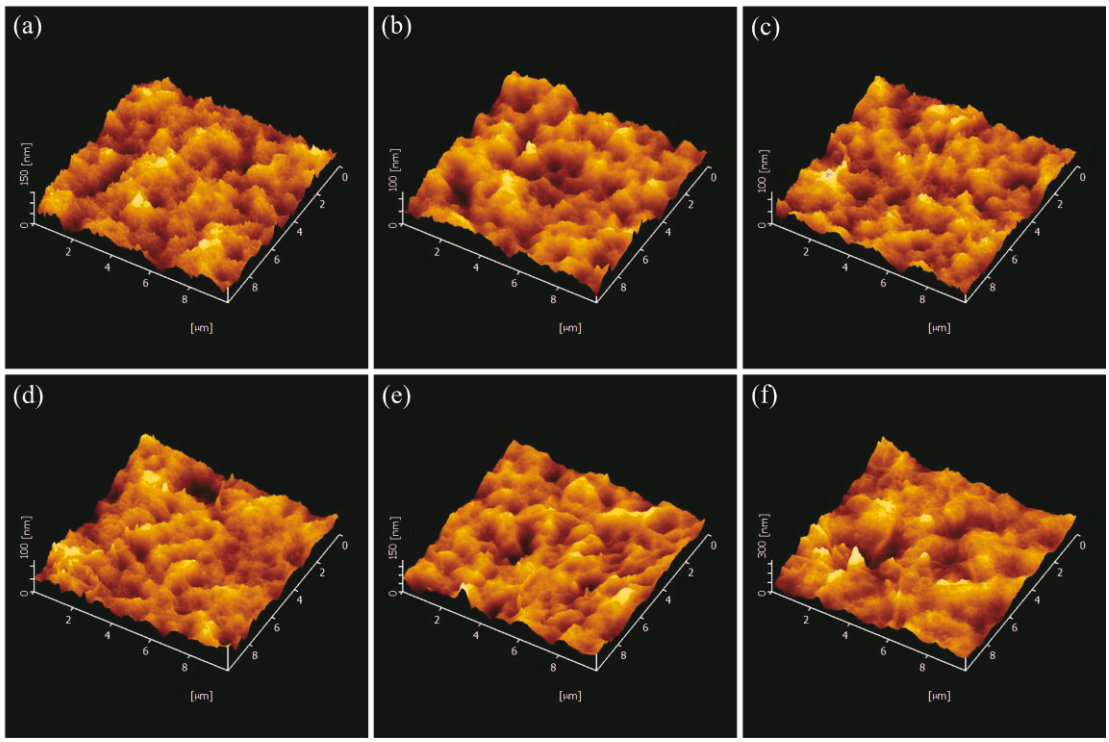

Fig.4-6 AFM images of NF membrane with MWCNTs-COOK dosage of: (a) 0ppm, (b) 30ppm, (c) 100ppm, (d) 150ppm, (e) 300ppm, and (f) 1000ppm.

Table 4-2 Roughness of NF membranes

Membrane	Ra (nm)	Rms (nm)
NF1	17.13	21.52
NF2	14.51	18.05
NF3	12.43	15.56
NF4	11.69	15.13
NF5	15.81	20.44
NF6	52.82	69.66

4.3.3 Surface properties characterization

The regulation effect of MWCNTs-COOK on the membrane surface hydrophilicity was proved by the contact angle test using pure water. As presented in Fig.4-7(a), an apparently reduced contact angle can be found after the formation of a polyamide layer on the substrate surface, which was related to the remained amine groups from PEI and carboxyl groups hydrolyzed from the unreacted acyl chloride groups on TMC. Note that the embedded MWCNTs-COOK nano-additives significantly reduced the contact angle of the NF membrane. And the contact angle reduced gradually with the further increase of MWCNTs-COOK nano-additives dosage in the membrane. The embedded hydrophilic MWCNTs-COOK would introduce more hydrophilic groups, thereby endowing the membrane surface with enhanced hydrophilicity. Notably, the improved hydrophilicity of membrane surface is essential for optimizing the permeability and anti-fouling properties [59, 60].

The zeta potential analysis was implemented to measure the chargeability of membrane surface. As shown in Fig.4-7(b), the NF membrane exhibited high positive chargeability after the polyamide layer emerged on the substrate surface. After interfacial polymerization, there were still many unreacted amine groups from PEI remain on the membrane surface, which would be protonated to $-NH_n^+$ (n=2, 3), giving the obtained membrane a high positive chargeability [61]. Note that when the pH value of the filtrate solution is higher than the isoelectric point, the membrane surface will exhibit negative chargeability, which was attributed to the deprotonated carboxyl group hydrolyzed by excess acyl chloride groups on TMC [13]. The incorporation of MWCNTs-COOK slightly reduced the isoelectric point of final NF membrane, matching the XPS results well. The introduced MWCNTs-COOK consumed some amine groups on PEI, leading to less free amine groups protonated to $-NH_n^+$, thereby weakening the positively charge in the membrane surface. On the other hand, the introduced MWCNTs-COOK also consumed some acyl chloride groups on TMC, resulting in less free acyl chloride groups hydrolyzed into the carboxyl group, thereby weakening the negatively charge on the membrane surface. Due to the combined

influence, we were surprised to find that, under the condition of using a neutral filter solution (pH ≈ 7), the NF membrane with 150ppm MWCNTs-COOK showed a similar zeta potential value with pristine NF membrane without MWCNTs-COOK. Besides, with high content MWCNTs-COOK of 1000ppm, the Zeta potential value of the obtained NF membrane reduced slightly under the condition of pH ≈ 7. In summary, the NF membrane with 150ppm MWCNTs-COOK presented high positive chargeability, which is proved to be vital for separating monovalent and multivalent cations.

Fig.4-7(c) shows the MWCO test results of NF membranes, which is further evidence for evaluating the changes of MWCNTs-COOK on the pore structure of the resultant NF membrane. The MWCO value of NF membranes with 150ppm MWCNTs-COOK was slightly higher than that of the pristine NF membranes with no MWCNTs-COOK, which was resulted from a tight network structure formed by PEI, MWCNTs-COOK, and TMC. The decreased pore size of the membrane would slightly strengthen transmission resistance during the filtration process. On the contrary, with excessive MWCNTs-COOK of 1000ppm, the resultant NF membrane showed a slightly increased MWCO value, which indicated a slight enlarged pore size of the membrane. Consistent with the above microstructure results, excessive MWCNTs-COOK nano-additives tend to cluster together and cause a looser polyamide layer, correspondingly reducing the pore size of the final NF membrane to a certain extent. Based on the above results, embedding low content MWCNTs-COOK nano-additives into the interfacial polymerization system is promising for fine-tuning the microstructure and surface properties of the final NF membranes.

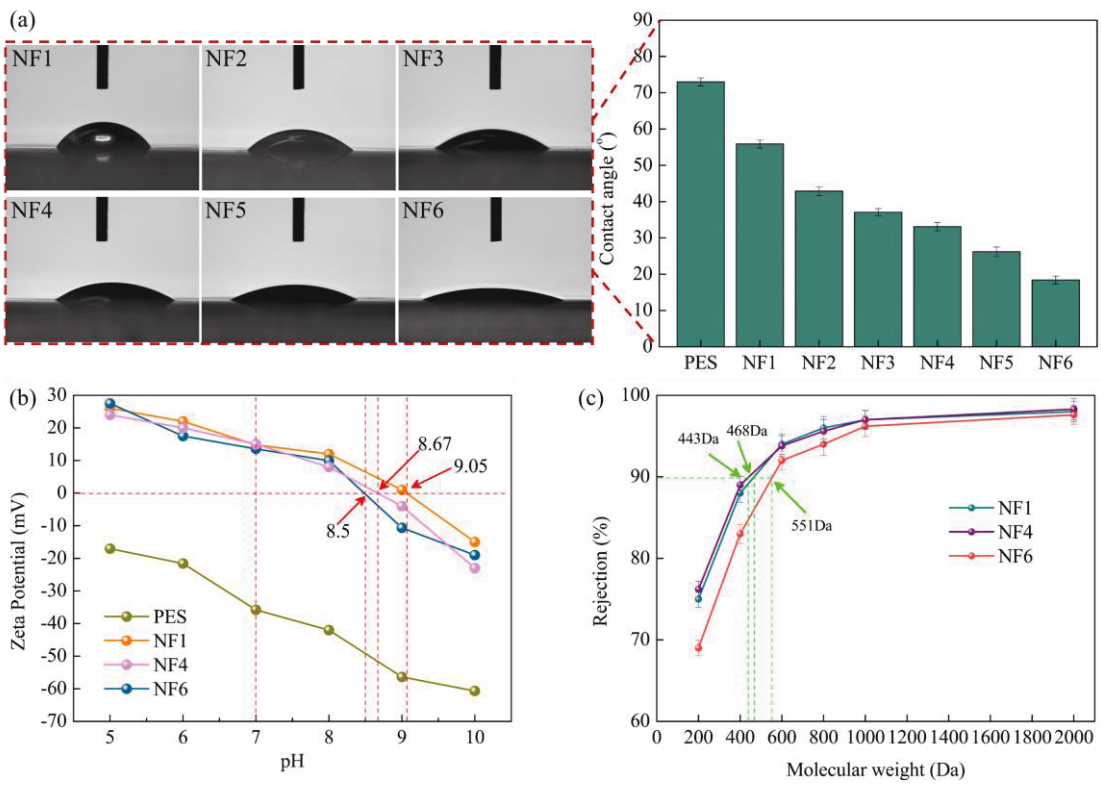

Fig.4-7 Surface properties characterization of membranes: (a) contact angle, (b) Zeta potential, (c) MWCO.

4.3.4 Separation performance characterization

Cross-flow, low operating pressure (3 bar), and continuous filtration tests were carried out to evaluate the changes of MWCNTs-COOK on the Li^+ enrichment and Mg^{2+} removal performance of NF membranes. According to the filtration results presented in Fig.4-8(a), each NF membrane showed a significant difference in the rejections of Li^+ and Mg^{2+}. After filtering the feed solution (Mg^{2+}/Li^+ mass ratio of 20) using these NF membranes, the mass ratio of Mg^{2+}/Li^+ in permeate solution was greatly decreased, which indicated the high rejection selectivity for Li^+ and Mg^{2+} during the transmission process. Divalent cation Mg^{2+} carries more positively charge than the monovalent cation Li^+. During the transmission process, higher-valence cation Mg^{2+} with larger size suffered stronger electrostatic repulsion and steric hindrance from the high positively charged membrane surface, which promoted the high difference between rejections of Li^+ and Mg^{2+} [21, 23]. Note that with a slight addition of

MWCNTs-COOK to 150ppm, the NF membrane presented a slightly higher rejection for Li^+ and Mg^{2+}, and the Mg^{2+}/Li^+ mass ratio in permeate solution decreased as low as 0.35. However, further increase of MWCNTs-COOK to 1000ppm caused a higher Mg^{2+}/Li^+ mass ratio in permeate solution and reduced rejection for Li^+ and Mg^{2+}. This phenomenon may be caused by the comprehensive effect of embedded MWCNTs-COOK on the structure and properties of the NF membrane. As discussed above, with an appropriate content of MWCNTs-COOK, the resultant NF membrane showed high positive chargeability and a slightly denser surface, contributing to a strong electrostatic repulsion and transmission resistance. On the contrary, excessive MWCNTs-COOK would hinder the formation of the selective layer, leading to a looser membrane surface with slightly weaker positive chargeability, which would weaken the electrostatic repulsion and transmission resistance during filtration.

On the other hand, as shown in Fig.4-8(b), the permeate flux of NF membrane was greatly improved after embedding MWCNTs-COOK nano-additives. The embedded MWCNTs-COOK introduced more hydrophilic groups into the NF membrane, which correspondingly improved the hydrophilicity of the membrane. In addition, the hollow tubular structure of MWCNTs-COOK and the inter-gap between MWCNTs-COOK nano-additives and the polymer matrix provided many nano-channels for water to penetrate through membrane. This phenomenon powerfully demonstrated the positive effect of MWCNTs-COOK on the permeate flux of NF membrane. After comprehensively considering the flux and rejections for Li^+ and Mg^{2+}, the NF membrane with an optimal MWCNTs-COOK content of 150ppm performed remarkably high separation ability ($R(Mg^{2+})$ = 98.64%, $R(Li^+)$ = 21.58%) and high permeate flux (12.23 L/m^2hbar) simultaneously. Note that the optimal NF4 membrane exhibited a superior permeation flux without a significant compromise in Li^+/Mg^{2+} separation ability.

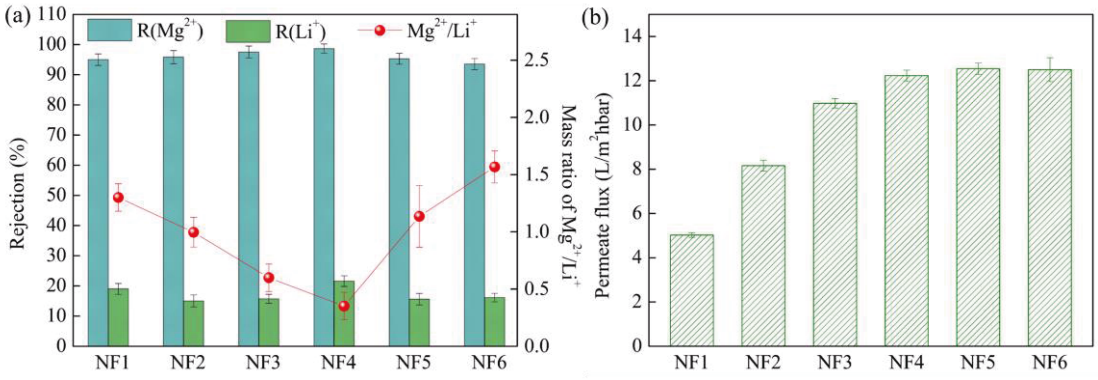

Fig.4-8 Li^+ enrichment and Mg^{2+} removal performance of NF membranes with different MWCNTs-COOK dosage:(a) rejections Mg^{2+} and Li^+, and mass ratio of Mg^{2+}/Li^+ in permeate solution, and (b) permeate flux.

Fig.4-9(a) shows the long-term separation performance of MWCNTs-COOK (150ppm)-assisted NF membrane. The NF membrane displayed a constant remarkably high rejection of Mg^{2+} around 98%, and the rejection of Li^+ was around 21% with a slight fluctuation due to the low concentration of Li^+. Additionally, the NF membrane also maintained a stable high permeate flux, which benefited from the robust and stable structure of the membrane. After 48h constant filtration, the flux of membrane showed a slight decrease to 11.6 L/m^2hbar, which may be caused by the compaction of membrane matrix. Overall, the MWCNTs-COOK-assisted NF membrane with high durability can work stably and outstandingly during lithium extraction. As shown in Table 4-3 and Fig.4-9(b), we summarized several reported NF membranes to evaluate the Li^+ enrichment and Mg^{2+} removal performance of the composite NF membrane prepared in this work. It can be found that each of the listed NF membranes shows a high difference in Li^+ and Mg^{2+} rejections, which indicated a superior separation ability of the NF membrane for Li^+ and Mg^{2+}. However, most NF membranes suffer from the low permeate flux, which limited the separation quality during filtration. Compared to these NF membranes, under the filtration conditions of low operating pressure and high Mg^{2+}/Li^+ mass ratio, the NF membrane proposed in this work displayed a high permeate flux and a significant rejection difference between Li^+ and Mg^{2+}, which can achieve quick and efficient Li^+ enrichment and Mg^{2+} removal. This phenomenon further verified the effective regulation of MWCNTs-COOK on the properties of the resultant

NF membrane. In summary, the prepared MWCNTs-COOK-assisted positively charged NF membrane is a promising candidate for rapid enrichment of high-purity lithium resources from salt-lake brines.

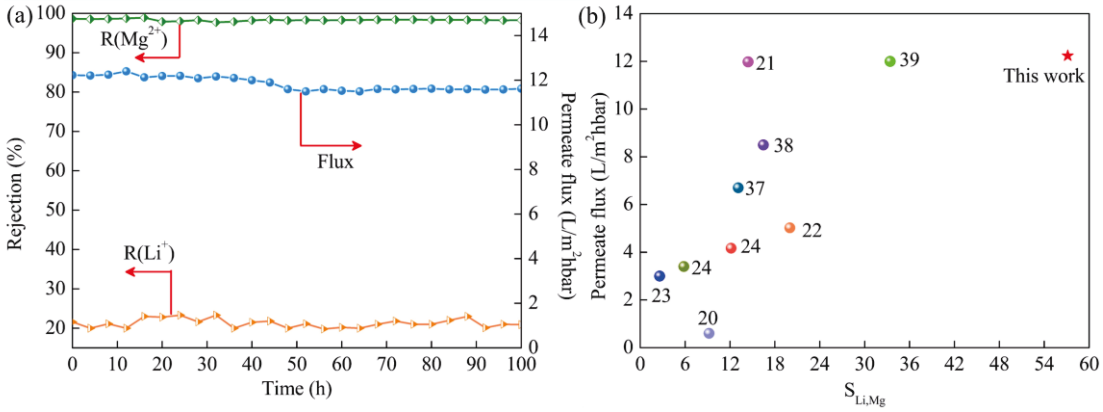

Fig.4-9 (a) Long-term separation performance of the MWCNTs-COOK (150ppm)-assisted NF membrane and (b) comparison of Li^+/Mg^{2+} separation properties with reported NF membranes.

Table 4-3 Comparison of Li^+/Mg^{2+} separation performance of several reported NF membranes

Selective layer	Operate pressure (bar)	Mg^{2+}/Li^+ mass ratio	$R(Mg^{2+})$	$R(Li^+)$	Ref
DAPP/TMC	3	20	46%	-40.7%	[23]
TMC/BPEI/EDTA	10	24	91.9%	20%	[20]
PIP-MWCNTs/PEI/ TMC	4	21.4	95% ($MgCl_2$)	18% ($MgCl_2$)	[38]
PIP-PHF/TMC	6	21.4	89.9	16.3	[37]
PEI/TMC	8	20	95%	19%	[22]
CNC-COOH/PEI/TMC	8	30	96.11	21.76	[24]
CNC-COOH/PEI/TMC	8	60	95.59	11.63	[24]
CQDs-NH_2/TMC	2	30	94.65% ($MgCl_2$)	22.86% (LiCl)	[21]
PIP/TMC/PEI	4	21.3	98.5% ($MgCl_2$)	46.2% (LiCl)	[39]
(MWCNTs-COOK)-PEI/TMC	3	20	98.64%	21.58%	This work

4.4 Conclusion

In summary, the MWCNTs-COOK-assisted highly permeable NF membrane with superior Li^+/Mg^{2+} separate-selectivity was successfully synthesized and optimized through interfacial polymerization. Results show that the incorporated MWCNTs-COOK intensified the network-crosslinking among PEI, MWCNTs-COOK, and TMC, achieving fine-tuning of structure and properties of resultant NF membranes. The presence of MWCNTs-COOK nano-additives significantly increased the flux of the NF membrane. The hollow tubular structure of MWCNTs-COOK and inter-gap between MWCNTs-COOK and membrane matrix furnished NF membrane with more channels for water to transport. Moreover, MWCNTs-COOK introduced more hydrophilic group and greatly improved the hydrophilicity of the membrane surface. However, excessive incorporation of MWCNTs-COOK would interfere with the interfacial polymerization, resulting in a loose selective layer structure and a weakened positively charge. Among several prepared NF membranes, the optimal NF membrane with 150ppm MWCNTs-COOK performed excellently during the filtration process. Benefiting from the synergistic effects of MWCNTs-COOK, the NF membrane was endowed with a dense selective layer with high hydrophilicity and positive chargeability. The obtained MWCNTs-COOK-assisted NF membrane showed a significantly improved flux of 12.23 L/m^2hbar without a compromise in Li^+/Mg^{2+} separate-selectivity, which greatly accelerated the filtration process. Importantly, the MWCNTs-COOK-assisted NF membrane exhibited a remarkably high separation factor $S_{Li,Mg}$ of 58, indicating the superior Li^+ enrich and Mg^{2+} remove capabilities. Moreover, the NF performance of the NF membrane remained stable even in long-term utilization. Overall, this work provides a feasible technique for quickly extracting high-purity lithium from salt-lake brine.

References

[1] X. Li, Y. Mo, W. Qing, S. Shao, C.Y. Tang, J. Li, Membrane-based technologies for

lithium recovery from water lithium resources: A review, Journal of Membrane Science, 591 (2019) 117317.

[2] Q.-B. Chen, Z.-Y. Ji, J. Liu, Y.-Y. Zhao, S.-Z. Wang, J.-S. Yuan, Development of recovering lithium from brines by selective-electrodialysis: Effect of coexisting cations on the migration of lithium, Journal of Membrane Science, 548 (2018) 408-420.

[3] B. Swain, Recovery and recycling of lithium: A review, Separation and Purification Technology, 172 (2017) 388-403.

[4] Y. Zhang, L. Wang, W. Sun, Y. Hu, H. Tang, Membrane technologies for Li^+/Mg^{2+} separation from salt-lake brines and seawater: A comprehensive review, Journal of Industrial and Engineering Chemistry, 81 (2020) 7-23.

[5] L. Kavanagh, J. Keohane, G. Garcia Cabellos, A. Lloyd, J. Cleary, Global lithium sources—Industrial use and future in the electric vehicle industry: A review, Resources, 7 (2018) 57.

[6] X. Xu, Y. Chen, P. Wan, K. Gasem, K. Wang, T. He, H. Adidharma, M. Fan, Extraction of lithium with functionalized lithium ion-sieves, Progress in Materials Science, 84 (2016) 276-313.

[7] P. Xu, J. Hong, X. Qian, Z. Xu, H. Xia, X. Tao, Z. Xu, Q.-Q. Ni, Materials for lithium recovery from salt lake brine, Journal of Materials Science, 56 (2020) 16-63.

[8] G. Liu, Z. Zhao, L. He, Highly selective lithium recovery from high Mg/Li ratio brines, Desalination, 474 (2020) 114185.

[9] L. He, W. Xu, Y. Song, Y. Luo, X. Liu, Z. Zhao, New insights into the application of lithium-ion battery materials: Selective extraction of lithium from brines via a rocking-chair lithium-ion battery system, Glob Chall, 2 (2018) 1700079.

[10] X. Wang, Y. Jing, H. Liu, Y. Yao, C. Shi, J. Xiao, S. Wang, Y. Jia, Extraction of lithium from salt lake brines by bis[(trifluoromethyl)sulfonyl]imide-based ionic liquids, Chemical Physics Letters, 707 (2018) 8-12.

[11] H. Wang, Y. Zhong, B. Du, Y. Zhao, M. Wang, Recovery of both magnesium and lithium from high Mg/Li ratio brines using a novel process, Hydrometallurgy, 175 (2018) 102-108.

[12] X. Liu, M. Zhong, X. Chen, Z. Zhao, Separating lithium and magnesium in brine by aluminum-based materials, Hydrometallurgy, 176 (2018) 73-77.

[13] T. Shintani, K. Akamatsu, S. Hamada, K. Nakagawa, H. Matsuyama, T. Yoshioka, Preparation of monoamine-incorporated polyamide nanofiltration membranes by interfacial polymerization for efficient separation of divalent anions from divalent cations, Separation and Purification Technology, 239 (2020) 116530.

[14] Y. Lin, Q. Shen, Y. Kawabata, J. Segawa, X. Cao, K. Guan, T. Istirokhatun, T. Yoshioka, H. Matsuyama, Graphene quantum dots (GQDs)-assembled membranes with intrinsic functionalized nanochannels for high-performance nanofiltration, Chemical Engineering Journal, (2020) 127602.

[15] M.J. Park, C. Wang, D.H. Seo, R.R. Gonzales, H. Matsuyama, H.K. Shon, Inkjet printed single walled carbon nanotube as an interlayer for high performance thin film composite nanofiltration membrane, Journal of Membrane Science, (2020) 118901.

[16] Z. Jiang, J. Miao, Y. He, K. Tu, S. Chen, R. Zhang, L. Zhang, H. Yang, A novel positively charged composite nanofiltration membrane based on polyethyleneimine with a tunable active layer structure developed via interfacial polymerization, RSC Advances, 9 (2019) 10796-10806.

[17] G.S. Lai, W.J. Lau, P.S. Goh, M. Karaman, M. Gürsoy, A.F. Ismail, Development of thin film nanocomposite membrane incorporated with plasma enhanced chemical vapor deposition-modified hydrous manganese oxide for nanofiltration process, Composites Part B: Engineering, 176 (2019) 107328.

[18] S.-Y. Sun, L.-J. Cai, X.-Y. Nie, X. Song, J.-G. Yu, Separation of magnesium and lithium from brine using a Desal nanofiltration membrane, Journal of Water Process Engineering, 7 (2015) 210-217.

[19] Q. Bi, Z. Zhang, C. Zhao, Z. Tao, Study on the recovery of lithium from high Mg^{2+}/Li^{+} ratio brine by nanofiltration, Water Sci Technol, 70 (2014) 1690-1694.

[20] W. Li, C. Shi, A. Zhou, X. He, Y. Sun, J. Zhang, A positively charged composite nanofiltration membrane modified by EDTA for $LiCl/MgCl_2$ separation, Separation and Purification Technology, 186 (2017) 233-242.

[21] C. Guo, X. Qian, F. Tian, N. Li, W. Wang, Z. Xu, S. Zhang, Amino-rich carbon quantum dots ultrathin nanofiltration membranes by double “one-step” methods: Breaking through trade-off among separation, permeation and stability, Chemical Engineering Journal, 404 (2021) 127144.

[22] P. Xu, W. Wang, X. Qian, H. Wang, C. Guo, N. Li, Z. Xu, K. Teng, Z. Wang, Positive charged PEI-TMC composite nanofiltration membrane for separation of Li^+ and Mg^{2+} from brine with high Mg^{2+}/Li^+ ratio, Desalination, 449 (2019) 57-68.

[23] X. Li, C. Zhang, S. Zhang, J. Li, B. He, Z. Cui, Preparation and characterization of positively charged polyamide composite nanofiltration hollow fiber membrane for lithium and magnesium separation, Desalination, 369 (2015) 26-36.

[24] C. Guo, N. Li, X. Qian, J. Shi, M. Jing, K. Teng, Z. Xu, Ultra-thin double Janus nanofiltration membrane for separation of Li^+ and Mg^{2+}: “Drag” effect from carboxyl-containing negative interlayer, Separation and Purification Technology, 230 (2020) 115567.

[25] J. Wang, Y. Wang, J. Zhu, Y. Zhang, J. Liu, B. Van der Bruggen, Construction of TiO_2@graphene oxide incorporated antifouling nanofiltration membrane with elevated filtration performance, Journal of Membrane Science, 533 (2017) 279-288.

[26] X. Zhang, L. Shen, C.-Y. Guan, C.-X. Liu, W.-Z. Lang, Y. Wang, Construction of SiO_2@MWNTs incorporated PVDF substrate for reducing internal concentration polarization in forward osmosis, Journal of Membrane Science, 564 (2018) 328-341.

[27] H. Zangeneh, A.A. Zinatizadeh, S. Zinadini, M. Feyzi, D.W. Bahnemann, Preparation ultrafine l-Methionine (C,N,S triple doped)-TiO_2-ZnO nanoparticles and their photocatalytic performance for fouling alleviation in PES nanocomposite membrane, Composites Part B: Engineering, 176 (2019) 107158.

[28] P. Wen, Y. Chen, X. Hu, B. Cheng, D. Liu, Y. Zhang, S. Nair, Polyamide thin film composite nanofiltration membrane modified with acyl chlorided graphene oxide, Journal of Membrane Science, 535 (2017) 208-220.

[29] J. Wang, C. Zhao, T. Wang, Z. Wu, X. Li, J. Li, Graphene oxide polypiperazine-amide nanofiltration membrane for improving flux and anti-fouling in water

purification, RSC Adv., 6 (2016) 82174-82185.

[30] M. Shan, H. Kang, Z. Xu, N. Li, M. Jing, Y. Hu, K. Teng, X. Qian, J. Shi, L. Liu, Decreased cross-linking in interfacial polymerization and heteromorphic support between nanoparticles: Towards high-water and low-solute flux of hybrid forward osmosis membrane, J Colloid Interface Sci, 548 (2019) 170-183.

[31] P. Zhao, R. Li, W. Wu, J. Wang, J. Liu, Y. Zhang, In-situ growth of polyvinylpyrrolidone modified Zr-MOFs thin-film nanocomposite (TFN) for efficient dyes removal, Composites Part B: Engineering, 176 (2019) 107208.

[32] C. Liu, W. Wang, L. Zhu, F. Cui, C. Xie, X. Chen, N. Li, High-performance nanofiltration membrane with structurally controlled PES substrate containing electrically aligned CNTs, Journal of Membrane Science, 605 (2020) 118104.

[33] Z. Zhou, Y. Hu, Q. Wang, B. Mi, Carbon nanotube-supported polyamide membrane with minimized internal concentration polarization for both aqueous and organic solvent forward osmosis process, Journal of Membrane Science, 611 (2020) 118273.

[34] L. Deng, Q. Wang, X. An, Z. Li, Y. Hu, Towards enhanced antifouling and flux performances of thin-film composite forward osmosis membrane via constructing a sandwich-like carbon nanotubes-coated support, Desalination, 479 (2020) 114311.

[35] H. Kang, W. Wang, J. Shi, Z. Xu, H. Lv, X. Qian, L. Liu, M. Jing, F. Li, J. Niu, Interlamination restrictive effect of carbon nanotubes for graphene oxide forward osmosis membrane via layer by layer assembly, Applied Surface Science, 465 (2019) 1103-1106.

[36] N. Nasrollahi, S. Aber, V. Vatanpour, N.M. Mahmoodi, The effect of amine functionalization of CuO and ZnO nanoparticles used as additives on the morphology and the permeation properties of polyethersulfone ultrafiltration nanocomposite membranes, Composites Part B: Engineering, 154 (2018) 388-409.

[37] Q. Shen, S.J. Xu, Z.L. Xu, H.Z. Zhang, Z.Q. Dong, Novel thin-film nanocomposite membrane with water-soluble polyhydroxylated fullerene for the separation of Mg^{2+}/Li^{+} aqueous solution, Journal of Applied Polymer Science, 136 (2019) 48029.

[38] H.-Z. Zhang, Z.-L. Xu, H. Ding, Y.-J. Tang, Positively charged capillary

nanofiltration membrane with high rejection for Mg^{2+} and Ca^{2+} and good separation for Mg^{2+} and Li^{+}, Desalination, 420 (2017) 158-166.

[39] Z. Yang, W. Fang, Z. Wang, R. Zhang, Y. Zhu, J. Jin, Dual-skin layer nanofiltration membranes for highly selective Li^{+}/Mg^{2+} separation, Journal of Membrane Science, (2020) 118862.

[40] Q. Kong, H. Xu, C. Liu, G. Yang, M. Ding, W. Yang, T. Lin, W. Chen, S. Gray, Z. Xie, Fabrication of high performance TFN membrane containing NH_2-SWCNTs via interfacial regulation, RSC Advances, 10 (2020) 25186-25199.

[41] L. Zhang, Q.-Q. Ni, Y. Fu, T. Natsuki, One-step preparation of water-soluble single-walled carbon nanotubes, Applied Surface Science, 255 (2009) 7095-7099.

[42] V. Vatanpour, M. Esmaeili, M.H.D.A. Farahani, Fouling reduction and retention increment of polyethersulfone nanofiltration membranes embedded by amine-functionalized multi-walled carbon nanotubes, Journal of Membrane Science, 466 (2014) 70-81.

[43] S.M. Xue, Z.L. Xu, Y.J. Tang, C.H. Ji, Polypiperazine-amide Nanofiltration Membrane Modified by Different Functionalized Multiwalled Carbon Nanotubes (MWCNTs), ACS Appl Mater Interfaces, 8 (2016) 19135-19144.

[44] A. Dourani, M. Haghgoo, M. Hamadanian, Multi-walled carbon nanotube and carbon nanofiber/ polyacrylonitrile aerogel scaffolds for enhanced epoxy resins, Composites Part B: Engineering, 176 (2019) 107299.

[45] S. Ramesh, A. Kathalingam, K. Karuppasamy, H.-S. Kim, H.S. Kim, Nanostructured CuO/Co_2O_4@ nitrogen doped MWCNT hybrid composite electrode for high-performance supercapacitors, Composites Part B: Engineering, 166 (2019) 74-85.

[46] J. Zhang, Z. Xu, M. Shan, B. Zhou, Y. Li, B. Li, J. Niu, X. Qian, Synergetic effects of oxidized carbon nanotubes and graphene oxide on fouling control and anti-fouling mechanism of polyvinylidene fluoride ultrafiltration membranes, Journal of Membrane Science, 448 (2013) 81-92.

[47] H. Zhao, S. Qiu, L. Wu, L. Zhang, H. Chen, C. Gao, Improving the performance of polyamide reverse osmosis membrane by incorporation of modified multi-walled

carbon nanotubes, Journal of Membrane Science, 450 (2014) 249-256.
[48] N.N. Gumbi, M. Hu, B.B. Mamba, J. Li, E.N. Nxumalo, Macrovoid-free PES/SPSf/O-MWCNT ultrafiltration membranes with improved mechanical strength, antifouling and antibacterial properties, Journal of Membrane Science, 566 (2018) 288-300.
[49] P. Wang, G. Deng, H. Zhu, H. Zhang, J. Yin, X. Xiong, X. Wu, Effect of MWCNT content on conductivity and mechanical and wear properties of copper foam/resin composite, Composites Part B: Engineering, 168 (2019) 572-580.
[50] S. Kang, J. Kim, J.H. Park, I. Jung, M. Park, Multiwalled carbon nanotube pretreatment to enhance tensile properties, process stability, and filler dispersion of polyamide 66 nanocomposites, Composites Part B: Engineering, 198 (2020) 108204.
[51] X. Liu, J. Luo, J. Fan, S. Lin, L. Jia, X. Jia, Q. Cai, X. Yang, Comprehensive enhancement in overall properties of MWCNTs-COOH/epoxy composites by microwave: An efficient approach to strengthen interfacial bonding via localized superheating effect, Composites Part B: Engineering, 174 (2019) 106909.
[52] M. Hu, Z. Cui, J. Li, L. Zhang, Y. Mo, D.S. Dlamini, H. Wang, B. He, J. Li, H. Matsuyama, Ultra-low graphene oxide loading for water permeability, antifouling and antibacterial improvement of polyethersulfone/sulfonated polysulfone ultrafiltration membranes, J Colloid Interface Sci, 552 (2019) 319-331.
[53] P. Xu, J. Hong, X. Qian, Z. Xu, H. Xia, Q.-Q. Ni, “Bridge” graphene oxide modified positive charged nanofiltration thin membrane with high efficiency for Mg^{2+}/Li^{+} separation, Desalination, 488 (2020) 114522.
[54] X. Li, L. Liu, Z. Xu, W. Wang, J. Shi, L. Liu, M. Jing, F. Li, X. Zhang, Gamma irradiation and microemulsion assisted synthesis of monodisperse flower-like platinum-gold nanoparticles/reduced graphene oxide nanocomposites for ultrasensitive detection of carcinoembryonic antigen, Sensors and Actuators B: Chemical, 287 (2019) 267-277.
[55] K. Goh, L. Setiawan, L. Wei, W. Jiang, R. Wang, Y. Chen, Fabrication of novel functionalized multi-walled carbon nanotube immobilized hollow fiber membranes for enhanced performance in forward osmosis process, Journal of Membrane Science, 446

(2013) 244-254.
[56] Y.-F. Mi, G. Xu, Y.-S. Guo, B. Wu, Q.-F. An, Development of antifouling nanofiltration membrane with zwitterionic functionalized monomer for efficient dye/salt selective separation, Journal of Membrane Science, 601 (2020) 117795.
[57] X. Song, L. Wang, C.Y. Tang, Z. Wang, C. Gao, Fabrication of carbon nanotubes incorporated double-skinned thin film nanocomposite membranes for enhanced separation performance and antifouling capability in forward osmosis process, Desalination, 369 (2015) 1-9.
[58] E.A.M. Hassan, L. Yang, T.H.H. Elagib, D. Ge, X. Lv, J. Zhou, M. Yu, S. Zhu, Synergistic effect of hydrogen bonding and π-π stacking in interface of CF/PEEK composites, Composites Part B: Engineering, 171 (2019) 70-77.
[59] N. Akther, Z. Yuan, Y. Chen, S. Lim, S. Phuntsho, N. Ghaffour, H. Matsuyama, H. Shon, Influence of graphene oxide lateral size on the properties and performances of forward osmosis membrane, Desalination, 484 (2020) 114421.
[60] Y. Li, Y. Su, X. Zhao, R. Zhang, Y. Liu, X. Fan, J. Zhu, Y. Ma, Y. Liu, Z. Jiang, Preparation of Antifouling Nanofiltration Membrane via Interfacial Polymerization of Fluorinated Polyamine and Trimesoyl Chloride, Industrial & Engineering Chemistry Research, 54 (2015) 8302-8310.
[61] K. Gu, S. Wang, Y. Li, X. Zhao, Y. Zhou, C. Gao, A facile preparation of positively charged composite nanofiltration membrane with high selectivity and permeability, Journal of Membrane Science, 581 (2019) 214-223.

Chapter 5

✵✵✵✵✵✵✵✵✵✵✵✵✵✵✵✵✵✵✵✵✵✵✵✵✵✵✵✵

Positively charged nanofiltration membrane based on (MWCNTs-COOK)-engineered substrate for fast and efficient lithium extraction

✵✵✵✵✵✵✵✵✵✵✵✵✵✵✵✵✵✵✵✵✵✵✵✵✵✵✵✵

5 Positively charged nanofiltration membrane based on (MWCNTs-COOK)-engineered substrate for fast and efficient lithium extraction

5.1 Introduction

Achieving high extraction rate of lithium resources from salt-lake is urgently needed to meet the increasing market requirement [1-4]. Reducing the Mg^{2+}/ Li^{+} mass ratio is an essential step for effective lithium extraction from salt-lake brine [5-13]. NF membrane separation technology is a promising approach for lithium separation and extraction [3, 14, 15]. In addition, NF membranes can selectively separate monovalent and multivalent ions due to the dual-effect of electrostatic interaction and steric hindrance [16-22]. Since Li^{+} (0.382 nm) and Mg^{2+} (0.428 nm) have similar ionic hydration radius [23], it is difficult to achieve separation of Mg^{2+} and Li^{+} by precisely controlling the pore size of the NF membrane during synthesize process. Therefore, electrostatic interaction is the dominant factor in designing NF membrane for separating the monovalent cation Li^{+} and divalent cation Mg^{2+}. Recently, researchers have proved that the positively charged NF membrane is more suitable for Mg^{2+}/Li^{+} separation due to the existence of electrostatic repulsion effect [3, 9, 24-26]. However, these reported NF membranes face the same difficulty of low flux, which extremely restrict the work efficiency of NF membranes during Mg^{2+}/Li^{+} separation.

Researchers have proved that the permeation performance of NF membrane can be improved by the addition of carbon-based nanomaterials, such as graphene oxide (GO) [27-31] and functional carbon nanotubes [32-35]. Shen et al. incorporated the polyhydroxylated fullerene (PHF) into the interfacial polymerization system to improve the flux and Mg^{2+}/Li^{+} separation property of NF membrane [7]. During Mg^{2+}/Li^{+}

separation test, the flux of NF membrane achieved 6.7 (L/m^{2}hbar). Zhang et al. grafted piperazine (PIP) on hydroxyl functionalized multi-walled carbon nanotubes, and then applied it as the additive during polyamide layer formation process [34]. They surprisingly demonstrated that the flux of the obtained NF membrane during Mg^{2+}/Li^+ separation was remarkably increased to 8.5 (L/m^{2}hbar). However, it is still difficult to simultaneously achieve high flux and separation performance due to the "trade-off" effect, which is a fatal problem that needs to be solved urgently. The structure and property of substrate membrane can directly affect the formation of the polyamide layer during interfacial polymerization [36]. However, there are few reports focus on the optimizing properties of the NF membrane by adjusting the substrate membrane. Herein, we proposed a new approach to optimize the NF membrane performance by regulating the substrate.

The unique structure and mechanical characteristics make Multi-walled carbon nanotubes (MWCNTs) an attractive nanomaterial in membrane field [37]. Especially, the hollow structure of MWCNTs and their inter-gaps in NF membrane can create more nanochannels for water molecular to pass through the membrane. Since MWCNTs tend to aggerate together, making it difficult to disperse them evenly in many common solvents [33, 34]. Among various functionalized MWCNTs [38-41], the oxidized MWCNTs with high hydrophilicity are popular nano-additives for improving membrane permeability. However, the oxidized MWCNTs are commonly synthesized by treating MWCNTs with acid solution (e.g., H_2SO_4 and HNO_3), which is acid-consuming and may cause environmental problems [42-45].

While ensuring the high perm-selectivity of Mg^{2+}/Li^+, increasing the permeation flux of the NF membrane is essential to achieve fast and efficient separation of Mg^{2+} and Li^+. In this work, we first synthesized the novel potassium carboxylate functionalized MWCNTs (MWCNTs-COOK) by one-step environmentally friendly oxidation process. The synthesized MWCNTs-COOK showed high solubility and can be uniformly dispersed in polar solvents. Then, we designed a novel NF membrane by anchoring the nano-additives MWCNTs-COOK into PES ultrafiltration substrate.

The MWCNTs-COOK grown in PES substrate can work as a “connector” and influence the formation of polyamide layer. We have systematically studied and discussed how the loaded MWCNTs-COOK alter the final NF membrane from many aspects, including microstructure, chemical composition, surface properties and Mg^{2+}/Li^{+} separation efficiency.

5.2 Experiment

5.2.1 Materials and chemicals

PES (M_W = 62000 Da) was purchased from Solvay Advanced Polymer (Belgium), and it was dried in the oven at 50 ℃ for 24 h before use. MWCNTs (10-20nm in diameter, 0.5-2μm in length) were obtained from Nanjing XFNANO Materials Tech. Co. Ltd. N, N-dimethylacetamide (DMAc), sodium dodecyl sulfate (SDS), n-hexane, PEI, TMC, polyethylene glycol (PEG), Sodium carbonate (Na_2CO_3), sodium chloride (NaCl), lithium chloride (LiCl), calcium chloride ($CaCl_2$), magnesium chloride ($MgCl_2$), magnesium sulfate ($MgSO_4$), sodium sulfate (Na_2SO_4), potassium persulfate ($K_2S_2O_8$) and potassium hydroxide (KOH) were all supplied by Wako Pure Chemical Industries Ltd., Japan.

5.2.2 Synthesis of MWCNTs-COOK

40mg pristine MWCNTs were firstly dispersed in 50ml deionized water by probe-sonication for 10 min at room temperature. Subsequently, 0.45g $K_2S_2O_8$ and 50ml KOH solution (1 wt%) were added, and then the mixture was vigorous stirred in the water bath at 80 ℃ for 3 h. The mixture was diluted with deionized water and dispersed with probe-sonication, and then centrifuged at 3000 rmp for 20min to eliminate residues. Finally, the functionalized MWCNTs-COOK powder was collected by filtering the supernatant though the membrane (47 mm/0.2μm) and dried at 50 ℃ for 24h.

5.2.3 Preparation of MWCNTs-COOK modified NF membrane

Firstly, the (MWCNTs-COOK)-engineered PES ultrafiltration substrate membranes were prepared via the non-solvent induced phase inversion method [46-48]. MWCNTs-COOK were ultrasonically dispersed in the DMAc solution for 3h at room temperature, and then PES and PEG were blended with the mixture by stirring at 50 ℃ for 6h. After fully degassing, the obtained casting solution was casted on the glass plat with a casting gap height of 200 μm, and then immediately immersed in the water bath to obtain the primary PES ultrafiltration membrane. The composition of casting solution with different MWCNTs-COOK contents was shown in Table 5-1.

The active layer of the MWCNTs-COOK modified NF membrane was formed through interfacial polymerization method [36, 49]. Briefly, immersing the obtained (MWCNTs-COOK)-engineered ultrafiltration substrate membrane in the PEI-contained aqueous phase solution (0.5 wt% PEI, 0.1wt% SDS, 0.1 wt% Na_2CO_3) for 5min, and removed excess solution using rubber roller. Subsequently, the membrane was immersed in the TMC contained organic solution (0.1 w/v% TMC in n-hexane) for 3 min to form a polyamide layer. Finally, the obtained membrane was cured at 70 ℃ for 10 min and stored in deionized water at 4 ℃ before test. The result MWCNTs-COOK modified NF membranes based on substate membrane UF0, UF1, UF2, UF3, UF4, UF5, UF6, and UF7 were denoted as NF0, NF1, NF2, NF3, NF4, NF5, NF6, and NF7, respectively.

Table 5-1 Composition of casting solution of ultrafiltration membrane

Membrane	PES (wt%)	PEG (wt%)	DMAc (wt%)	MWCNTs-COOK (wt%)
UF0	18	10	72	0
UF1	18	10	71.996	0.004
UF2	18	10	71.992	0.008
UF3	18	10	71.988	0.012
UF4	18	10	71.98	0.02
UF5	18	10	71.97	0.03

UF6	18	10	71.95	0.05
UF7	18	10	71.9	0.1

5.2.4 Membrane characterization

The morphologies of membranes were visualized using the field emission scanning electron microscopy (FESEM, Hitachi S-5000, Japan). The atomic force microscopy (AFM, Shimadzu SPM-9500 J3, Japan) was used to characterize the topography and roughness of the obtained membranes surface. The functional groups and chemical composition of membrane surface and MWCNTs-COOK were examined via Fourier-transform infrared spectroscopy (ATR-FTIR, Shimadzu Co., Ltd., Japan) and X-ray photoelectron spectroscopy (XPS, AXIS-ULTRA DLD, KRATOS). The contact angle (CA, digidrop, GBX, Whitestone way, France) was applied to analyze the changes in hydrophilicities of membranes. Each sample was tested more than 5 times to minimize the error. The membrane surface chargeability was tested by the electrokinetic analyzer (Sur-PASS TM3 Anton Paar, GmbH, Austria). The Raman spectra of MWCNTs before and after modification were analyzed by Raman spectroscope (Kaiser Optical Systems, Inc.) The porosity of UF membrane was measured using the dry-wet weight method [43, 50], and the value of membrane porosity ε (%) can be calculated with the following Eq. (1):

$$\varepsilon = \frac{W_W - W_d}{\rho S \theta} \times 100\% \quad (1)$$

Where W_W (g) and W_d (g) represent the wet weight and dry weight of UF membranes, respectively. ρ (g/cm^3) presents the pure water density. S (cm^2) and θ (cm) present the area and thickness of UF membranes, respectively.

5.2.5 Separation performance measurement

The cross-flow filtration setup was applied to evaluate the separation performance of membranes with a permeate area of 12.56 cm^2. Each membrane was pre-compacted with the pure water at 4 bar for 1 h to get a stable flux, and then operate pressure was

reduced to 3 bar to collect the permeate flux. The flux F (L/m^{2}hbar) of membrane was measured according to the Eq. (2):

$$F = \frac{V}{S \times T \times P} \quad (2)$$

Where V (L) presents the volume of the permeate solution. S (m^2) presents the permeate area of membrane, T (h) is denoted as the test time, and P (bar) is the operate pressure during filtration process. in addition, the rejection R (%) of the NF membrane was calculated according to Eq. (3):

$$R = \left(1 - \frac{C_P}{C_F}\right) \times 100\% \quad (3)$$

Where C_P (ppm) and C_F (ppm) are the concentrations of permeate solution and feed solution, respectively. To assess the effect of MWCNTs-COOK on changes in Mg^{2+}/Li^+ separation performance of the NF membrane, the separation test was conducted by filtering the simulated brine (2000ppm, Mg^{2+}/Li^+ mass ratio of 20) under an operate pressure of 3 bar. The Mg^{2+}/Li^+ separation of NF membrane was evaluated by the separation factor $S_{Li,Mg}$, which can be calculated according to Eq. (4):

$$S_{Li,Mg} = \frac{P_{Li}/P_{Mg}}{F_{Li}/F_{Mg}} \quad (4)$$

Where P_{Li} and F_{Li} represent the concentrations of Li^+ in the permeate solution and feed solution, respectively. Similarly, P_{Mg} and F_{Mg} represent the concentrations of Mg^{2+} in the permeate solution and feed solution, respectively. The concentrations of Mg^{2+} and Li^+ in solution were measured by the inductively coupled plasma optical emission spectroscopy (ICPOES,10000IV, Shimadzu, Japan).

5.3 Result and discussion

5.3.1 Characterization of MWCNTs

Fig.5-1 shows the Raman spectrum results of the pristine MWCNTs and MWCNTs-COOK, which is a representative tool to evaluate the structural integrity of MWCNTs. On each spectrum, there are two peaks located on 1351cm^{-1} and 1538 cm^{-1}, corresponding to disorder mode (D band) and tangential mode (G band). The intensity

ratio of D band and G band (I_D/I_G) is relate to the disorder degree of MWCNTs structure and the amount of sp^2-hybridized carbons [51, 52]. It can be found in Fig.5-1(a) that the I_D/I_G value of MWCNTs-COOK (1.25) was significantly high than the pristine MWCNTs (0.89). The increased I_D/I_G value was related to the high functionalization degree of MWCNTs. The XPS spectra results were applied to further clarify and analyze the introduced functional groups on the MWCNTs. Fig.5-1(b) presents that both the pristine MWCNTs and the modified MWCNTs- COOK spectra show a strong peak of C1s around 285 eV. Three new peaks appeared on the MWCNTs-COOK spectra around 292.8 eV, 377.5 eV, and 531.5eV, corresponding to K2s, K2p, and O1s, respectively, which confirmed the success of the modification reaction. As shown in Fig.5-1(c), C1s spectrum can be divided into three statues of C-C, C-O, and O-C=O. In addition, O1s spectrum contains two main peaks of O-C=O and C-O, which can be seen in Fig.5-1(d). The XPS results prove the success of introducing functional groups (-COOK, -OH) on MWCNTs, which will greatly enhance the hydrophilicity of MWCNTs.

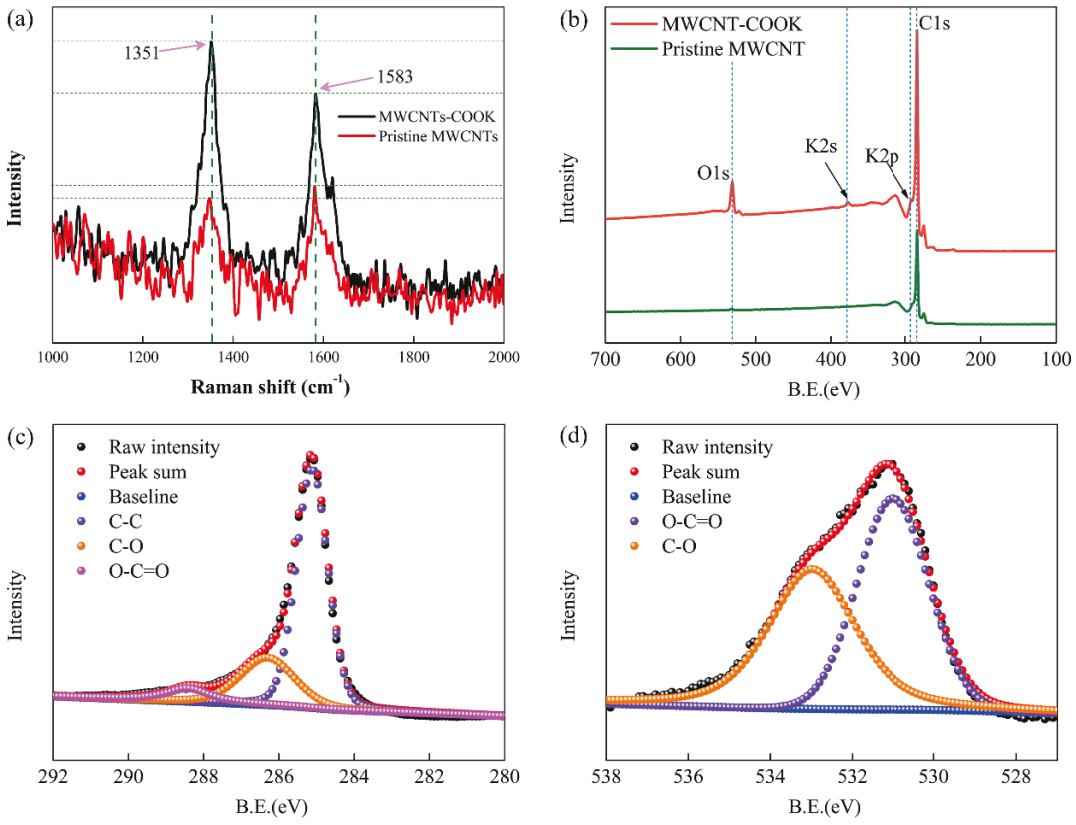

Fig.5-1. Characterization of the MWCNTs-COOK: (a) roman spectra, (b) XPS spectra wide scan spectra, (c) deconvolution of C1s, and (d) deconvolution of O1s.

5.3.2 Characterization of membranes

5.3.2.1 Chemical composition of membranes

The functional groups in UF substrates and NF membranes were characterized by ATR-FTIR. According to Fig.5-2(a), a new characteristic peak at 3316cm^{-1}~3689 cm^{-1} appeared on each (MWCNTs-COOK)-engineered UF membrane, which is corresponding to the -OH vibration stretch of MWCNTs-COOK [31, 53]. Additionally, the peak intensity of -OH tends to strengthen with the increase of MWCNTs-COOK content in the UF substrate. Fig.5-2 (b) compares the FTIR spectrum of pure UF substrate UF0, pure NF membrane NF0, and NF membranes fixed with different content of MWCNTs-COOK. Compared to the UF membrane, the new peaks at 1648cm^{-1} attributes to C=O vibration (amide-I) and 1536 cm^{-1} attributes to N-H (amide-II) [54] appeared on the spectra of each NF membrane, which was due to the existence of new polyamide layer emerged on the UF substrate. Compared to the pure UF0 membrane, a stronger peak at 3128cm^{-1}~3667cm^{-1} can be observed on the spectra of the NF membrane, which can be attributed to not only -OH but also -NH stretching groups [9, 18, 34]. Besides, a new peak at 2924 cm^{-1} can be found on the spectra of each NF membrane, which was related to both C-H and -NH_n^+ (n=2,3) [25, 34]. After immersing the PEI-contained aqueous solution on the surface of the substrate membrane UF3, the membrane was denoted as M3. As shown in Fig.5-2(c), compared to the membrane UF3, the new weak peak located at 1648cm^{-1} (C=O, amide-I) and 1536cm^{-1} (N-H, amide-II) can also be observed on the spectra of membrane M3. The result confirmed the crosslink reaction between MWCNTs-COOK and PEI, which is beneficial to strengthen the connection between the UF substrate and the polyamide layer.

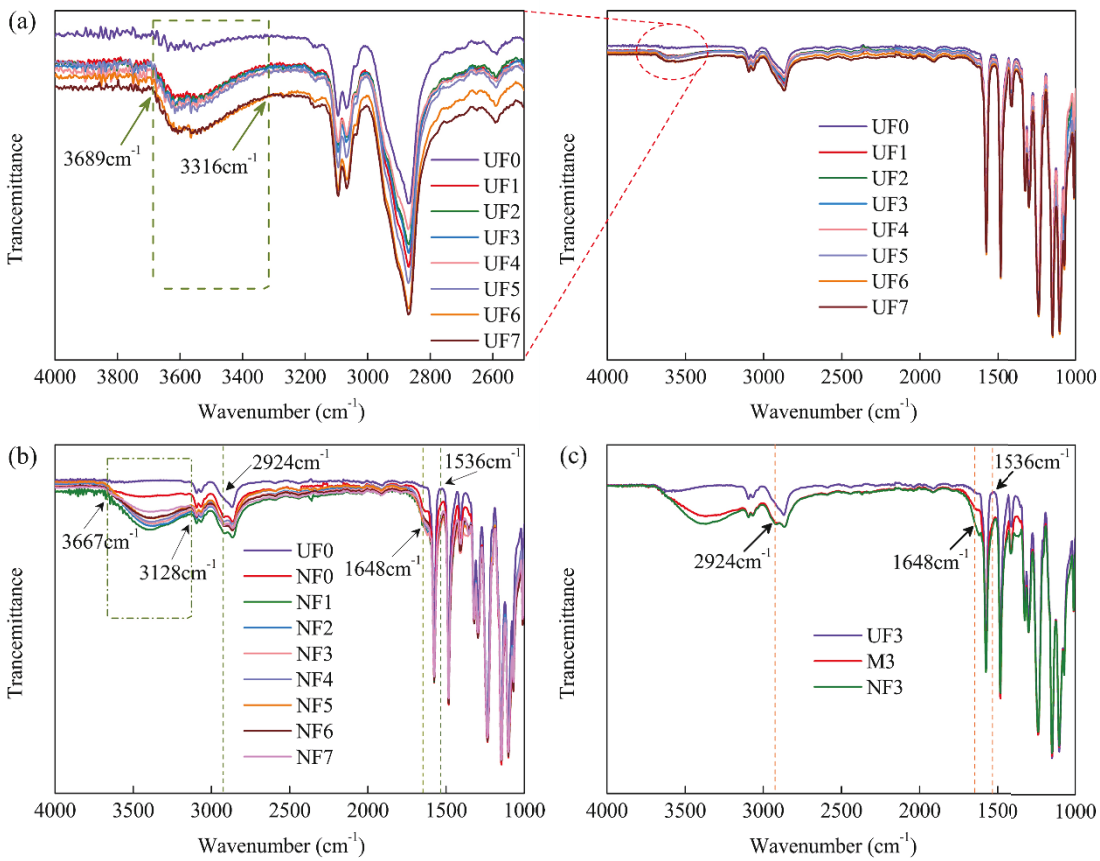

Fig.5-2. FTIR spectra of membranes: (a) UF substrate with different contents of MWCNTs-COOK, (b) substrate membrane UF0 and MWCNTs-COOK modified NF membrane, and (c) UF3, M3, and NF3.

The result of XPS spectra was applied to further quantify and analyze the changes in the chemical composition of NF membranes with different loading contents of MWCNTs-COOK. According to the deconvolution results of C1s in Fig.5-3, the C1s spectra contained five carbon statues located around 284.6, 285.7, 286.3, 287.8, and 288.4 eV, which were originated from C-C, C-N, C-O, N-C=O, and O-C=O, respectively. Among these carbon species, N-C=O was related to the amide group (-CONH-), and O-C=O was derived from carboxyl group (-COOH) that hydrolyzed by acid chloride group (-COCl) in the TMC monomers. As presented in Fig.5-3 and Table 5-2, with the content of MWCNTs-COOK in the NF membrane increased from 0 wt% to 0.1 wt%, the percent of N-C=O and O-C=O accordingly increased from 9.16 % to 12.87 % and from 3.19% to 6.13 %, respectively. The ratio of N-C=O to O-C=O is usually related to the chemical cross-linking degree between PEI and TMC. The

potassium carboxylate group (-COOK) on MWCNTs-COOK can connect with the amine group (-NH_2) on PEI during the immersion of the UF substrate into the aqueous phase solution, consuming part of -NH_2 on PEI. As a result, there will be more unreacted -COCl remains on the membrane surface after interfacial polymerization between PEI and TMC. In summary, the increased content of MWCNTs-COOK in the NF membrane may lead to a decrease in the ratio of N-C=O/O-C=O, reducing the chemical cross-linking degree between PEI and TMC to a certain extent.

On the other hand, the N1s spectra can be divided into three species located at 389.9, 399.9, and 401.1 eV, which were related to C-N, N-C=O, and -NH_n^+ (n=2, 3), respectively. According to Fig.5-4 and Table 5-2, the percent of -NH_n^+ decreased from initial 16.35 % to 8.4% with the increase of MWCNTs-COOK content from 0 wt% to 0.1 wt%. Besides, the percent of N-C=O increased with the increase of MWCNTs-COOK content, which was similar with the deconvoluted result of C1s. The nitrogen specie -NH_n^+ (n=2, 3) was derived from the protonation of remained amine groups on the membrane surface. MWCNTs-COOK in the UF substrate membrane may consume some amine groups on PEI. In addition, more MWCNTs-COOK may consume more amine groups, leading to less amine groups remaining on the NF membrane surface. Importantly, the cross-linking between the fixed MWCNTs-COOK and PEI may strengthen the connection between the UF substrate and the formed polyamide layer, which was conducive to the stability of the NF membrane performance.

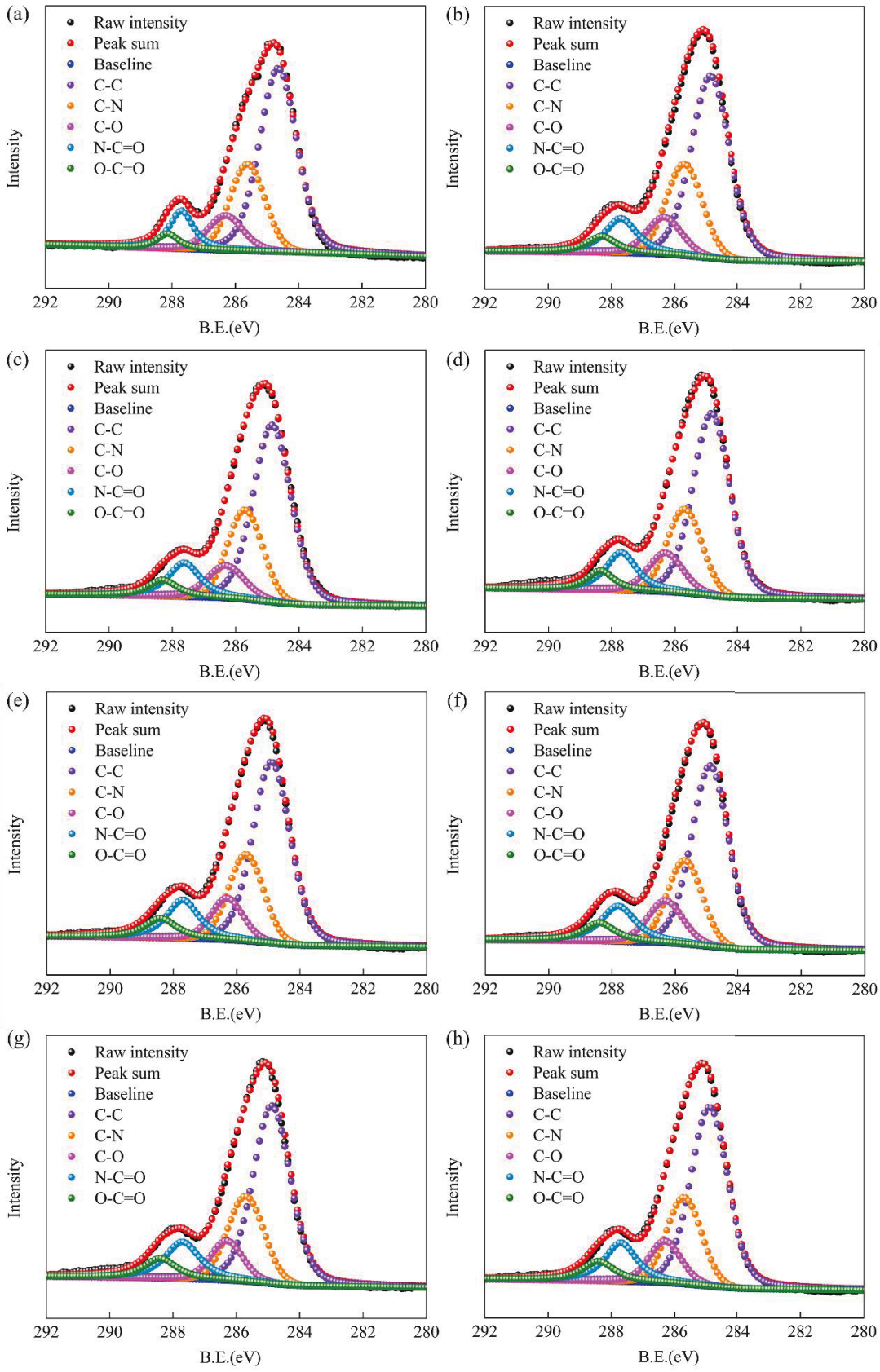

Fig.5-3. Deconvoluted C1s of NF membrane: (a) NF0, (b) NF1, (c) NF2, (d) NF3, (e) NF4, (f) NF5, (g) NF6, and (h) NF7.

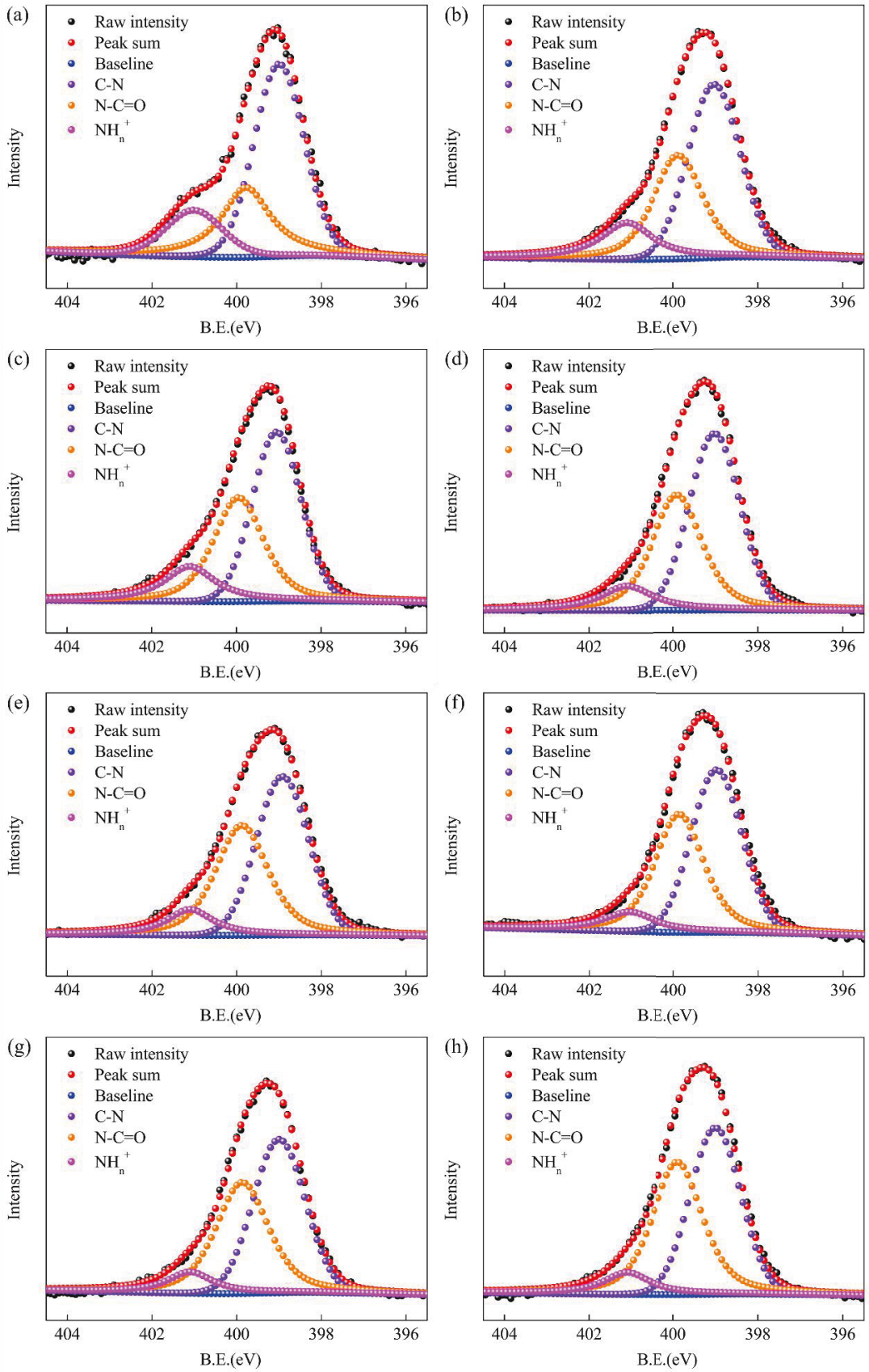

Fig.5-4. Deconvoluted N1s of NF membrane: (a) NF0, (b) NF1, (c) NF2, (d) NF3, (e) NF4, (f) NF5, (g) NF6, and (h) NF7.

Table 5-2 XPS results of NF membranes originated from C1s and N1s

Membranes	C1s		N1s	
	Species	Percent (%)	Species	Percent (%)
NF0	O-C=O	3.19	NH_n^+	16.35
	N-C=O	9.16	N-C=O	28.27
	C-O	9.8	C-N	55.35
	C-N	22.32		
	C-C	55.54		
NF1	O-C=O	4.38	NH_n^+	15.58
	N-C=O	10.24	N-C=O	35.06
	C-O	9.69	C-N	49.35
	C-N	22.66		
	C-C	53.02		
NF2	O-C=O	4.59	NH_n^+	15.25
	N-C=O	10.52	N-C=O	37.28
	C-O	9.55	C-N	47.46
	C-N	22.41		
	C-C	52.91		
NF3	O-C=O	4.9	NH_n^+	10.62
	N-C=O	11.16	N-C=O	39.82
	C-O	10.45	C-N	49.55
	C-N	20.69		
	C-C	52.79		
NF4	O-C=O	5.45	NH_n^+	10.2
	N-C=O	11.55	N-C=O	41.68
	C-O	11.48	C-N	48.11
	C-N	20.21		
	C-C	51.31		
NF5	O-C=O	5.91	NH_n^+	8.98

	N-C=O	11.65	N-C=O	42.7
	C-O	10.23	C-N	48.31
	C-N	21.03		
	C-C	15.16		
NF6	O-C=O	6.04	NH_n^+	8.67
	N-C=O	12.08	N-C=O	43.37
	C-O	9.66	C-N	47.94
	C-N	21.45		
	C-C	50.75		
NF7	O-C=O	6.13	NH_n^+	8.4
	N-C=O	12.87	N-C=O	45.38
	C-O	11.71	C-N	46.21
	C-N	20.85		
	C-C	48.44		

5.3.2.2 Microstructure of membranes

The effect of MWCNTs-COOK dosage on the morphology structure of UF substrates and NF membranes was obseved by FESEM. Obviously, as the content of MWCNTs-COOK increases, the color of the UF membrane gradually darkens (Figs. 5-5a, 5-5b, 5-5c). This indicates that the doped MWCNTs-COOK spontaneously migrate to the surface of the film, thereby helping to improve the surface properties of the mixed membrane. Similar phenomenon has also been reported by others when doping functionalized MWCNTs into the PES membrane matrix [43, 55]. As displayed in Figs. 5-5a, 5-5b, and 5-5c, each UF membrane shows a dense surface and the membrane surface morphology changes slightly after anchoring MWCNTs-COOK. More nano-porous can be observed on the surface of UF3, which was due to the accelerated solvent-nonsolvent exchange caused by MWCNTs-COOK. Besides, with a high MWCNTs-COOK content in UF7, the membrane surface had a tendency to become denser, which

was due to the increased viscosity of the mixed casting solution [56, 57].

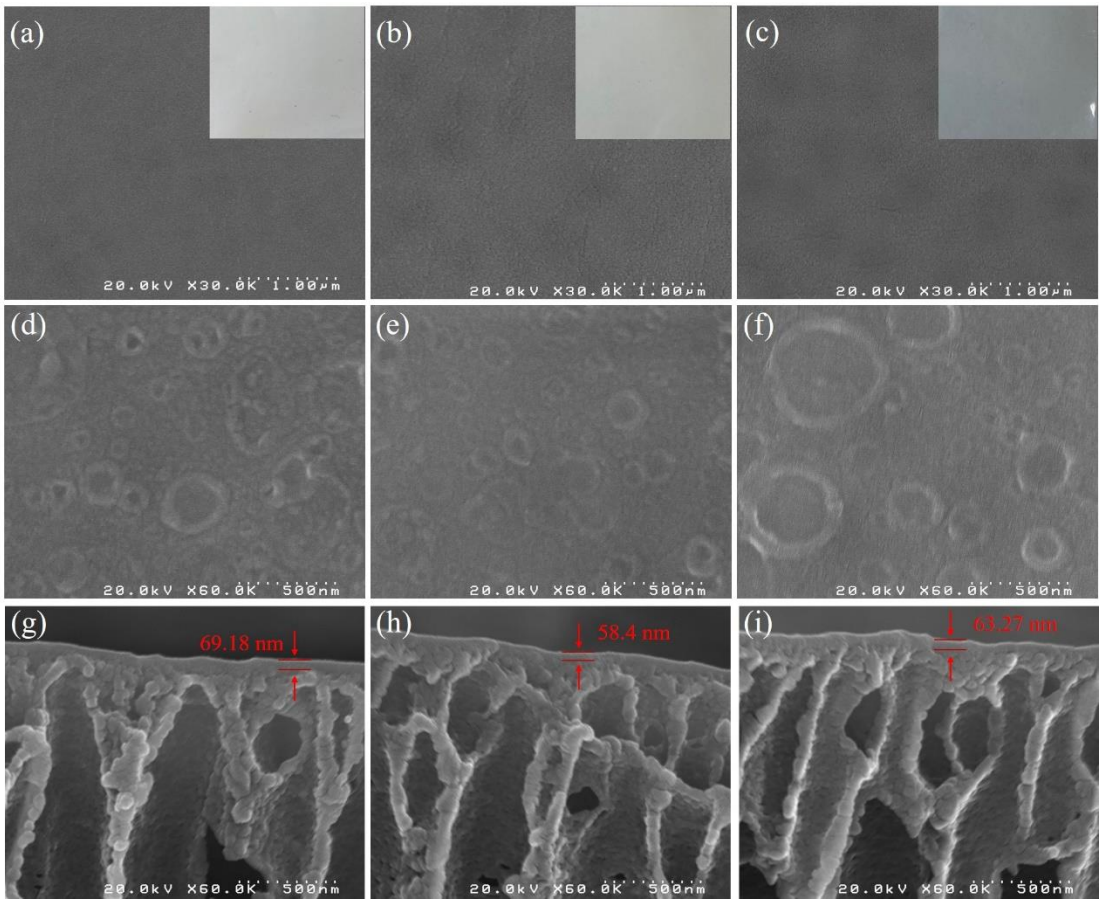

Fig.5-5. FESEM images of UF substrate membranes with different loading content of MWCNTs-COOK: (a) 0 wt%, (b) 0.012 wt%, and (c) 0.1 wt%; FESEM surface images of NF membranes with different loading content of MWCNTs-COOK: (d) 0 wt%, (e) 0.012 wt%, and (f) 0.1 wt%; and FESEM cross images of NF membranes with different loading content of MWCNTs-COOK: (g) 0 wt%, (h) 0.012 wt%, and (i) 0.1 wt%.

After the interfacial polymerization process, obvious changes can be found on the NF membrane surface. As shown in Fig.5-5, each NF memrbane presented a typical ridge-vally structure formed by polymerization between PEI and TMC, which demonstrated the occurance of the polyamide layer. Note that the ridge-vally structure of NF membrane surface gradually became looser with the increase of MWCNTs-COOK dosage in the UF substrate membrane. On the other hand, Fig.5-5 also shows that the NF membranes modified with MWCNTs-COOK exhibited slightly thinner polyamide layer than that of the pure NF membrane. As disscussed in the section of chemical analysis, MWCNTs-COOK in UF substrate can connect with PEI during the

contact between the base film and the aqueous solution. As a result, some PEI branches were fixed on the UF substrate and the number of free amine groups was reduced, reducing the polymerization rate with TMC and leading to a thinner and looser polyamide layer. Importantly, compared to the pure NF membrane, the transmission resistance through the modified NF membrane would be reduced due to the occurrence of the thinner and looser polyamide layer, which can contribute to a higher permeate flux and accelerate the separation process.

The AFM topology was adopted to further study the roughness difference of the UF substrate and NF membranes after anchoring MWCNTs-COOK. It can be seen in Fig.5-6 that the surface of the pure substrate UF0 (Ra=14.08, Rms=17.85) is slightly smoother than (MWCNTs-COOK)-engineered UF membranes. With the increase of MWCNTs-COOK anchoring content in the UF substrate, the roughness of UF substrate surface increased accordingly. The changes in membrane surface was related to the accelerated exchange of solvent-nonsolvent during phase inversion due to the hydrophilic MWCNTs-COOK in casting solution. According to previous reports, the accelerated exchange of solvent-nonsolvent may cause shrinkage of surface PES polymer chain, which is their response to the sudden existence of the non-solvent [58]. This may result in the presence of spheres or spherical nodules, which in turn increases the roughness of membrane surface. Besides, hydrophilic MWCNTs-COOK can migrate to the membrane surface during phase inversion, thereby changing the roughness of membrane surface.

Figs. 5-6(d), 5-6(e), and 5-6(f) show that the NF membrane surface became rougher compared to the corresponding UF substrate, which was due to existence of the typical ridge-vally polyamide layer formed between PEI and TMC. With the increase of MWCNTs-COOK content in UF substrate, the reaction rate and cross-linking degree between PEI and TMC was slowed down to a certain extent, leading to a looser polyamide layer with larger ridge-vally structure. On the other hand, the hydrophilic MWCNTs-COOK in casting solution can cause a rougher UF substrate, which in turn increase the roughness of the final NF membrane. Note that the increased roughness of

UF substrate and NF membrane is conducive to improve the flux during filtration process.

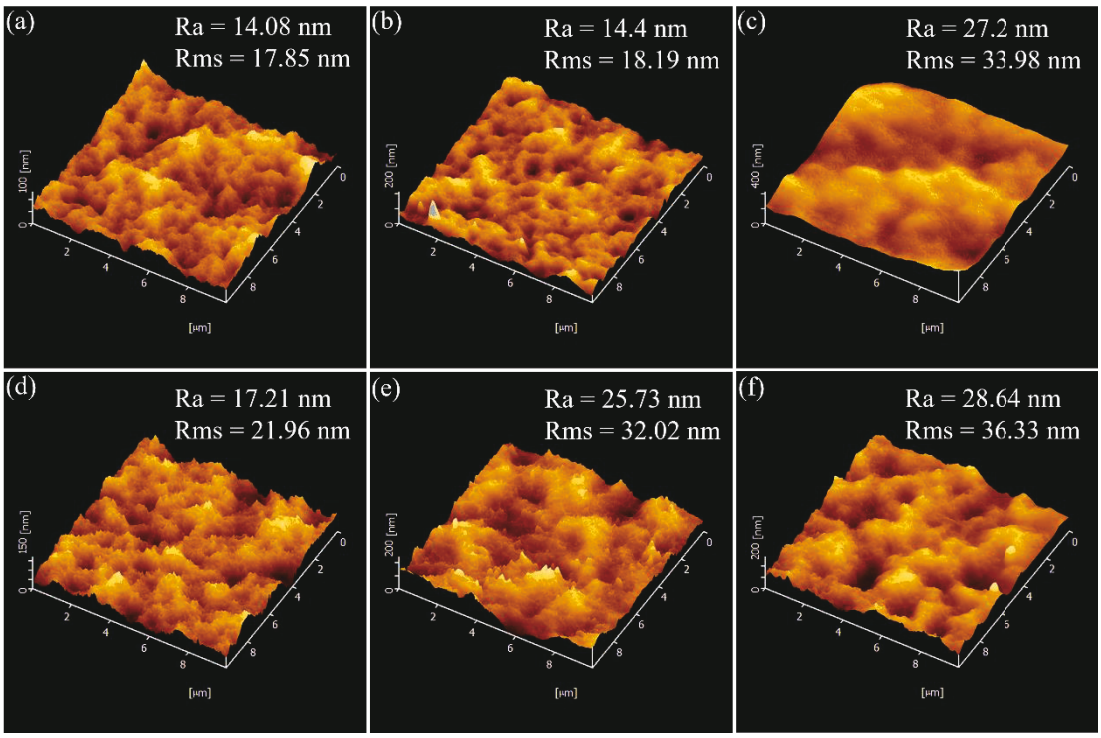

Fig.5-6. AFM topology images of UF substrate membranes with different loading content of MWCNTs-COOK: UF substrate: (a) 0 wt%, (b) 0.012 wt%, and (c) 0.1 wt%; AFM topology images of modified NF membranes with different loading content of MWCNTs-COOK (d) 0 wt%, (e) 0.012 wt%, and (f) 0.1 wt%.

5.3.2.3 Surface properties of UF membranes

The change in hydrophilicity of the UF substrate membrane before and after anchoring with MWCNTs-COOK was measured by the contact angle analysis. As shown in Fig.5-7(a), the contact angle of UF membrane significantly reduced with the increase of MWCNTs-COOK anchoring content in UF substrate, which indicated that the hydrophilicity of the UF membrane was greatly improved. During phase inversion process, the hydrophilic MWCNTs-COOK would migrate and disperse evenly in the UF substrate, thereby improving the hydrophilicity of the UF membrane. Note that a more hydrophilic membrane surface helps prevent the adhesion of pollutants due to the formation of hydrate layer on the membrane surface [59]. According to Fig.5-7(b), as

the anchoring content of MWCNTs-COOK increased from 0 wt% to 0.05 wt%, the porosity of obtained UF substrate gradually increased from initial 67.71% to 80%. And the porosity of the UF substrate reduced slightly to 78.15 % with further increase of MWCNTs-COOK content to 0.1 wt%. This phenomenon was contributed to the dual-effect of the thermodynamic and kinetic effect of MWCNTs-COOK addition [58]. The high affinity of the hydrophilic MWCNTs-COOK to non-solvent water promoted the thermodynamic instability of the polymer system and accelerated the exchange between the water and the solvent DMAc, resulting in higher porosity of the obtained UF substrate membrane. However, a high MWCNTs-COOK anchoring content of 0.1 wt% would cause increase of the viscosity of the casting solution, leading to higher kinetic hindrance during water-DMAc exchange and reducing the porosity of the UF substrate membrane.

Fig.5-7(c) shows the permeation flux of UF substrate membranes fixed with different content of MWCNTs-COOK. As the content of MWCNTs-COOK increased from 0 wt% to 0.05 wt%, the water flux of UF membrane was significantly increased from 210 (L/m^2hbar) to 621 (L/m^2hbar). And then the water flux of UF membrane decreased to 477 (L/m^2hbar) with a further addition of MWCNTs-COOK content to 0.1 wt%. According to the results of contact angle and porosity analysis, after anchoring hydrophilic MWCNTs-COOK in the UF membrane, both the hydrophilicity and porosity of UF membrane were accordingly improved, which can lead to high water flux of the obtained UF membrane. On the other hand, as illustrated in Fig.5-7(d), the nanotube of MWCNTs-COOK and their inter-gaps in the membrane matrix can provide water channels for water molecules to fast permeate through the UF membrane. However, with a high MWCNTs-COOK anchoring content of 0.1 wt%, the reduced porosity of the UF membrane would lead to a decrease in the water flux to a certain extent.

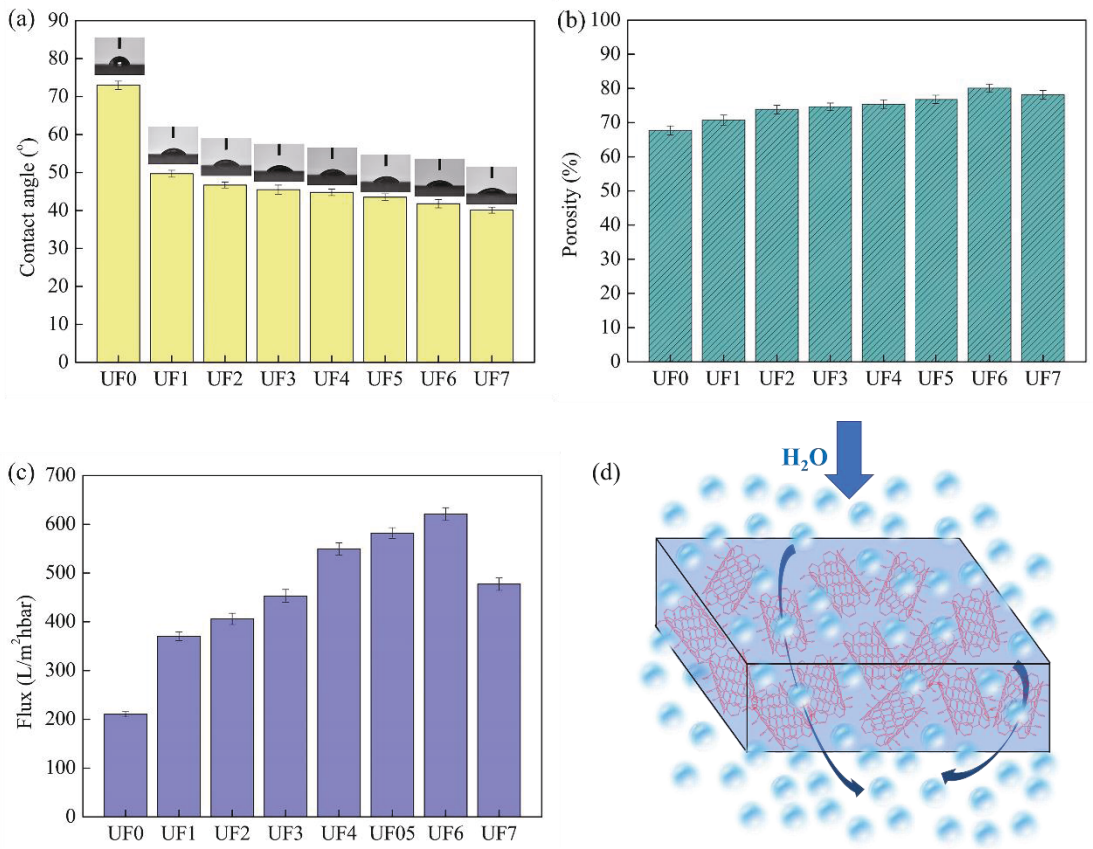

Fig.5-7. Characterization of UF membranes fixed with different content of MWCNTs-COOK: (a) contact angle, (b) porosity, (c) water flux, and (d) schematic illustration of water molecules passing through the UF membrane.

5.3.2.4 Separation performance of NF membranes

The contact angle result of NF membrane before and after modification was presented in Fig.5-8 (a). As the MWCNTs-COOK anchoring content in the UF membrane increased, the contact angle of the final NF membrane gradually decreased, which indicated that the hydrophilicity of the NF membrane was improved. The result can be explained that the hydrophilic MWCNTs-COOK additives greatly improved the hydrophilicity of the UF membrane, which is also benefit for the hydrophilicity of the final NF membrane. Additionally, the increased roughness of the MWCNTs-COOK modified NF membrane increases the effective area, thereby improving the hydrophilicity of membrane surface. As described in the chemical composition results, the fixed MWCNTs-COOK in the UF membrane may contribute to more un-react acid

chloride group (-COCl) remaining on membrane surface, which will be hydrolyzed to carboxyl (-COOH) and improve the hydrophilicity of NF membrane surface. Briefly, the fixed MWCNTs-COOK additives were beneficial to improve the hydrophilicity of both UF substrate and NF membranes.

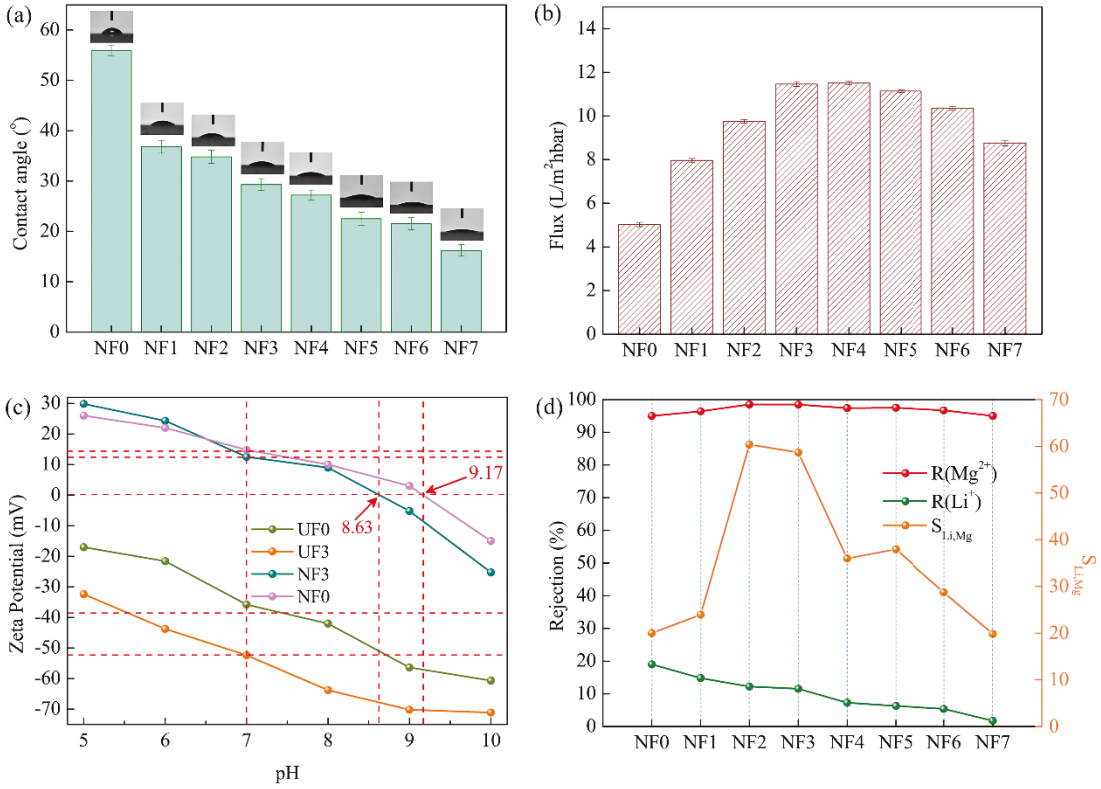

Fig.5-8. Characterization of NF membranes: (a) contact angle, (b) water flux, (c) zeta potential, and (d) separation performance of NF membranes for Mg^{2+} and Li^{+}.

As shown in Fig.5-8(b), the flux of NF membrane increased from 5.01 to 11.51 (L/m^{2}hbar) with the increase of MWCNTs-COOK anchoring content from 0 wt% to 0.02 wt%, and then slightly decreased to 8.76 (L/m^{2}hbar) with further addition of MWCNTs-COOK content to 0.1 wt%. The increased flux of NF membrane is critical for accelerated the separation process. After anchoring the hydrophilic MWCNTs-COOK, the hydrophilicity of both UF substrate and NF membranes were greatly improved, thereby speeding up the passage of water through the membrane. In addition, the MWCNTs-COOK may weaken the cross-linking degree between PEI and TMC and lead to a slightly looser polyamide layer, thereby reducing the transmission resistance to a certain extent. However, as shown in Fig.5-7(b), a high loading content of

MWCNTs-COOK can contribute to a denser UF membrane, increasing the transmission resistance of water molecules through the membrane. Moreover, excessive MWCNTs-COOK in UF membrane may connect with more PEI, hindering the migration of some PEI branches and reducing the reaction rate between PEI and TMC to a certain extent. Since the interfacial polymerization between PEI and TMC is self-inhibited process, the remarkably reduction of the reaction rate can result in the formation of a slightly thicker polyamide layer, thereby increasing the transmission resistance of water molecules and decreasing the water flux of the NF membrane.

According to the zeta potential result shown in Fig.5-8(c), the UF substrate surface was negatively charged in the pH range of 5 to 10. After the formation of the polyamide layer on the UF substrate, the NF membrane was highly positively charged due to the protonation of the free amine groups remaining on the membrane surface. Compared to the pure NF0 membrane, the MWCNTs-COOK-modified NF membrane NF3 showed a slightly lower isoelectric point, which was related to the reduce of the unreacted amine groups on membrane surface. Note that, under the applied condition in this work (pH ≈ 7), the membrane NF3 exhibited a similar high positively charged surface to that of membrane NF0. Fig.5-8(d) shows the Mg^{2+}/Li^{+} separation capacity of NF membranes prepared with different content of MWCNTs-COOK. Each NF membrane had a significant difference in the rejection of Mg^{2+} and Li^{+}, which confirmed the effective separation of $Mg^{2+}$and Li^{+}. Compare to the membrane NF0, the modified NF membranes with a low MWCNTs-COOK anchoring content had little change in the rejection of Mg^{2+} and Li^{+}. According to previous reports, it is the collective effect of electrostatic interaction and steric hindrance determined the Mg^{2+}/Li^{+} separation ability of NF membrane during the Mg^{2+}/Li^{+} separation process. On the one hand. the ionic hydration radius of Mg^{2+} (0.428nm) is slightly larger than that of Li^{+} (0.382nm), which made Mg^{2+} face higher transmission resistance. Compared to the monovalent Li^{+} with low positive charge, the divalent Mg^{2+} faced greater electrostatic repulsion from the positively charged NF membrane during the filtering process, resulting in higher rejection of Mg^{2+}. However, the high anchoring content of MWCNTs-COOK in

membrane resulted in poor Mg^{2+}/Li^{+} separation capacity of the final NF membrane, which was due to the combined effect of the changed morphology and surface properties of the final NF membrane. After comprehensively considering the rejections and flux of these prepared NF membrane, membrane NF3 exhibited not only high permeation flux of 11.46 (L/m^2hbar) but also high rejection difference of Mg^{2+} and Li^{+} reached 86.94%, which is a promising approach for fast and efficient Mg^{2+}/Li^{+} separation.

Fig.5-9(a) presents the rejection result of membrane NF3 for several inorganic salts, which was corresponds to the separation performance of positively charged NF membrane. The stronger electrostatic repulsion of positively charged NF membrane to divalent cation resulted in high rejection of Mg^{2+} than that of Na^{+}, Li^{+}. In addition, the electrostatic attraction of the membrane to divalent anions SO_4^{2-} was higher than that of monovalent anions Cl^{-}. The hydrated radius of Ca^{2+}, Mg^{2+}, Na^{+}, Li^{+}, SO_4^{2-}, Cl^{-} are 0.412nm, 0.428nm, 0.358, 0.383nm, 0.379nm, and 0.332nm, respectively. Ions with larger hydrated radius will face higher transmission resistance during filtration process. Therefore, the rejections ratio of inorganic salts by the NF membrane were determined by the combined effect of electrostatic interaction and steric hindrance. In order to evaluate the Mg^{2+}/Li^{+} separation stability of the MWCNTs-COOK modified NF membrane, a long-term filtration test for membrane NF0 and NF 3 was carried out. According to Fig.5-9, during a long-time filtration test, there was no obvious fluctuation on the rejections of Mg^{2+} and Li^{+} for both NF3 and NF0. Besides, the MWCNTs-COOK modified NF membrane NF3 also maintained a stable high permeate flux during the filtration process. However, it can be found in Fig.5-9 that the permeate flux of membrane NF0 showed a decline trend after a long-term running test. Compared to the pure NF membrane, the fixed MWCNTs-COOK in membrane could connect with the PEI monomer during immersing the UF substrate surface in the aqueous phase solution, thereby enhancing the connection between the UF substrate and the polyamide layer. As a result, the fixed MWCNTs-COOK endowed the final NF membrane with high stability during filtration process.

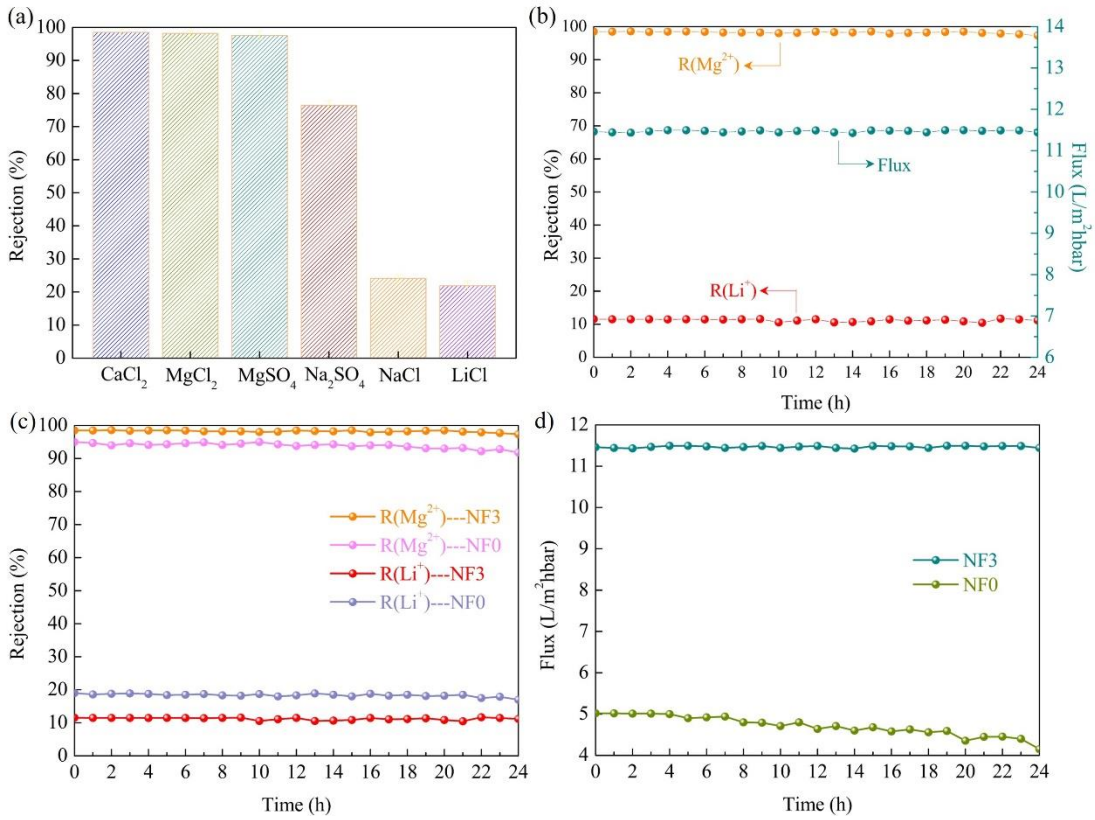

Fig.5-9 (a) Rejections of membrane NF3 for several inorganic salts and (b) long-time Mg^{2+}/Li^{+} separation test of membrane NF3; long-term filtration test for membrane NF0 and NF3: (c) rejection performance for Mg^{2+} and Li^{+}, and (d) permeate flux.

Table 5-3 compares the Mg^{2+}/Li^{+} separation performance of several reported NF membranes and the MWCNTs-COOK-modified NF membrane prepared in this work. As shown in Table 5-3, each NF membrane exhibits a significantly difference between the rejection of Li^{+} and Mg^{2+}, indicates their separation ability for Li^{+} and Mg^{2+}. Note that most NF membrane in Table 5-3 face a problem of low flux, which will significantly reduce the work efficiency of membrane when separating Li^{+} and Mg^{2+}. Importantly, compared to other listed NF membrane, the MWCNTs-COOK-modified NF membrane formed in this work shows not only high Mg^{2+}/Li^{+} rejection difference of 86.94% but also highest flux of 11.46 (L/m^2hbar). The comparison result revealed that the positively charged NF membrane prepared in this work is promising alternative for fast and efficient separation of Li^{+} and Mg^{2+} during lithium extraction process.

Table 5-3 Mg^{2+}/Li^{+} separation performance comparison of several reported NF membranes and the MWCNTs-COOK-modified NF membrane prepared in this work.

Membrane	Feed solution	Separation performance	Flux (L/m^2hbar)	Ref
NF90 NF membrane	Mg^{2+}/Li^{+}=20	$R(Mg^{2+})$ = 60.5 %	-	[24]
	2000ppm	$R(Li^{+})$ = 15%		
Polyacrylonitrile/DAPP-TMC	Mg^{2+}/Li^{+}=20	$R(Mg^{2+})$ = 46 %	-	[24]
	2000ppm	$R(Li^{+})$ =−40.7%		
Polyetherimide/TMC-BPEI/EDTA	Mg^{2+}/Li^{+}=24	$R(Mg^{2+})$ = 91.9 %	0.6	[9]
	2000ppm	$R(Li^{+})$ = 20%		
PES/PIP-MWCNTs-PEI-TMC	Mg^{2+}/Li^{+}=21.4	$R(MgCl_2)$ = 95 %	8.5	[34]
	2000ppm	R(LiCl) = 18%		
PES/(PIP-PHF)-TMC	Mg^{2+}/Li^{+}=21.4	$R(MgCl_2)$ = 89.9 %	6.7	[7]
	2000ppm	R(LiCl) = 16.3%		
PES/PEI-TMC	Mg^{2+}/Li^{+}=20	$R(Mg^{2+})$ = 95 %	5.02	[26]
	2000ppm	$R(Mg^{2+})$ ≈ 19%		
PES-(CNC-COOH)/ PEI/TMC	Mg^{2+}/Li^{+}=30	$R(Mg^{2+})$ = 96.11%	4.17	[25]
	2000ppm	$R(Li^{+})$ = 21.76%		
PES-(CNC-COOH)/ PEI/TMC	Mg^{2+}/Li^{+}=60	$R(Mg^{2+})$ = 95.59 %	3.4	[25]
	2000ppm	$R(Li^{+})$ = 11.63%		
PES-GO/PEI-TMC	Mg^{2+}/Li^{+}=20	$R(Mg^{2+})$ = 95.14 %	11.15	[36]
	2000ppm	$R(Li^{+})$ = 20.93%		
PES-MWCNTs-COOK/PEI-TMC	Mg^{2+}/Li^{+}=20	$R(Mg^{2+})$ = 98.49 %	11.46	This
	2000ppm	$R(Li^{+})$ = 11.54%		work

5.4 Conclusion

The fast and efficient separation of Li^{+} and co-existing Mg^{2+} is an urgent matter in lithium extracting application. In this work, a novel MWCNTs-COOK with high water solubility was synthesized by a one-step environmentally friendly oxidation process.

We fixed the MWCNTs-COOK additives into the UF substrate membrane, and then formed the polyamide layer on the MWCNTs-COOK-engineered substrate surface through interfacial polymerization.

The fixed MWCNTs-COOK endowed the substrate with high hydrophilicity and porosity, contributing to higher water permeability of the UF membrane. Chemical composition analysis revealed that the fixed MWCNTs-COOK in UF substrate can connect with the -NH_2 on PEI, leading to less free -NH_2 on membrane and reducing the crosslinking degree between PEI and TMC. On the other hand, the connection between UF substrate and the polyamide layer was strengthened by the "connector" MWCNTs-COOK, which directly improved the performance stability of the final NF membrane. The membrane performance characterization indicated that with an optimal MWCNTs-COOK content of 0.012 wt%, the obtained membrane NF3 showed best Mg^{2+}/Li^{+} separation efficiency. The separation factor $S_{Li,Mg}$ reached 58.66, and the difference between rejections of Li^{+} and Mg^{2+} reached 86.94%, which were much higher than that of most reported NF membrane. Importantly, the flux of membrane NF3 was 11.46 (L/m^2hbar), which was over 120% higher than that of the NF membrane with no MWCNTs-COOK. The obtained high separation factor and flux of membrane NF3 indicated its great potential for fast and efficient separation of Mg^{2+} and Li^{+}. This work proved that anchoring MWCNTs-COOK into the UF substrate membrane is an effective way to improve the Mg^{2+}/Li^{+} separation performance of NF membrane, thereby accelerating the rate of lithium enrichment during lithium extraction.

References

[1] L. Kavanagh, J. Keohane, G. Garcia Cabellos, A. Lloyd, J. Cleary, Global Lithium Sources—Industrial Use and Future in the Electric Vehicle Industry: A Review, Resources, 7 (2018) 57.

[2] P. Xu, J. Hong, X. Qian, Z. Xu, H. Xia, X. Tao, Z. Xu, Q.-Q. Ni, Materials for lithium recovery from salt lake brine, Journal of Materials Science, (2020).

[3] X. Li, Y. Mo, W. Qing, S. Shao, C.Y. Tang, J. Li, Membrane-based technologies for

lithium recovery from water lithium resources: A review, Journal of Membrane Science, 591 (2019) 117317.

[4] V. Flexer, C.F. Baspineiro, C.I. Galli, Lithium recovery from brines: A vital raw material for green energies with a potential environmental impact in its mining and processing, Sci Total Environ, 639 (2018) 1188-1204.

[5] X. Xu, Y. Chen, P. Wan, K. Gasem, K. Wang, T. He, H. Adidharma, M. Fan, Extraction of lithium with functionalized lithium ion-sieves, Progress in Materials Science, 84 (2016) 276-313.

[6] G. Liu, Z. Zhao, L. He, Highly selective lithium recovery from high Mg/Li ratio brines, Desalination, 474 (2020) 114185.

[7] Q. Shen, S.J. Xu, Z.L. Xu, H.Z. Zhang, Z.Q. Dong, Novel thin-film nanocomposite membrane with water-soluble polyhydroxylated fullerene for the separation of Mg^{2+}/Li^{+} aqueous solution, Journal of Applied Polymer Science, 136 (2019) 48029.

[8] X.-J. Pan, Z.-H. Dou, D.-L. Meng, X.-X. Han, T.-A. Zhang, Electrochemical separation of magnesium from solutions of magnesium and lithium chloride, Hydrometallurgy, 191 (2020) 105166.

[9] W. Li, C. Shi, A. Zhou, X. He, Y. Sun, J. Zhang, A positively charged composite nanofiltration membrane modified by EDTA for $LiCl/MgCl_2$ separation, Separation and Purification Technology, 186 (2017) 233-242.

[10] S.H. Park, J.H. Kim, S.J. Moon, J.T. Jung, H.H. Wang, A. Ali, C.A. Quist-Jensen, F. Macedonio, E. Drioli, Y.M. Lee, Lithium recovery from artificial brine using energy-efficient membrane distillation and nanofiltration, Journal of Membrane Science, 598 (2020) 117683.

[11] G. Liu, Z. Zhao, A. Ghahreman, Novel approaches for lithium extraction from salt-lake brines: A review, Hydrometallurgy, 187 (2019) 81-100.

[12] B. Swain, Recovery and recycling of lithium: A review, Separation and Purification Technology, 172 (2017) 388-403.

[13] X. Zhao, H. Yang, Y. Wang, Z. Sha, Review on the electrochemical extraction of lithium from seawater/brine, Journal of Electroanalytical Chemistry, 850 (2019)

113389.

[14] S.-Y. Sun, L.-J. Cai, X.-Y. Nie, X. Song, J.-G. Yu, Separation of magnesium and lithium from brine using a Desal nanofiltration membrane, Journal of Water Process Engineering, 7 (2015) 210-217.

[15] G. YANG, H. SHI, W. LIU, W. XING, N. XU, Investigation of Mg^{2+}/Li^{+} Separation by Nanofiltration, Chinese Journal of Chemical Engineering, 19 (2011) 586-591.

[16] H. Peng, Q. Tang, S. Tang, J. Gong, Q. Zhao, Surface modified polyamide nanofiltration membranes with high permeability and stability, Journal of Membrane Science, 592 (2019) 117386.

[17] K. Shen, C. Cheng, T. Zhang, X. Wang, High performance polyamide composite nanofiltration membranes via reverse interfacial polymerization with the synergistic interaction of gelatin interlayer and trimesoyl chloride, Journal of Membrane Science, 588 (2019) 117192.

[18] M.B.M.Y. Ang, C.A. Trilles, M.R. De Guzman, J.M. Pereira, R.R. Aquino, S.-H. Huang, C.-C. Hu, K.-R. Lee, J.-Y. Lai, Improved performance of thin-film nanocomposite nanofiltration membranes as induced by embedded polydopamine-coated silica nanoparticles, Separation and Purification Technology, 224 (2019) 113-120.

[19] J. Wang, C. Zhao, T. Wang, Z. Wu, X. Li, J. Li, Graphene oxide polypiperazine-amide nanofiltration membrane for improving flux and anti-fouling in water purification, RSC Adv., 6 (2016) 82174-82185.

[20] J. Tian, H. Chang, S. Gao, R. Zhang, How to fabricate a negatively charged NF membrane for heavy metal removal via the interfacial polymerization between PIP and TMC?, Desalination, 491 (2020) 114499.

[21] Y. Qi, L. Zhu, X. Shen, A. Sotto, C. Gao, J. Shen, Polythyleneimine-modified original positive charged nanofiltration membrane: Removal of heavy metal ions and dyes, Separation and Purification Technology, 222 (2019) 117-124.

[22] R. Weng, X. Huang, D. Liao, S. Xu, L. Peng, X. Liu, A novel cellulose/chitosan composite nanofiltration membrane prepared with piperazine and trimesoyl chloride by

interfacial polymerization, RSC Advances, 10 (2020) 1309-1318.

[23] A.G. Volkov, S. Paula, D.W. Deamer, Two mechanisms of permeation of small neutral molecules and hydrated ions across phospholipid bilayers, Bioelectrochemistry and Bioenergetics, 42 (1997) 153–160.

[24] X. Li, C. Zhang, S. Zhang, J. Li, B. He, Z. Cui, Preparation and characterization of positively charged polyamide composite nanofiltration hollow fiber membrane for lithium and magnesium separation, Desalination, 369 (2015) 26-36.

[25] C. Guo, N. Li, X. Qian, J. Shi, M. Jing, K. Teng, Z. Xu, Ultra-thin double Janus nanofiltration membrane for separation of Li^+ and Mg^{2+}: "Drag" effect from carboxyl-containing negative interlayer, Separation and Purification Technology, 230 (2020) 115567.

[26] P. Xu, W. Wang, X. Qian, H. Wang, C. Guo, N. Li, Z. Xu, K. Teng, Z. Wang, Positive charged PEI-TMC composite nanofiltration membrane for separation of Li^+ and Mg^{2+} from brine with high Mg^{2+}/Li^+ ratio, Desalination, 449 (2019) 57-68.

[27] A. Anand, B. Unnikrishnan, J.-Y. Mao, H.-J. Lin, C.-C. Huang, Graphene-based nanofiltration membranes for improving salt rejection, water flux and antifouling–A review, Desalination, 429 (2018) 119-133.

[28] S. Bano, A. Mahmood, S.-J. Kim, K.-H. Lee, Graphene oxide modified polyamide nanofiltration membrane with improved flux and antifouling properties, Journal of Materials Chemistry A, 3 (2015) 2065-2071.

[29] Z. Xu, T. Wu, J. Shi, W. Wang, K. Teng, X. Qian, M. Shan, H. Deng, X. Tian, C. Li, F. Li, Manipulating Migration Behavior of Magnetic Graphene Oxide via Magnetic Field Induced Casting and Phase Separation toward High-Performance Hybrid Ultrafiltration Membranes, ACS Appl Mater Interfaces, 8 (2016) 18418-18429.

[30] Z. Xu, T. Wu, J. Shi, K. Teng, W. Wang, M. Ma, J. Li, X. Qian, C. Li, J. Fan, Photocatalytic antifouling PVDF ultrafiltration membranes based on synergy of graphene oxide and TiO2 for water treatment, Journal of Membrane Science, 520 (2016) 281-293.

[31] G.S. Lai, W.J. Lau, P.S. Goh, A.F. Ismail, N. Yusof, Y.H. Tan, Graphene oxide

incorporated thin film nanocomposite nanofiltration membrane for enhanced salt removal performance, Desalination, 387 (2016) 14-24.

[32] H. Zarrabi, M.E. Yekavalangi, V. Vatanpour, A. Shockravi, M. Safarpour, Improvement in desalination performance of thin film nanocomposite nanofiltration membrane using amine-functionalized multiwalled carbon nanotube, Desalination, 394 (2016) 83-90.

[33] S.M. Xue, Z.L. Xu, Y.J. Tang, C.H. Ji, Polypiperazine-amide Nanofiltration Membrane Modified by Different Functionalized Multiwalled Carbon Nanotubes (MWCNTs), ACS Appl Mater Interfaces, 8 (2016) 19135-19144.

[34] H.-Z. Zhang, Z.-L. Xu, H. Ding, Y.-J. Tang, Positively charged capillary nanofiltration membrane with high rejection for Mg^{2+} and Ca^{2+} and good separation for Mg^{2+} and Li^{+}, Desalination, 420 (2017) 158-166.

[35] S. Gholami, J. López, A. Rezvani, V. Vatanpour, J.L. Cortina, Fabrication of thin-film nanocomposite nanofiltration membranes incorporated with aromatic amine-functionalized multiwalled carbon nanotubes. Rejection performance of inorganic pollutants from groundwater with improved acid and chlorine resistance, Chemical Engineering Journal, 384 (2020) 123348.

[36] P. Xu, J. Hong, X. Qian, Z. Xu, H. Xia, Q.-Q. Ni, “Bridge” graphene oxide modified positive charged nanofiltration thin membrane with high efficiency for Mg^{2+}/Li^{+} separation, Desalination, 488 (2020) 114522.

[37] L. Deng, Q. Wang, X. An, Z. Li, Y. Hu, Towards enhanced antifouling and flux performances of thin-film composite forward osmosis membrane via constructing a sandwich-like carbon nanotubes-coated support, Desalination, 479 (2020) 114311.

[38] L. Dumée, J. Lee, K. Sears, B. Tardy, M. Duke, S. Gray, Fabrication of thin film composite poly(amide)-carbon-nanotube supported membranes for enhanced performance in osmotically driven desalination systems, Journal of Membrane Science, 427 (2013) 422-430.

[39] H. Zhao, S. Qiu, L. Wu, L. Zhang, H. Chen, C. Gao, Improving the performance of polyamide reverse osmosis membrane by incorporation of modified multi-walled

carbon nanotubes, Journal of Membrane Science, 450 (2014) 249-256.
[40] E.-S. Kim, G. Hwang, M. Gamal El-Din, Y. Liu, Development of nanosilver and multi-walled carbon nanotubes thin-film nanocomposite membrane for enhanced water treatment, Journal of Membrane Science, 394-395 (2012) 37-48.
[41] X. Zhang, L. Shen, C.-Y. Guan, C.-X. Liu, W.-Z. Lang, Y. Wang, Construction of SiO_2@MWNTs incorporated PVDF substrate for reducing internal concentration polarization in forward osmosis, Journal of Membrane Science, 564 (2018) 328-341.
[42] F. Yu, H. Shi, J. Shi, K. Teng, Z. Xu, X. Qian, High-performance forward osmosis membrane with ultra-fast water transport channel and ultra-thin polyamide layer, Journal of Membrane Science, 616 (2020) 118611.
[43] N.N. Gumbi, M. Hu, B.B. Mamba, J. Li, E.N. Nxumalo, Macrovoid-free PES/SPSf/O-MWCNT ultrafiltration membranes with improved mechanical strength, antifouling and antibacterial properties, Journal of Membrane Science, 566 (2018) 288-300.
[44] K.A. Wepasnick, B.A. Smith, K.E. Schrote, H.K. Wilson, S.R. Diegelmann, D.H. Fairbrother, Surface and structural characterization of multi-walled carbon nanotubes following different oxidative treatments, Carbon, 49 (2011) 24-36.
[45] H. Kang, J. Shi, L. Liu, M. Shan, Z. Xu, N. Li, J. Li, H. Lv, X. Qian, L. Zhao, Sandwich morphology and superior dye-removal performances for nanofiltration membranes self-assemblied via graphene oxide and carbon nanotubes, Applied Surface Science, 428 (2018) 990-999.
[46] M. Hu, Z. Cui, J. Li, L. Zhang, Y. Mo, D.S. Dlamini, H. Wang, B. He, J. Li, H. Matsuyama, Ultra-low graphene oxide loading for water permeability, antifouling and antibacterial improvement of polyethersulfone/sulfonated polysulfone ultrafiltration membranes, J Colloid Interface Sci, 552 (2019) 319-331.
[47] A. Rahimpour, M. Jahanshahi, S. Khalili, A. Mollahosseini, A. Zirepour, B. Rajaeian, Novel functionalized carbon nanotubes for improving the surface properties and performance of polyethersulfone (PES) membrane, Desalination, 286 (2012) 99-107.

[48] J. Zhang, Z. Xu, M. Shan, B. Zhou, Y. Li, B. Li, J. Niu, X. Qian, Synergetic effects of oxidized carbon nanotubes and graphene oxide on fouling control and anti-fouling mechanism of polyvinylidene fluoride ultrafiltration membranes, Journal of Membrane Science, 448 (2013) 81-92.

[49] M. Shan, H. Kang, Z. Xu, N. Li, M. Jing, Y. Hu, K. Teng, X. Qian, J. Shi, L. Liu, Decreased cross-linking in interfacial polymerization and heteromorphic support between nanoparticles: Towards high-water and low-solute flux of hybrid forward osmosis membrane, J Colloid Interface Sci, 548 (2019) 170-183.

[50] M. Chandrashekhar Nayak, A.M. Isloor, Inamuddin, B. Lakshmi, H.M. Marwani, I. Khan, Polyphenylsulfone/multiwalled carbon nanotubes mixed ultrafiltration membranes: Fabrication, characterization and removal of heavy metals Pb^{2+}, Hg^{2+}, and Cd^{2+} from aqueous solutions, Arabian Journal of Chemistry, 13 (2020) 4661-4672.

[51] R. Graupner, Raman spectroscopy of covalently functionalized single-wall carbon nanotubes, Journal of Raman Spectroscopy, 38 (2007) 673-683.

[52] X. Li, L. Liu, Z. Xu, W. Wang, J. Shi, L. Liu, M. Jing, F. Li, X. Zhang, Gamma irradiation and microemulsion assisted synthesis of monodisperse flower-like platinum-gold nanoparticles/reduced graphene oxide nanocomposites for ultrasensitive detection of carcinoembryonic antigen, Sensors and Actuators B: Chemical, 287 (2019) 267-277.

[53] S. Li, C. Li, X. Song, B. Su, B. Mandal, B. Prasad, X. Gao, C. Gao, Graphene Quantum Dots-Doped Thin Film Nanocomposite Polyimide Membranes with Enhanced Solvent Resistance for Solvent-Resistant Nanofiltration, ACS Appl Mater Interfaces, 11 (2019) 6527-6540.

[54] S. Xu, F. Li, B. Su, M.Z. Hu, X. Gao, C. Gao, Novel graphene quantum dots (GQDs)-incorporated thin film composite (TFC) membranes for forward osmosis (FO) desalination, Desalination, 451 (2019) 219-230.

[55] V. Vatanpour, S.S. Madaeni, R. Moradian, S. Zinadini, B. Astinchap, Fabrication and characterization of novel antifouling nanofiltration membrane prepared from oxidized multiwalled carbon nanotube/polyethersulfone nanocomposite, Journal of Membrane Science, 375 (2011) 284-294.

[56] J.-H. Choi, J. Jegal, W.-N. Kim, Fabrication and characterization of multi-walled carbon nanotubes/polymer blend membranes, Journal of Membrane Science, 284 (2006) 406-415.

[57] S. Qiu, L. Wu, X. Pan, L. Zhang, H. Chen, C. Gao, Preparation and properties of functionalized carbon nanotube/PSF blend ultrafiltration membranes, Journal of Membrane Science, 342 (2009) 165-172.

[58] A. Abdel-Karim, S. Leaper, M. Alberto, A. Vijayaraghavan, X. Fan, S.M. Holmes, E.R. Souaya, M.I. Badawy, P. Gorgojo, High flux and fouling resistant flat sheet polyethersulfone membranes incorporated with graphene oxide for ultrafiltration applications, Chemical Engineering Journal, 334 (2018) 789-799.

[59] G. Zhao, R. Hu, J. Li, H. Zhu, Graphene oxide quantum dots embedded polysulfone membranes with enhanced hydrophilicity, permeability and antifouling performance, Science China Materials, 62 (2019) 1177-1187.

Chapter 6

Conclusions

6 Conclusions

In this work, we adopted several carbon nano-additives to improve the Mg^{2+}/Li^{+} separation capability and efficiency of NF membranes, and comprehensively discussed the results and mechanism of the resulted carbon-based NF membranes from the perspectives of multiple aspects. Based on the above research process, the results of this paper are as follows:

In chapter 1, an overview of global lithium resources and distribution, commonly used lithium retraction methods, and research status and difficulties of Mg^{2+}/Li^{+} separation using NF membrane has been reviewed.

In chapter 2, we successfully optimized the Mg^{2+}/Li^{+} separation efficiency of NF membrane by doping a small amount of GO additives in the PES UF substrate membrane. The polyamide thin layer was formed through polymerization between PEI and TMC on the GO-doped UF membrane surface. A large amount of unreacted protonated amine groups in the polyamide layer gave the membrane surface high positive chargeability. The “bridge” GO greatly enhanced the interaction between the substrate membrane and polyamide layer. On the other hand, a small increase of the hydrophilic GO additives (from 0 wt% to 0.05 wt%) greatly improved the porosity and permeability of UF membrane, and the pore size of final NF membrane was enlarged slightly, and the thickness of polyamide layer was decreased slightly, which correspondingly improved the flux of the prepared NF membrane during the filtration process. The optimized NF membrane exhibited an optimal Mg^{2+}/Li^{+} separation performance and efficiency, the rejection for Mg^{2+} and Li^{+} and the flux were 95.14%, 20.93%, and 11.15 L/m^2hbar, respectively. In addition, the obtained NF membrane performed a high stability after a 7-day long-time filtration, which may be due to the improved hydrophilicity and mechanical properties by GO modification. This work successfully optimized the performance of the NF membrane by modifying the substrate membrane with ultra-low content of GO, which provides a reference direction

for future NF membrane optimization research.

In chapter 3, a novel high positively charged NF membrane containing GQDs-NH_2 was synthesized by interfacial polymerization on the PSE base membrane. Due to the multi-effect caused by GQDs-NH_2, the final obtained NF membranes were endowed with thinner and smoother polyamide layer, enhanced positively chargeability and improved hydrophilicity, and shorter path water channel formed between GQDs-NH_2 monomers and polyamide layer. After filtering the feed solution using optimized NF membrane, the mass ratio of Mg^{2+}/Li^{+} decreased from an initial 20 to 0.7, and rejections of membrane for Mg^{2+} and Li^{+} were 97.16 % and 20.02%, respectively. Note that the permeation flux of the NF membrane improved to 11.94 L/m^2hbar, which was 137.8 % more than that of pure NF membrane with no GQDs-NH_2. Additionally, the improved hydrophilicity and smoother surface endowed the final NF membrane with higher anti-fouling performance, allowing it to work stably for a long time in practical applications. In summary, the NF membrane incorporated with GQDs-NH_2 is effective for enrich and extract lithium from salt-lake brines with a high mass ratio of Mg^{2+}/Li^{+}.

In chapter 4, the MWCNTs-COOK-assisted highly permeable NF membrane with superior Li^{+}/Mg^{2+} separate-selectivity was successfully synthesized and optimized. Results show that the incorporated MWCNTs-COOK intensified the network-crosslinking among PEI, MWCNTs-COOK, and TMC, achieving fine-tuning of structure and properties of resultant NF membranes. The presence of MWCNTs-COOK nano-additives significantly increased the flux of the NF membrane. The hollow tubular structure of MWCNTs-COOK and inter-gap between MWCNTs-COOK and membrane matrix furnished NF membrane with more channels for water to transport. Moreover, MWCNTs-COOK introduced more hydrophilic group and greatly improved the hydrophilicity of the membrane surface. The modified MWCNTs-COOK-assisted NF membrane showed a significantly improved flux of 12.23 L/m^2hbar without a compromise in Li^{+}/Mg^{2+} separate-selectivity, which greatly accelerated the filtration process. Importantly, the MWCNTs-COOK-assisted NF membrane exhibited a remarkably stable Li^{+} enrich and Mg^{2+} remove capabilities in long-term utilization.

Overall, this work provides a feasible technique for quickly extracting high-purity lithium from salt-lake brine.

In chapter 5, we fixed the MWCNTs-COOK additives into the UF substrate membrane, and then formed the polyamide layer on the MWCNTs-COOK-engineered substrate surface through interfacial polymerization. The fixed MWCNTs-COOK endowed the substrate with high hydrophilicity and porosity, contributing to higher water permeability of the UF membrane. The connection between UF substrate and the polyamide layer was strengthened by the "connector" MWCNTs-COOK, which directly improved the performance stability of the final NF membrane. The membrane performance characterization indicated that with an optimal MWCNTs-COOK content of 0.012 wt%, the obtained NF membrane showed a high Mg^{2+}/Li^{+} separation ability and the difference between rejections of Li^{+} and Mg^{2+} reached 86.94%, which were much higher than that of most reported NF membrane. Importantly, the flux of the optimized NF membrane was 11.46 (L/m^2hbar), which was over 120% higher than that of the NF membrane with no MWCNTs-COOK. The obtained high separation factor and flux of the NF membrane indicated its great potential for fast and efficient separation of Mg^{2+} and Li^{+}. This work proved that anchoring MWCNTs-COOK into the UF substrate membrane is an effective way to improve the Mg^{2+}/Li^{+} separation performance of NF membrane, thereby accelerating the rate of lithium enrichment during lithium extraction.

In chapter 6, we comprehensively summarized the results and application prospects of the carbon nano-additives on the Mg^{2+}/Li^{+} separation capability and efficiency of NF membranes.

In summary, the incorporation of carbon nanomaterials is an effective way to improve the Mg^{2+}/Li^{+} separation efficiency of NF membrane. This work opens a simple and effective pathway for accelerating Li^{+} enrichment and Mg^{2+} removal, which has great potential for lithium extraction application from salt-lake brines that loaded with high concentration of Mg^{2+}.

ACCOMPLISHMENTS

LIST OF PUBLICATION

❋❋❋❋❋❋❋❋❋❋❋❋❋❋❋❋❋❋❋❋❋❋❋❋❋❋❋❋❋❋❋❋❋

Journal Publications

[1] **Ping Xu**, J. Hong, X. Qian, Z. Xu, H. Xia, Q.-Q. Ni, "Bridge" graphene oxide modified positive charged nanofiltration thin membrane with high efficiency for Mg^{2+}/Li^{+} separation, Desalination 488 (2020), 114522.

[2] **Ping Xu**, J. Hong, Z. Xu, H. Xia, Q.-Q. Ni, Novel aminated graphene quantum dots (GQDs-NH_2)-engineered nanofiltration membrane with high Mg^{2+}/Li^{+} separation efficiency, Separation and Purification Technology 258 (2021) 118042.

[3] **Ping Xu**, J. Hong, Z. Xu, H. Xia, Q.-Q. Ni, MWCNTs-COOK-assisted high positively charged composite membrane: Accelerating Li^{+} enrichment and Mg^{2+} removal, Composites Part B: Engineering 212 (2021), 108686.

[4] **Ping Xu**, J. Hong, Z. Xu, H. Xia, Q.-Q. Ni, Positively charged nanofiltration membrane based on (MWCNTs-COOK)-engineered substrate for fast and efficient lithium extraction, Separation and Purification Technology 270 (2021), 118796.

[5] **Ping Xu**, J. Hong, X. Qian, Z. Xu, H. Xia, X. Tao, Z. Xu, Q.-Q. Ni, Materials for lithium recovery from salt lake brine, Journal of Materials Science 56 (2021), 16–63.

Conference

[1] **Ping Xu**, J. Hong, H. Xia, Q.-Q. Ni (2020), "Bridge" graphene oxide modified nanofiltration membrane with high efficiency for Mg^{2+}/Li^{+} separation, MEMBRANE SYMPOSIUM, Japan, 2020.

[2] **Ping Xu**, Q-Q. Ni, "Bridge" graphene oxide modified nanofiltration membrane with high efficiency for Mg^{2+}/Li^{+} separation, China-Japan Academic and Technical Exchange Conference on Composite Material, Wuhu, China, 2021.

ACKNOWLEDGMENTS

Graduation is approaching, and I have basically completed the study and exploration of the graduation research. I want to give my sincerely gratitude to the persons who give me help and advice.

First, I would like to express my sincere gratitude to my supervisor Prof. Qing-Qing Ni for providing me the opportunity to study at Shinshu University. Thanks to his guidance, I can successfully overcome every difficulty and complete my PhD. Meanwhile, I like to express my gratitude to Dr. Hong Xia for her continuous guidance and support to my research work. I also want to express my thanks to Prof. Toshiaki Natsuki for his help for my research and living. We often have good discussion related to my work and his suggestions are always helpful.

Thank all former and current members of Ni Lab: Hairong Chen, Xiaoyu Guan, Chongchao Li, Canyi Huang, Yajun Liu, Lina Cui, Si Chen, Fengyu Li, Baoji Hu, Jingyan Qu, Guangyu Su and Hao Wang. I also want to thank all my friends at Shinshu University. I am grateful to meet you. It is you who gave me great support and encouragement in the course of my living and PhD. I wish you all the best and a bright future.

Special thanks to Prof. Xiaoming Qian and Prof. Zhiwei Xu in Tiangong University and Prof. Zhenzhen Xu at Anhui Polytechnic University for their constructive suggestions and warm encouragement.

Here, I want to express my gratitude to Rotary Yoneyama Memorial Foundation for financial support.

Last but not least, I want to express my thank to my lovely family for their tolerance, encouragement, warm care and help in life during my PhD period at Shinshu University.